NTNU – Trondheim
Norwegian University of
Science and Technology

Wave slamming forces on truss support structures for wind turbines

Miriam Zakri Aashamar

Civil and Environmental Engineering (2 year)
Submission date: June 2012
Supervisor: Øivind Asgeir Arntsen, BAT
Co-supervisor: Alf Tørum, BAT

Norwegian University of Science and Technology
Department of Civil and Transport Engineering

NORWEGIAN UNIVERSITY OF SCIENCE AND TECHNOLOGY
DEPARTMENT OF CIVIL AND TRANSPORT ENGINEERING

Report Title: Wave slamming forces on truss support structures for wind turbines		Date: 07.06.2012 Number of pages (incl. appendices): 166			
		Master Thesis	X	Project Work	
Name:	Miriam Zakri Aashamar				
Professor in charge/supervisor:	Øivind Asgeir Arntsen Alf Tørum				
Other external professional contacts/supervisors:					

Abstract:

This thesis is a study of the slamming forces from plunging breaking waves on truss support structures in shallow water. The main parts have been model testing and analysis on an existing 1:50 scale model of a truss support structure for wind turbines at NTNU.

An expanding building of offshore structures has led to increased focus on wave forces. Large slamming forces from breaking waves can occur in shallow water. These forces will impact the structure in a much bigger way than non-breaking wave forces. Several researches have been investigating wave slamming forces on single vertical and inclined piles for the last 50 years, but there are still uncertainties at this area. This causes uncertainties in the dimension of structures exposed to these kinds of forces, and are therefore still under investigation.

A large number of measurements have been executed. The tests have been run with both regular and irregular waves, with different frequencies and wave lengths. This give waves with different wave heights and breaking points, so that maximum forces can be determined.

A "new" analyzing method described by Määtänen (1979) is applied to obtain the wave slamming force for response force time series. This is a simplified analysis based on an assumption of a single degree of freedom system subjected to a total force.

The probability of occurrence of plunging breakers on the foreshore is investigated by Reedijk, et al. (2009). The method is used to find the probability of occurrence of plunging breakers on the truss structure for irregular waves.

Maximum force response is given by waves that broke some distance away from the structure and not when the wave broke directly at the structure. The wave broke ahead and surged against the structure, which imposed forces with a slamming character in both the top and bottom force transducers.

It is significant air entrained in the water during the breaking process, which may influence the results differently in small-scale model testing and in reality. The reason for this may be scale-effects that may impact interpretation of the results. The measured crest height is smaller due to air entrance in the waves as well.

Keywords:

1. Truss structure
2. Plunging breaking waves
3. Response
4. Scale effects

TASK DESCRIPTION

Wind turbine foundation structures in shallow water may be prone to slamming forces from breaking waves, typically plunging breaking waves.

Reinertsen A/S has been involved in the design of a truss support structure for wind turbines on the Thornton Bank, Belgian Coast. Plunging breaking waves has been specified for this area. Calculations show that the forces from the plunging breaking waves are governing the responses of the structure and the foundations. However, there are considerable uncertainties on the calculated plunging breaking wave forces.

The thesis work will mainly be model testing of such a structure in a wave flume using an existing 1:50 scale model of a truss structure. The test program may be changed as results are obtained. But the following tasks are envisaged: The tests will be run with regular as well as irregular waves. It is planned to split the structure in different parts to measure the wave forces on the individual parts. The bottom slope has been approximately 1:10 in the tests run by Ros (2011) and Aune (2011). However, if time permits, tests should be run also with an additional slope, say 1:30 or 1:50.

PREFACE

This report is the result of my Master's thesis work done in the course TBA4920 Marine Civil Engineering, Master Thesis. This report is a continuation of my project work done in the course TBA4250 Marine Civil Engineering, Specialization Project. The main part of the project work was a literature study of wave slamming forces on truss support structures for wind turbines.

This thesis is an experimental study of plunging breaking waves on truss support structures for wind turbines in shallow water. The theory concerning this topic is amplified. I have executed a large number of tests on an existing 1:50 scale model of a truss structure, and the results are analyzed.

I would like to thank my supervisors Alf Tørum and Øiving Asgeir Arntsen for good help during the writing of this report. I would also like to thank Torgeir Jensen and Gustav Jakobsen at SINTEF for their help with the experimental set-up and instrumentation.

Miriam Zakri Aashamar, June 7th, 2012

SUMMARY

This thesis is a study of the slamming forces from plunging breaking waves on truss support structures in shallow water.

An expanding building of offshore structures has led to increased focus on wave forces. Non-breaking wave forces appear in deep water. These wave forces have been investigated for many years. Morison's equation (Morison et al. 1950) is the most frequently used equation to calculate forces from non-breaking waves:

$$dF = dF_D + dF_M = \frac{1}{2}\rho_w C_D D|u|udz + \rho_w \frac{\pi D^2}{4} C_M \frac{du}{dt} dz \quad (1)$$

F_D is the drag force, F_M is the inertia force, ρ_w is the water density, C_d is the drag coefficient, C_M is the inertia coefficient, D is the diameter of the cylinder, u is the water particle velocity, du/dt is the water particle acceleration, z is the upward vertical direction and t is the time.

Large slamming forces from breaking waves can occur in shallow water. These forces will impact the structure in a much bigger way than non-breaking wave forces. Several researches have been investigating wave slamming forces on single vertical and inclined piles for the last 50 years, but there are still uncertainties at this area. The researchers have agreed on the formulas used to calculate the slamming force, but have different theories on the value of the slamming factor, C_S, curling factor, λ, and duration of impact, τ. This causes uncertainties in the dimension of structures exposed to these kinds of forces, and are therefore still under investigation. The total force from breaking waves is:

$$F = F_D + F_M + F_S \quad (2)$$

The slamming force is commonly written as:

$$F_S = \frac{1}{2}\rho_w C_S D C_b^2 \lambda \eta_b \quad (3)$$

C_s is the slamming factor, $C_b = C$ is the wave celerity, λ is the curling factor and η_b is the maximum surface elevation of the wave at breaking.

The main parts of this thesis work have been model testing and analysis on an existing 1:50 scale model of a truss support structure for wind turbines at NTNU.

The test set-up is shown in Figure 1.

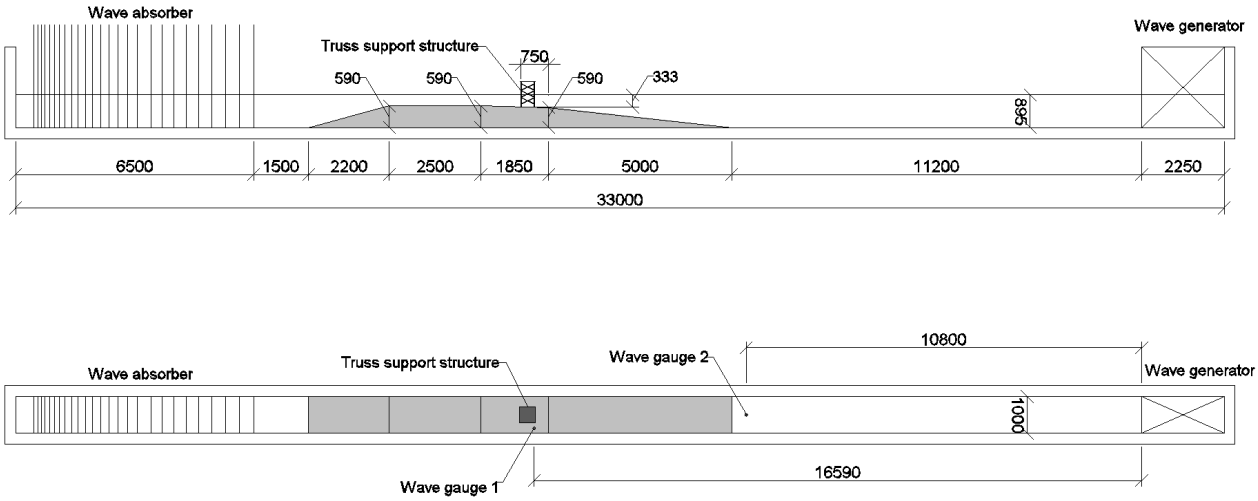

Figure 1: Wave channel [mm]

A large number of measurements have been executed. The tests have been run with both regular and irregular waves, with different frequencies and wave lengths. This give waves with different wave heights and breaking points, so that maximum forces can be determined. The sampling frequency during testing was 19200Hz.

The truss structure, Figure 2, is equipped with four force transducers, two at the bottom and two at the top of the structure. The water depth at the middle of the structure is 0,333m.

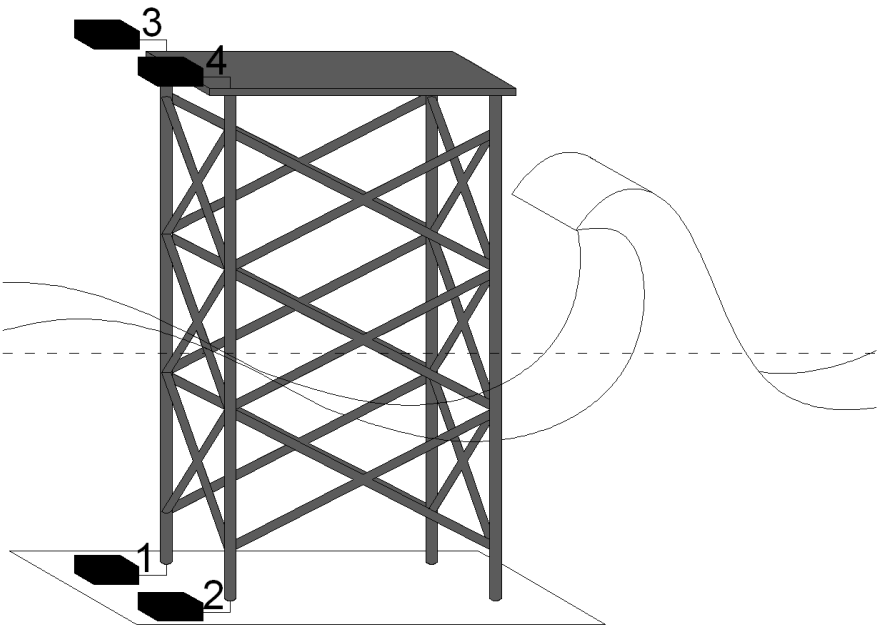

Figure 2: Truss support structure with force transducers, scale 1:50

A "new" analyzing method described by Määtänen (1979) is applied to obtain the wave slamming force for response force time series. This is a simplified analysis based on an assumption of a single degree of freedom system subjected to a total force.

An impulse hammer is used to find the transfer function. The structure is hit by the impulse hammer several places, in the approximate location of the wave slamming resultant load. The frequency response function (FRF), *H(ω)*, is obtained from the measured impulse force and the simultaneously measured response forces in the four force transducers on the structure.

The inverse fast Fourier transform (IFFT) of S(ω)/H(ω) has a high frequency component. This high frequency component has been filtered away by a low-pass filter, and it is obtained a force time series that show the wave slamming force. *S(ω)* is the linear spectrum of the applied force.

The probability of occurrence of plunging breakers on the foreshore is investigated by Reedijk, et al. (2009). The method is used to find the probability of occurrence of plunging breakers on the truss structure for irregular waves.

Maximum force response is given by waves that broke some distance away from the structure and not when the wave broke directly at the structure. The wave broke ahead and surged against the structure, which imposed forces with a slamming character in both the top and bottom force transducers. See Figure 3.

Figure 3: Snap-shot, Mf045e270_1

The slamming force obtained from model testing is about half the measured response. The calculated slamming forces are larger than the measured slamming force in all the analyzed cases of regular waves. The reason for this may be scale effects.

It is significant air entrained in the water during the breaking process, which may influence the results differently in small-scale model testing and in reality. The reason for this may be scale-effects that may impact interpretation of the results. The measured crest height is smaller due to air entrance in the waves as well.

The use of freshwater in the model testing can be considered valid, as previous investigation have shown that there are only minor differences between the process of air entrainment by breaking waves in freshwater and seawater. The bubble sizes are also comparable.

SAMMENDRAG

Denne masteroppgaven er en studie av slagkrefter fra styrtbrytende bølger på støttekonstruksjoner av fagverk i grunt vann.

En ekspansiv utbygging av offshorekonstruksjoner har ført til økt fokus på bølgekrefter. Ikkebrytende bølgekrefter oppstår på dypt vann. Disse bølgekreftene har blitt gransket i mange år. Morisons ligning (Morison et al. 1950) er den mest brukte ligningen for å beregne krefter fra ikkebrytende bølger:

$$dF = dF_D + dF_M = \frac{1}{2}\rho_w C_D D|u|udz + \rho_w \frac{\pi D^2}{4} C_M \frac{du}{dt} dz \tag{4}$$

F_D er dragkraften, F_M er treghetskraften, ρ_w er vannets tetthet, C_d er dragkoeffisienten, C_M er treghetskoeffisienten, D er sylinderens diameter, u er vannets partikkelhastighet, du/dt er vannets partikkelakselerasjon, z er vertikal retning oppover og t er tid.

Store slagkrefter fra styrtbrytende bølger kan oppstå i grunt vann. Disse kreftene vil støte konstruksjonen mye hardere enn ikkebrytende bølgekrefter. Flere forskere har gransket slagkrefter fra bølger på enkle vertikale og skrå peler de siste 50 årene, men det er fortsatt usikkerheter rundt dette temaet. Forskerne er enige om hvilke formler som skal benyttes for å beregne slagkraften, men har forskjellige teorier om verdien på slagfaktoren, C_S, krumningsfaktoren, λ, og varigheten av slaget, τ. Dette fører til usikkerheter rundt dimensjonering av konstruksjoner utsatt for denne type krefter, og er derfor fortsatt under gransking. Den totale kraften fra styrtbrytning er:

$$F = F_D + F_M + F_S \tag{5}$$

Slagkraften er vanligvis skrevet som:

$$F_S = \frac{1}{2}\rho_w C_S D C_b^2 \lambda \eta_b \tag{6}$$

C_s er slagfaktoren, $C_b = C$ er bølgens hastighet, λ er krumningsfaktoren og η_b er maks overflateelevasjon av bølgen ved brytning.

Hoveddelen av denne masteroppgaven har vært modelltesting og analyse på en eksisterende modell i skala 1:50 av en støttekonstruksjon av fagverk for vindturbiner på NTNU.

Testoppsettet er vist i Figur 4.

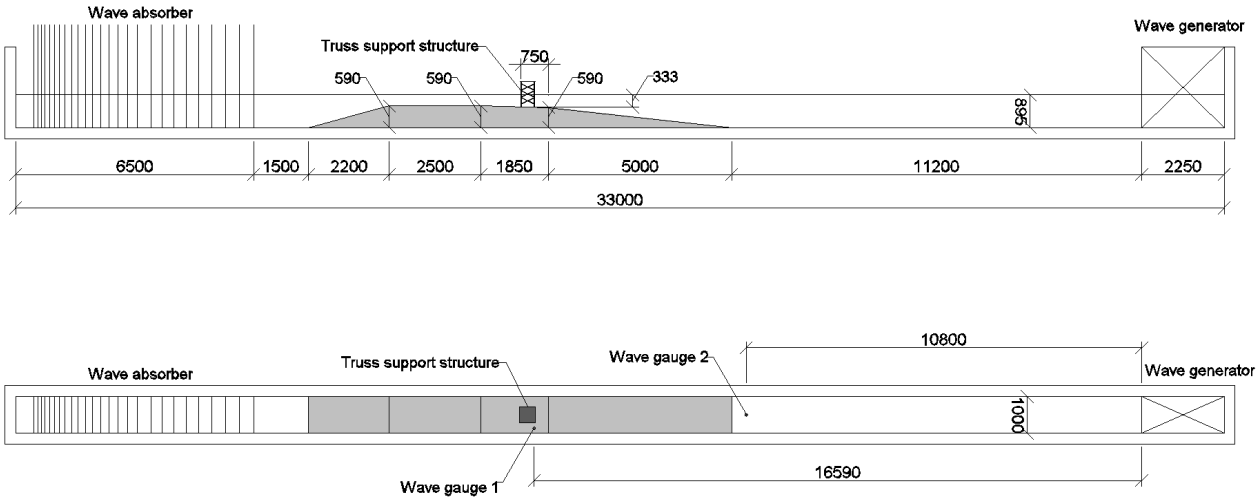

Figur 4: Bølgekanal [mm]

Et stort antall målinger har blitt utført. Testene har blitt kjørt med både regelmessige og uregelmessige bølger, med forskjellige frekvenser og bølgelengder. Dette gir bølger med forskjellige bølgehøyder og brytningspunkt, slik at maksimale krefter kan fastsettes. Samplingsfrekvensen under testing var 19200Hz.

Fagverkskonstruksjonen, Figur 5, er utstyrt med fire kraftmålere, to i bunn og to i toppen av konstruksjonen. Vanndybden i midten av kostruksjonen er 0,333m.

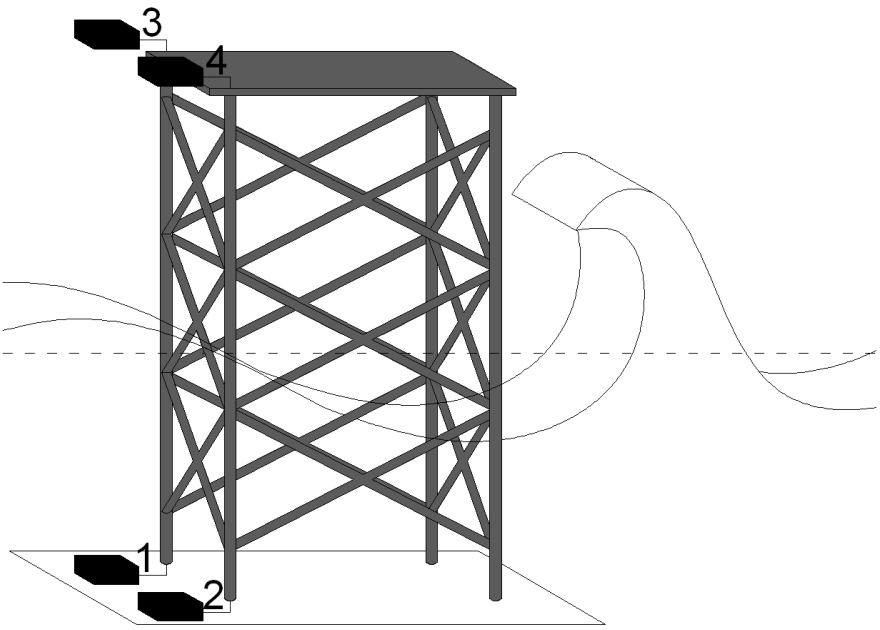

Figur 5: Fagverkskonstruksjon med kraftmålere, skala 1:50

En "ny" analysemetode beskrevet av Määtänen (1979) er anvendt for å oppnå bølgeslagkraften for tidsserier av responskraften. Dette er en forenklet analyse basert på en antakelse om et system med èn frihetsgrad utsatt for en total kraft.

En impulshammer er brukt til å finne transferfunksjonen. Det er slått flere steder på konstruksjonen med impulshammeren, tilnærmet de stedene bølgeslagkraftens resultantkraft oppstår. Frekvensresponsfunksjonen (FRF), $H(\omega)$, er oppnådd fra den målte impulskraften og den samtidig målte responskraften i de fire kraftmålerene på konstruksjonen.

Den inverse Fast Fourier transform (IFFT) av S(ω)/H(ω) har en høyfrekvent komponent. Denne høyfrekvente komponenten har blitt filtrert bort med et lavpassfilter, og det oppnås en tidsserie som viser bølgeslagkraften. $S(\omega)$ er det lineære spektrumet av den påførte kraften.

Sannsynligheten for forekomst av styrtbrytende bølger på en strandlinje er gransket av Reedijk, et al. (2009). Denne metoden er brukt til å finne sannsynligheten for forekomst av styrtbrytende bølger på fagverkskonstruksjonen når den er utsatt for uregelmessige bølger.

Maks kraftrespons er gitt av bølger som brøt en viss avstand unna konstruksjonen og ikke når bølgen brøt rett på. Bølgen brøt foran og fosset mot konstruksjonen, noe som påtvang krefter med en slagkarakter på kraftmåleren i både topp og bunn. Se Figur 6.

Figur 6: Bilde, Mf045e270_1

Slagkraften oppnådd fra modelltesting er rundt halvparten av den målte responsen. De beregnede slagkreftene er større enn målt slagkraft i alle tilfellene av regelmessige bølger. Grunnen til dette kan være skalaeffekter.

En betydelig mengde luft er brakt med i vannet under brytningsprosessen, noe som kan påvirke resultatet forskjellig i småskala modelltesting og i virkeligheten. Grunnen til dette kan være skalaeffekter som kan innvirke på tolkningen av resultatene. Den målte bølgekamhøyden er også mindre enn observert på grunn av luft i bølgene.

Bruk av ferskvann i modelltestingen kan ses på som gyldig, siden tidligere forskning har vist at det bare er små forskjeller mellom luft brakt med i vannet under brytningsprosessen i ferskvann og saltvann. Størrelsen på boblene kan også sammenlignes.

TABLE OF CONTENTS

LIST OF FIGURES

LIST OF TABLES

1. INTRODUCTION

This thesis is a study of the slamming forces from plunging breaking waves on truss support structures for wind turbines in shallow water.

Focus on wave forces has increased the last decades due to an increase in construction of offshore structures in shallow water. Non-breaking wave forces have been investigated in many years. These wave forces appear in deep water. Morison's equation (Morison, et al. 1950) is the most frequently used equation to calculate forces from non-breaking waves.

In shallow water, large slamming forces from plunging breaking waves can occur. These forces will impact the structure in a much bigger way than non-breaking wave forces. For the last 50 years, several researches have investigated wave slamming forces on single vertical and inclined piles, but there are still uncertainties at this area.

Reinertsen AS has been involved in the design of a truss support structure for wind turbines on the Thornton Bank outside the Belgian Coast, see Figure 7. Plunging breaking waves have been specified in this area.

A large research project has been proposed, involving large scale experiments in the Large Wave Channel in Hannover, Germany. This is to obtain improved knowledge of wave kinematics and forces from breaking waves, especially wave slamming forces on truss structures through model tests on a large scale, 1:8. The experiments in the large wave channel in Hannover are planned to be in the spring of 2013. Some of the challenges in these tests are to resolve the slamming forces on the individual members of the truss structure.

Figure 7: Truss structure for support of wind turbines (Tørum, 2011)

2. BREAKING WAVES IN SHALLOW WATER

2.1. Short description of water waves

Water waves are fluctuations of the water level. They are accompanied by water particle velocities, accelerations and pressure fluctuations. A regular wave, the simplest wave form, is defined by the sine (or cosine) function, Figure 8. The vertical distance between a crest and a trough is the wave height, *H*. The wavelength, *L*, is the distance over which the wave pattern repeats itself. The wave propagates with a celerity, *C*, the phase speed. The wave period, *T*, is the time a wave uses to pass a particular location. *d* is the water depth, η is the instantaneous water surface elevation above still water level and *a* is the wave amplitude.

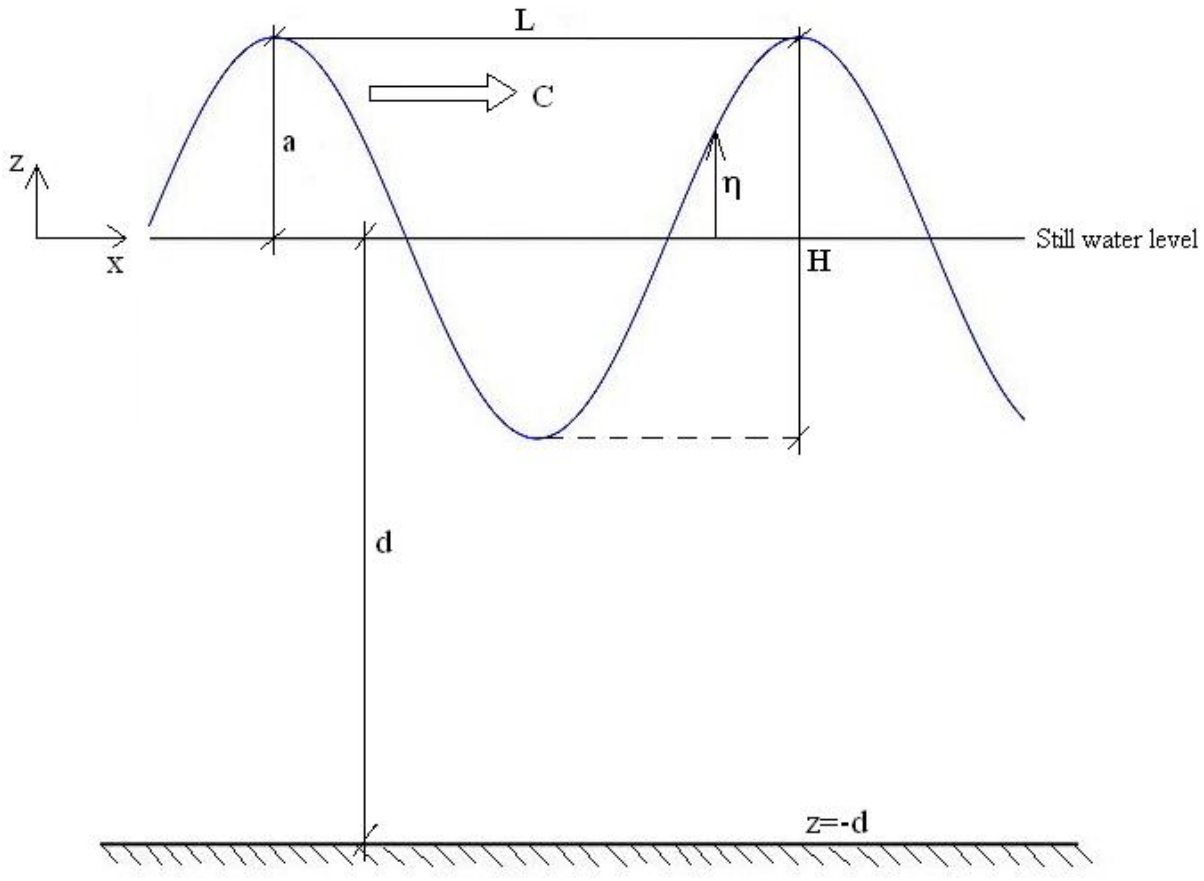

Figure 8: Regular wave

2.2. Definition of breaking waves

Figure 9: Breaking wave

Wave shoaling is the effect of change of wave height when surface waves enter shallower water. *H/L* is the physical limit to the steepness of the waves, so the wave breaks and dissipates its energy when this limit is exceeded.

When the wave breaks, it may have one of several shapes as defined below. The breaker type is a function of the wave steepness, *H/L*, and the seabed slope, *tanθ*. The surf similarity is defined as:

$$\xi_0 = \frac{\tan\theta}{\sqrt{\frac{H_0}{L_0}}} \tag{7}$$

tanθ is the beach slope, H_0 is deep water wave height and L_0 is the wave length in deep water. (Battjes, 1974).

2.2.1. Spilling breaking waves

Breaking waves are predominantly spilling breakers, Figure 10. They occur for steep waves on flat beach slopes, often called dissipative beaches. Small parts of the wave crest breaks gently, and several of the crests may break simultaneously. $\xi_0 < 0{,}5$ according to Battjes (1974).

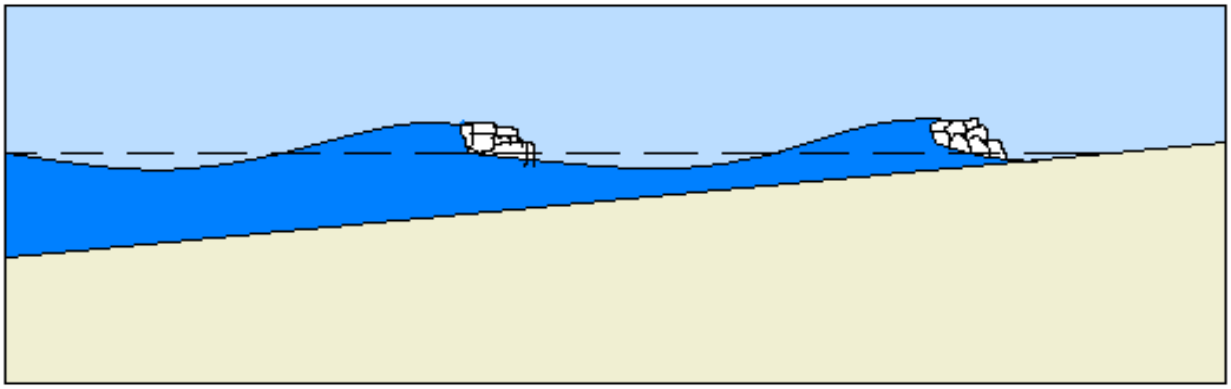

Figure 10: Spilling breaking wave

2.2.2. Plunging breaking waves

A typical plunging breaking wave is shown in Figure 9. Plunging breakers occur for flatter waves on steeper beaches, Figure 11. The wave crest runs ahead of the main body of the wave and plunges forward. $0{,}5 < \xi_0 < 3{,}3$ according to Battjes (1974).

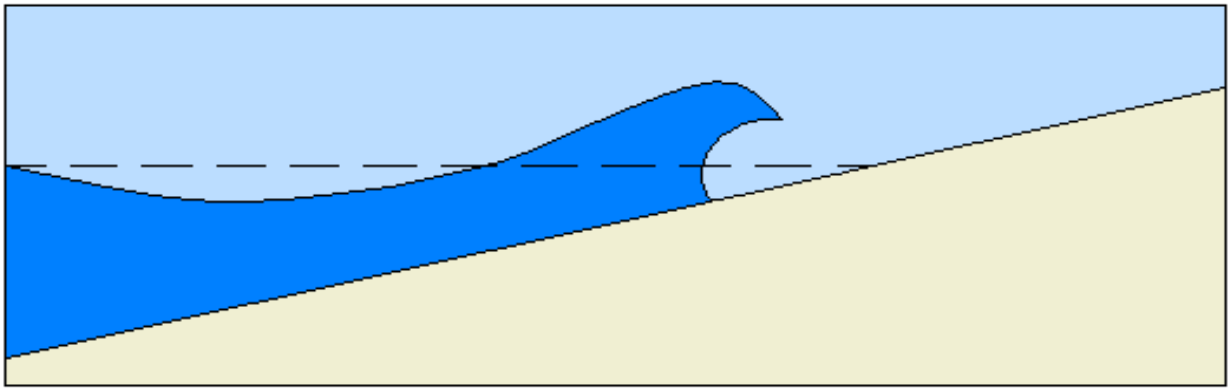

Figure 11: Plunging breaking wave

2.2.3. Surging breaking waves

Surging breakers occur on very steep beaches, often called reflective beaches, Figure 12. The wave surge up and down the beach and makes little or no breaking. $\xi_0 > 3{,}3$ according to Battjes (1974).

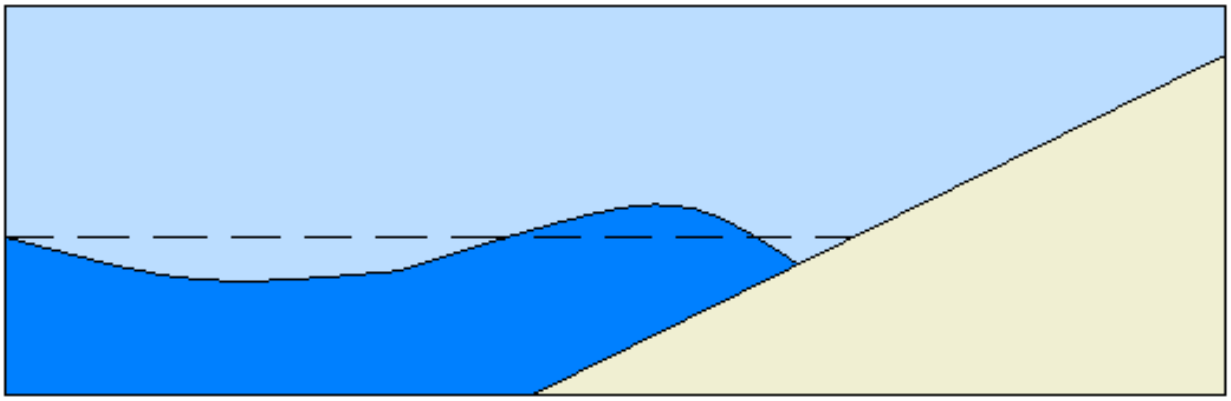

Figure 12: Surging breaking wave

2.2.4. Collapsing breaking waves

Collapsing breakers occur on steep beaches, also often called reflective beaches, Figure 13. These waves may be found on steep beaches made up of coarse material.

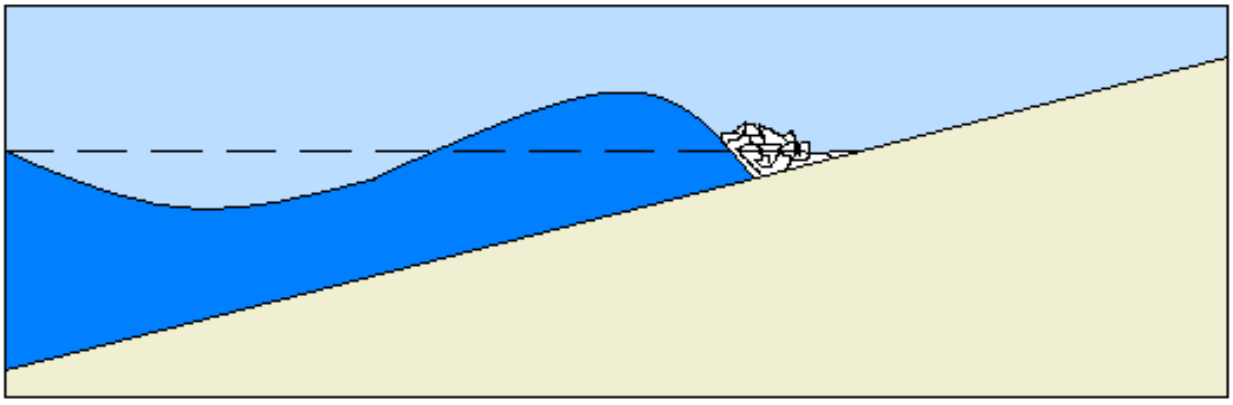

Figure 13: Collapsing breaking wave

2.2.5. Breaker index criterion

The breaker criterion *(H_b/L_b)* defines where and how the wave breaks. The breaker index criterion *(H_b/d_b)* is synonymous with the breaker criterion, but is easier to use in many calculations.

There are developed different equations for the breaker index criterion. It is common to use the Solitary Wave Theory criterion (8), (McCowan, 1894); (Munk, 1949):

$$\frac{H_b}{d_b} = 0.78 \tag{8}$$

The Solitary Wave Theory criterion defines wave breaking when the depth of water at breaking, d_b, limits the wave breaking wave height, H_b. (Kamphuis, 2000)

2.3. Scour

Scour is also a problem for truss support structures in shallow water at sandy sea beds. There are two types of scour that can occur, see Figure 14:

- Local scour:
  Scour around each element.
- Global scour:
  Scour around the "envelope" of elements.

Global scour is most unfortunate for the truss support structure, and is a result of the interaction of the flow between the individual elements. (Holmedal, 2009)

Figure 14: Global and local scour (Holmedal, 2009)

Scour would in reality be a big problem for truss support structures in shallow water, where global scour is most unfortunate. It is usual to design the structure for a larger water depth to account for the developing scour. This may be cheaper than investing in scour protection for this type of structure.

3. WAVE SLAMMING FORCES ON VERTICAL CYLINDERS

Several researches have been investigating wave slamming forces on single vertical and inclined piles on a flat or uniformly sloping seabed, e.g. Goda, et al. (1966), Swaragi and Nochino (1984), Tanimoto, et al. (1986), Wienke and Oumeraci (2005) and Arntsen, et al. (2011).

3.1. Morison's equation

The Morison equation (Morison, et al. 1950) is a good approximation used to calculate the forces acting on a slender vertical pile when the pile is hit by non-breaking waves. This equation is used in investigations of slender cylinders since 1950. The total force is a sum of the drag force, F_D, and the inertia force, F_M. Morison's equation:

$$dF = dF_D + dF_M = \frac{1}{2}\rho_w C_D D|u|udz + \rho_w \frac{\pi D^2}{4} C_M \frac{du}{dt} dz \tag{9}$$

ρ_w is the water density, C_d is the drag coefficient, C_M is the inertia coefficient, D is the diameter of the cylinder, u is the water particle velocity, du/dt is the water particle acceleration, z is the upward vertical direction and t is the time.

The drag coefficient, C_D, and the inertia coefficient, C_M, depends on Reynolds number, *Re* (10), and the Keulegan-Carpenter number, *KC* (11).

$$\mathrm{Re} = \frac{uD}{\nu} \tag{10}$$

ν is the kinematic viscosity of the fluid.

$$KC = \frac{uT}{D} \tag{11}$$

T is the wave period.

3.2. The slamming force

High slamming forces on a slender structure may be induced by breaking waves, especially plunging breakers. The high duration of these slamming forces is extremely short, which makes it difficult to analyze the breaking wave forces. In structural or stability analysis, the slamming force, F_S, must be included in Morison's equation due to the short duration, as an additional part of the wave force. Total force:

$$F = F_D + F_M + F_S \tag{12}$$

A model for the slamming force can be found by considering the breaking wave as a vertical wall of water that hits the cylinder. The method of von Karman (von Karman, 1929) is based on this assumption, and is usually used to calculate the impact force on slender cylinders, see Figure 15. The cylinder is approximated by a flat plate with a width equal to the width of the immersed part of the cylinder at each instant of the impact. The force on the plate can be calculated by considering the potential flow below the plate and integrating the pressures calculated by the Bernoulli equation. The line force is:

$$f_l(t) = \rho_w R C^2 C_S \tag{13}$$

$$C_S = \pi(1 - \frac{C}{R}t) \tag{14}$$

C_S is the slamming factor, C is the wave celerity, R is the radius of the cylinder and t is time.

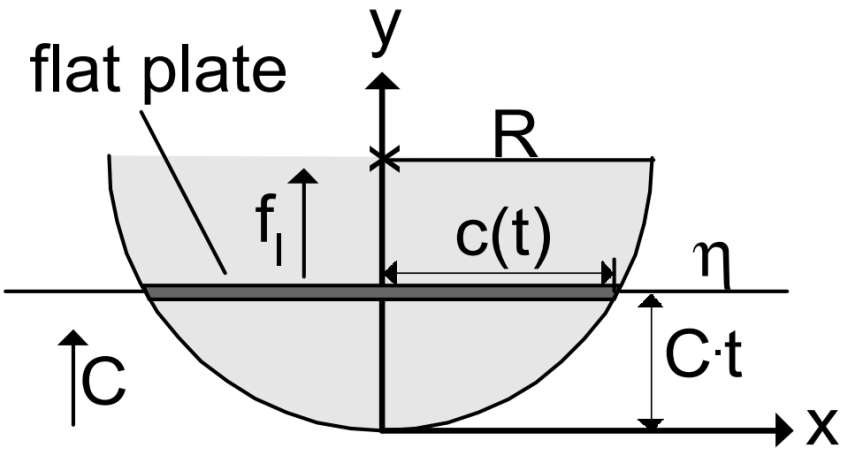

Figure 15: Von Karman's model

Von Karman's method is related to a cylinder of infinite length. Applying this method for breaking waves, the force must be integrated over the height of the impact area as shown in Figure 16.

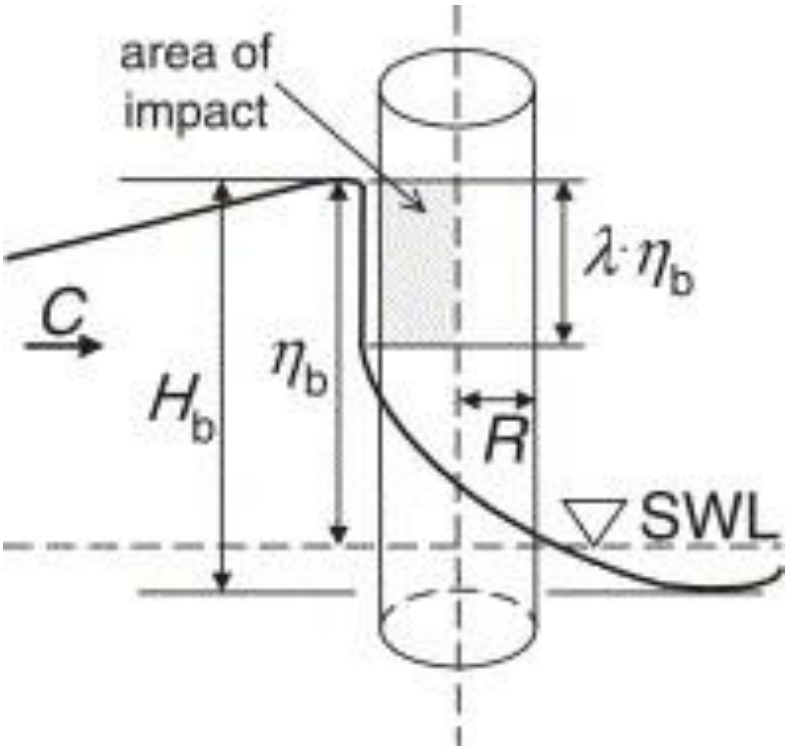

Figure 16: Definition sketch (Wienke and Oumeraci, 2005)

Goda, et al. (1966) proposed that the height of the impact area should be equal to the curling factor, λ, multiplied with the maximum elevation of the wave at breaking, η_b. The total impact force is then:

$$F_S(t) = \lambda \eta_b \pi \rho R C^2 (1 - \frac{C}{R} t) \tag{15}$$

C is the wave celerity, R is the radius of the cylinder, η_b is the maximum elevation of the breaking wave, λ is the curling factor, ρ is the density of water and t is time. See Figure 16.

The most interesting point is when the slamming force is maximum, i.e. t = 0. The slamming force is commonly written as:

$$F_S = \frac{1}{2} \rho_w C_S D C_b^2 \lambda \eta_b \tag{16}$$

C_s is the slamming factor, $C_b = C$ is the wave celerity, λ is the curling factor and η_b is the maximum surface elevation of the wave at breaking.

From Equation (14) and (15) one can see that the value π as Goda, et al. (1966) used is changed to C_S.

Equation (16) is, as mentioned, for the maximum slamming force. Wagner introduced a model for the so-called pile-up effect, see Figure 17 (Wagner, 1932). This also accounts for the flow beside the flat plate. The "immersion" of the pile occurs earlier due to this effect, which leads to decreased duration of the impact and higher line force. According to Wagner's theory (1932), the maximum line force is:

$$f_l = 2\pi\rho_w R C_b^2 \tag{17}$$

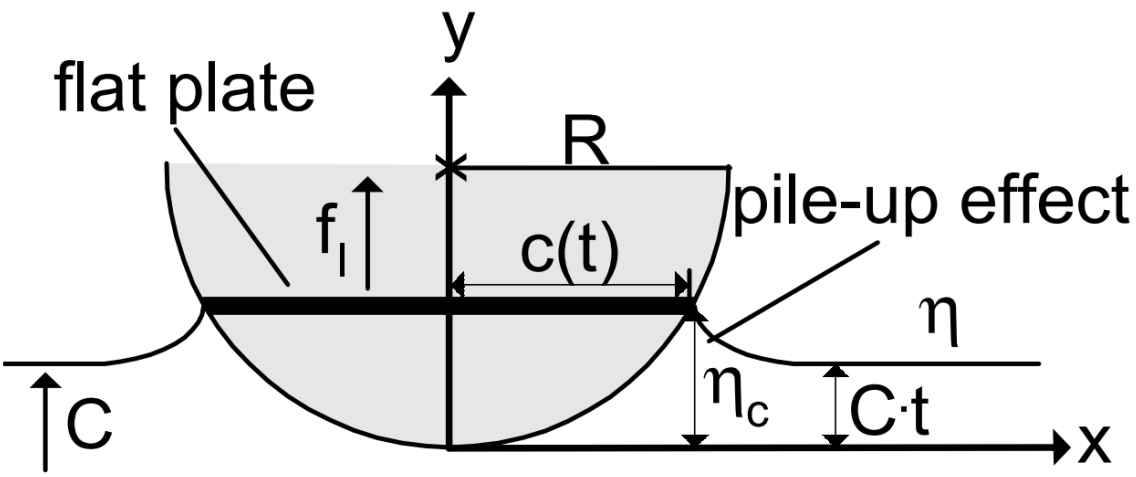

Figure 17: Wagner's model

As you can see from Equation (13), (14) and (17), Wagner's maximum line force is twice that of von Karman's maximum line force. The maximum line force is often described as a function of the slamming coefficient:

$$f_l = C_S \rho_w R C_b^2 \tag{18}$$

3.3. Slamming and curling factor

The slamming factor, C_S, is the most investigated factor related to breaking waves, along with the curling factor, λ, and the duration of impact, τ. Different values have been obtained by different researchers. The slamming factor was set to $C_S = \pi$ by Goda, et al. (1966), and this is the most frequently used value.

Based on Wagner's theory, Wienke and Oumeraci (2005) investigated wave slamming forces on cylinders in a large scale model set-up with $C_S = 2\pi$, and obtained values of the curling factor, λ, as shown in Figure 18 for different inclinations of the pile. The maximum value for zero inclination is $\lambda = 0.46$.

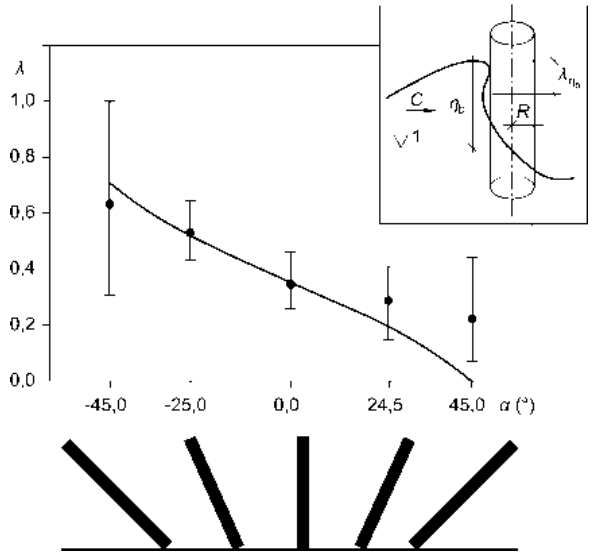

Figure 18: Curling factor vs. pile inclination (Wienke and Oumeraci, 2005)

Ros Collados (2011) investigated specially the slamming factor, C_S, on a vertical cylinder in his Master's thesis. The results of his testing led to a $C_S = 4.3$ and a triangular vertical force distribution.

Aune (2011) also investigated the slamming factor, C_S, in his Master's thesis, but this was on a truss support structure as shown in Figure 21 on page 21, with a result of $C_S = 4.77$.

3.4. The duration of impact

Another important factor is the duration of impact, τ. This factor describes the time of impact duration, and is also varying by the results of different researchers.

Table 1: Duration of impact

Study	Duration of impact factor, τ
Wienke and Oumeraci (2005)	$\frac{13}{64}\frac{D}{C_b}$
Tanimoto et al. (1986)	$\frac{1}{4}\frac{D}{C_b} to \frac{1}{2}\frac{D}{C_b}$
Goda (1966)	$\frac{1}{2}\frac{D}{C_b}$
von Karmen (1929)	$\frac{D}{2u}$

D is the diameter of the pile, C_b is the breaking wave celerity and u is the water particle velocity.

The duration of impact factor was introduced by von Karmen. The researchers listed in Table 1 adopted τ as the impact time duration, but assumed that the water particle velocity changed to the breaking wave celerity.

The time history of the impact line force for several researchers is plotted in Figure 19.

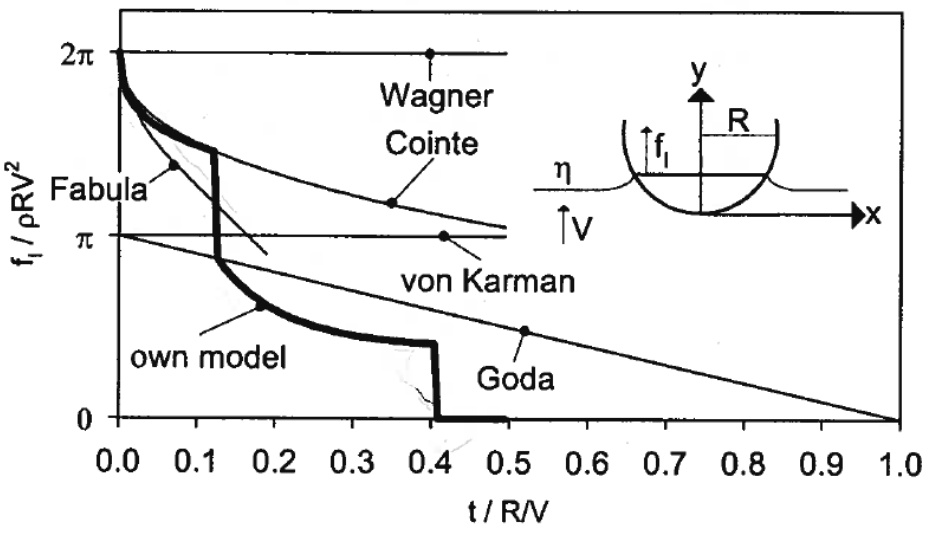

Figure 19: Time history of the line force, different theories (Wienke and Oumeraci, 2005)

3.5. International Standards

ISO 21650 (2007) is an International Standard which deals with the actions from waves and currents on structures in the coastal zone, and is the first of its kind. This standard sums up the different theories. An agreement of all the coefficients values is not present in this standard, but the slamming factor is assumed to be $C_S = \pi$ (von Karmen theory) and the curling factor $\lambda = 0.5$ (Goda, et al. 1966).

For vertical and inclined cylinders, total slamming force is obtained as (ISO 21650, 2007):

$$F_S = 0,5\rho_w C_S D C_b^2 \lambda \eta_b \tag{19}$$

C_s is the slamming factor, C_b is the wave celerity, λ is the curling factor and η_b is the maximum surface elevation of the wave at breaking, ρ_w is the mass density of water, D is the member diameter.

ISO 21650 (2007) does not specify a formula to calculate the duration of impact, it just sums up the different studies.

The International Electrotechnical Commission (IEC) has published an International Standard for wind turbines, Wind turbines - Part 3: Design requirements for offshore wind turbines (IEC 61400-3, 2009). IEC is a worldwide organization for standardization comprising all national electrotechnical committees. This standard assumes a slamming factor, C_S, between 3 and 7, and the curling factor $\lambda \approx 0.5$.

Slamming force per unit length (IEC 61400-3, 2009):

$$F_S = \frac{1}{2} C_S \rho_w D U^2 \tag{20}$$

C_s is the slam coefficient, ρ_w is the density of water, D is the member diameter.

The velocity U is not simply the water particle velocity for slam in waves. U can be determined from a wave theory by resolving the particle velocities at the point of impact, which is defined as the wave celerity, C_b.

IEC 61400-3 (2009) defines the total duration of impact for a vertical cylinder as:

$$T' = \frac{13R}{32V\cos\gamma} = \frac{13\frac{D}{2}}{32V} = \frac{13\frac{D}{2}}{32C_b} = \frac{13D}{64C_b} \tag{21}$$

R is the member radius, D is the member diameter, $V = C_b$ is the wave celerity and γ is the angle between motion of the mass of water and the perpendicular to the cylinders axis ($\cos\gamma=1$).

The duration of impact is based on the results of Wienke and Omeraci (2005).

The slamming force is, as you can see from above, defined in the same way in both standards. The total force from breaking waves is as defined in section 3.2. Figure 16 on page 11 is used as a reference scetch to define the impact area in both standards.

3.6. Study summary

Different researchers of breaking waves have agreed on the formulas used to calculate the slamming force, but have different theories on the values of the slamming and curling factor, see Table 2. This causes uncertainties in the dimension of structures exposed to these kinds of forces.

The design standard for offshore wind turbines, IEC 61400-3 (2009), have clearer guidelines than the first standard made of this subject, ISO 21650 (2007), but some assumptions still need to be done here as well.

The standards are based on previous research.

Table 2: Different studies of forces on cylinders

Study	Slamming factor, C_S	Curling factor, λ_{max}	Vertical force distribution
Wienke and Oumeraci (2005)	2π	0.46	Uniform
Goda (1966)	π	0.40	Uniform
Swaragi and Nochino (1986)	π	0.90	Triangular
Tanimoto et al. (1986)	π	0.66	Triangular
Ros (2011)	4.3	0.67	Triangular
Aune (2011) Truss structure	4.77	0.50	Uniform
ISO 21650 (2007)	π	0.50	Uniform
IEC 61400-3 (2009)	3-7	0.50	Uniform

3.7. Air entrainment measurements and scale effects in breaking waves

Breaking waves at sea is a complex process. The presence of air bubbles entrained by breaking waves has been shown to have a strong influence on wave impact forces on coastal structures.

Blenkinsopp and Chaplin (2011) wrote a paper following the work of Blenkinsopp and Chaplin (2007). The paper describes detailed measurements of the time-varying distribution of void fractions generated by breaking waves in freshwater, artificial seawater and natural seawater under laboratory conditions. Flow visualization of the entrainment process is also described.

Their experiments were carried out in a 17m long and 0,42m wide wave flume, with a water depth 0,7m.

The result of the experiments of Blenkinsopp and Chaplin (2011) suggest that there are only minor differences between the process of air entrainment by breaking waves in freshwater, artificial seawater and seawater. Flow visualization also suggested comparable bubble sizes in all water types. The exception was an additional population of very small bubbles which remained at the end of each wave period in the two seawater cases, and was augmented by each subsequent breaking wave. These small bubbles did not make a significant contribution to the total volume of entrained air.

Scale effects on the evolution of the bubble plume evolution after entrainment are very important. Blenkinsopp and Chaplin (2011) analyzed the issue by applying small-scale measurements of air entrainment to field conditions. This suggested that the total volume of air entrained would scale geometrically, though pressure effects will increase with scale, but the bubble sizes would remain approximately the same at all scales. It must therefore be large differences in the temporal evolution of bubble plumes generated at model and full scale. Their results demonstrate that the entrained bubble plume in breaking waves disperses much more slowly in large-scale than in small-scale. This will have the effect of significantly increasing the compressibility of the air-water mixture and will reduce the propagation speed of pressure waves.

Since the bubble sizes of entrained air are the same at all scales, small-scale model testing may have a cushion effect. The entrained air will cushion the pressure on the structure in small-scale.

4. TEST ANALYSIS METHOD

This chapter gives an illustration on how the testing on the 1:50 scale model is carried out. The testing has taken place at Valgrinda, NTNU. A theoretical description on how to analyze measured response is also given.

4.1. Wave channel

The wave channel is 33m long and 1m wide. The truss support structure is placed 16.95m from the wave generator, see Figure 20. The bottom slope in front of the truss structure is 1:10. This slope is necessary to make the waves break. The wave channel is then divided into one part with “deep” water and one with shallow water. The deep water, which in reality is intermediate water, have a constant water depth d = 0.895m. The water depth is 0.333m at the middle of the structure. The shallow water starts 11.2m after the wave generator. Wave absorbers, which are made of perforated steel plates, are placed in the end of the wave channel to prevent disturbance of reflecting waves.

The wave generator is hydraulic. The waves are generated by a plate that moves back and forth, a piston-type wave generator. The frequency and the eccentricity is the input.

The testing has been run with both regular and irregular waves.

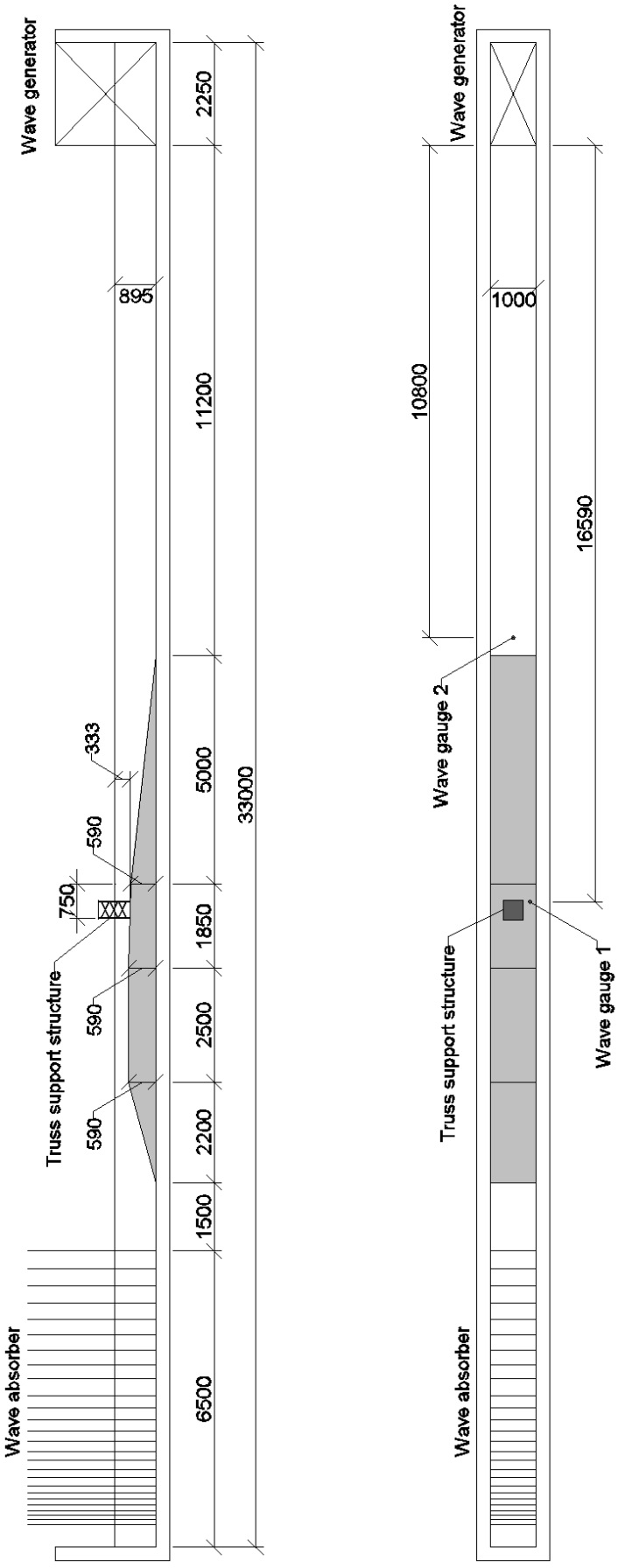

Figure 20: Wave flume [mm]

4.2. Truss support structure

The truss support structure is a model based on a structure that Reinertsen AS has designed for the Thornton Bank. The slamming forces from plunging breaking waves govern the design of this structure. The model (Figure 21) is made of PVC plastic pipes in a scale of 1:50. The vertical pipes have a diameter 16mm and the crossing pipes have a diameter 12mm. The thickness is 1mm. Total height is 0.693m and total width is 0.416m. The four sides are identical with three crossings. The four vertical pipes are stiffened with steel pipes inside and fixed to a 10mm thick plate on top of the structure.

There have also been made a one-sided model; the structure is split in different parts to measure the wave forces on the individual parts. The one-sided model is made of aluminum. The plan of this thesis work was to perform measurements on this model as well as the plastic model, but this part was eliminated due to lack of time.

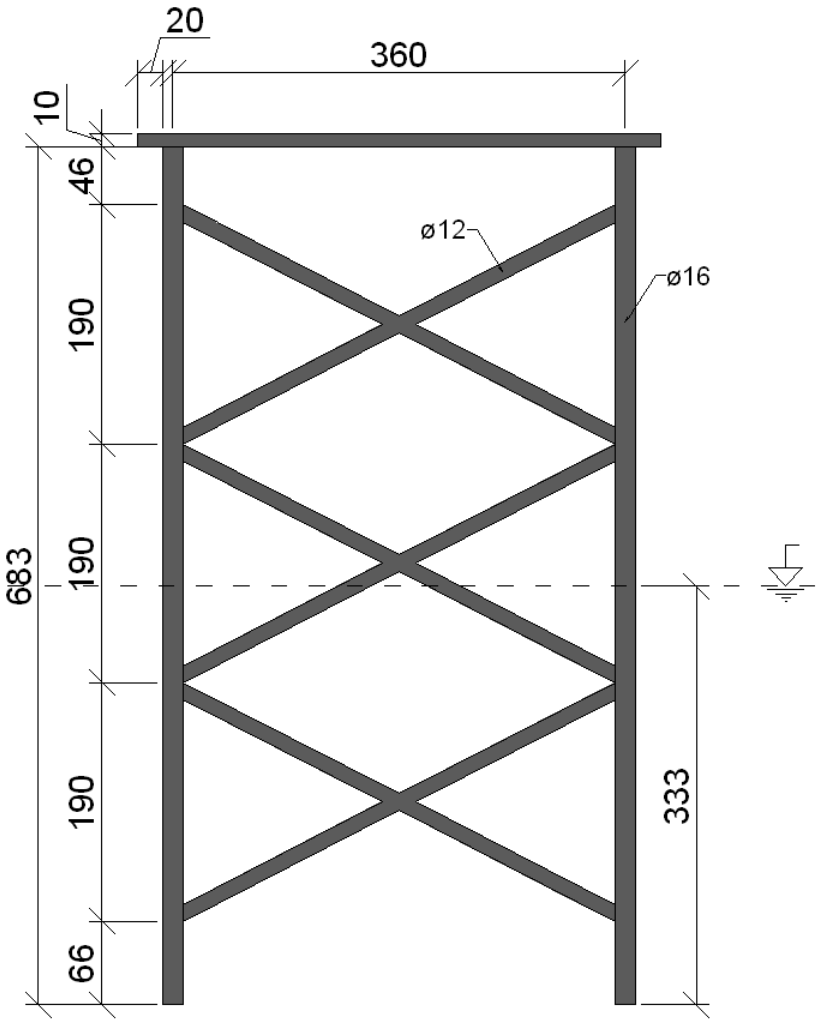

Figure 21: Truss support structure [mm]

4.3. Wave gauge

It is placed two wave gauges in the wave channel. One is placed by the truss support structure, 16.95m from the wave generator, and one in the deep water area, 10.8m from the wave generator (Figure 20).

The wave gauge is made of two plastic pipes that have electrical tension between them, see Figure 22 and 23.

The wave gauges must be calibrated before tests are run. The calibration is done by lifting and sinking the gauge ±10cm while the channel is connected to a voltmeter. When the gauge is lifted 10cm, the voltmeter is adjusted to 5V, and -5V when the gauge is sunk 10cm. This is done to get more accurate measurements.

The quality of the measured wave height by the use of the wave gauges is uncertain when the wave breaks. There are many air gaps in breaking waves, and the wave gauge is therefore possibly measuring a lower breaking wave height then what really occurs. The results are used as they are.

Figure 22: Wave gauge

Figure 23: Wave gauge, close-up

4.4. Force transducers

The force transducers (Figure 24) are designed for measuring static and dynamic tensile and/or compressive forces within the load limits 500N to 2000N, see Figure 25. They provide highly accurate static and dynamic force measurements. The force transducers only measure horizontal loads.

Figure 24: Force transducer (HBM)

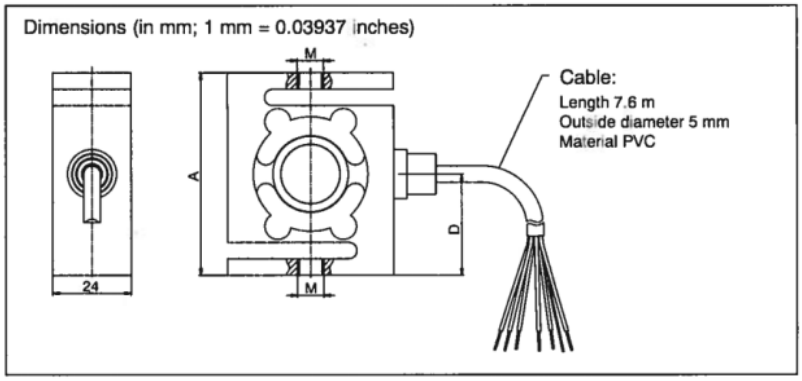

Nominal (rated) force	A	B	C	D	M
500 N	62	50.8	25.4	31	M8
1 kN	62	50.8	25.4	31	M8
2 kN	87.3	57.2	28.6	43.7	M12

Figure 25: Dimensions of force transducer (HBM)

The truss support structure is equipped with four force transducers, two at top of the structure and two at the bottom (Figure 26). It is therefore possible to measure forces at each transducer, the forces on top and bottom of the structure and the total force.

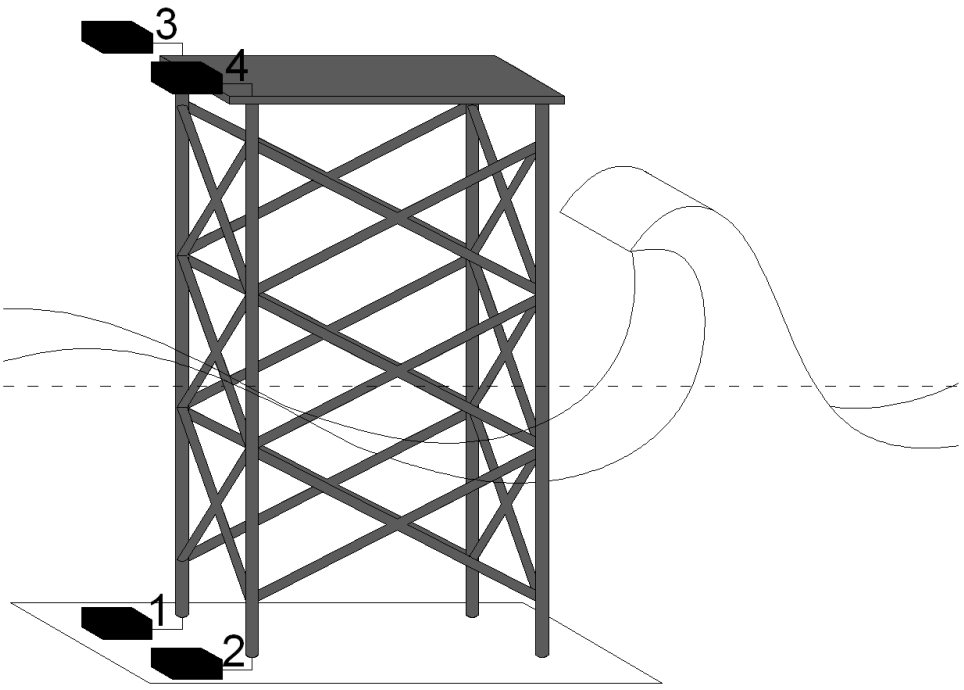

Figure 26: Structure with force transducers

Figure 27: Force transducer

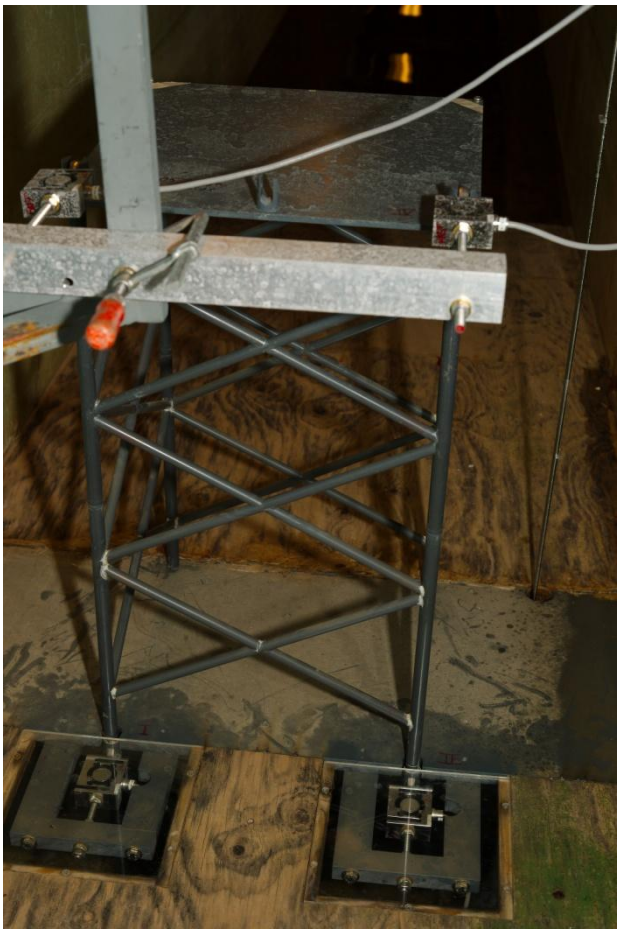

Figure 28: Structure with force transducers

Figure 27 and 28 are pictures taken in the laboratory of the force transducers and their placement on the structure.

4.5. Eigenfrequency

The eigenfrequency of the structure is measured by the use of an impulse hammer, see Figure 29 and 30. This hammer is connected to the same spectrum analyzer as the force transducers and the wave gauges. The force transducers measure a force in Volts. The impulse hammer measures an impulse in Volts. This force and impulse must be converted into Newton by setting the range in the spectrum analyzer from 0V to 1V and 0N to 468,2339N, as shown in Equation (22).

Calibration:
1mV=9,5mV/LbF
1LbF=4,44822N

$$1V = 1000mV \cdot \frac{1}{9{,}5\,{}^{mV}\!/_{LbF}} \cdot 4{,}44822\,{}^{N}\!/_{LbF} = 468{,}2339N \tag{22}$$

Figure 29: Impulse hammer

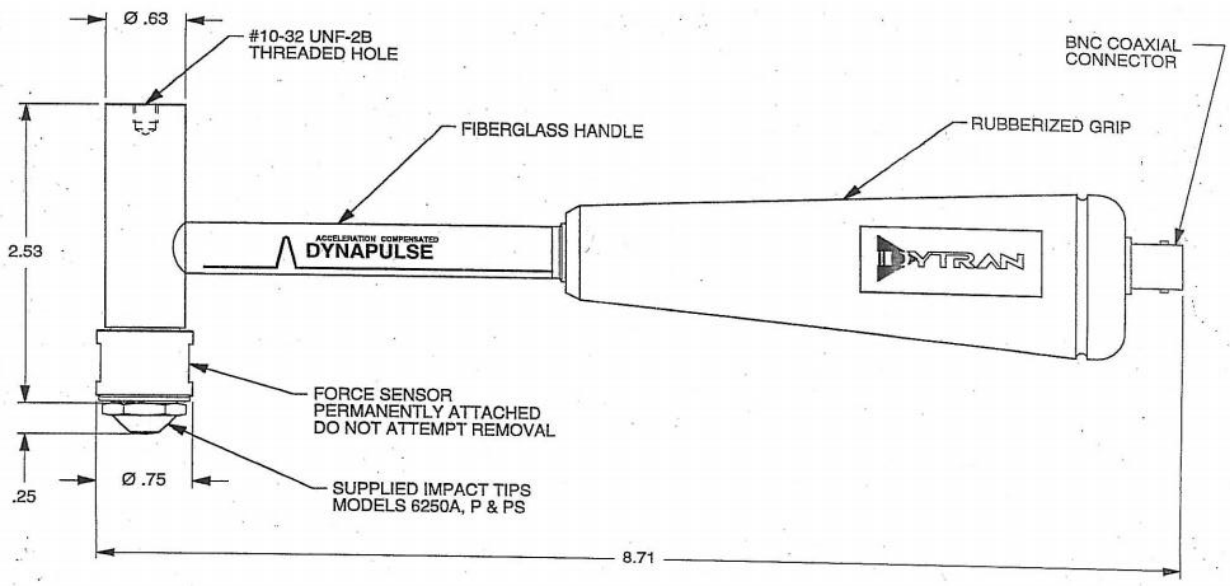

Figure 30: Impulse hammer (Dytran Instruments)

4.6. Experimental set-up

The force transducers, wave gauges and the impulse hammer is connected to a spectrum analyzer. The spectrum analyzer is connected to a computer that has installed the program CatmanEasy, which analyses the results. Figure 31 shows a typical system interconnects for measuring systems. The bin-files saved in CatmanEasy is exported to asc-files, and then converted in the program CommandPrompt into csv-files. This is done because the force transducers and the impulse hammer have different time series than the wave gauges, the wave gauges is logged with finer resolution. The CommandPrompt program interpolates these files, so that the force transducers and the impulse hammer have the same time series as the wave gauges. This is very important because the program Matlab need same length of time series to analyze the files.

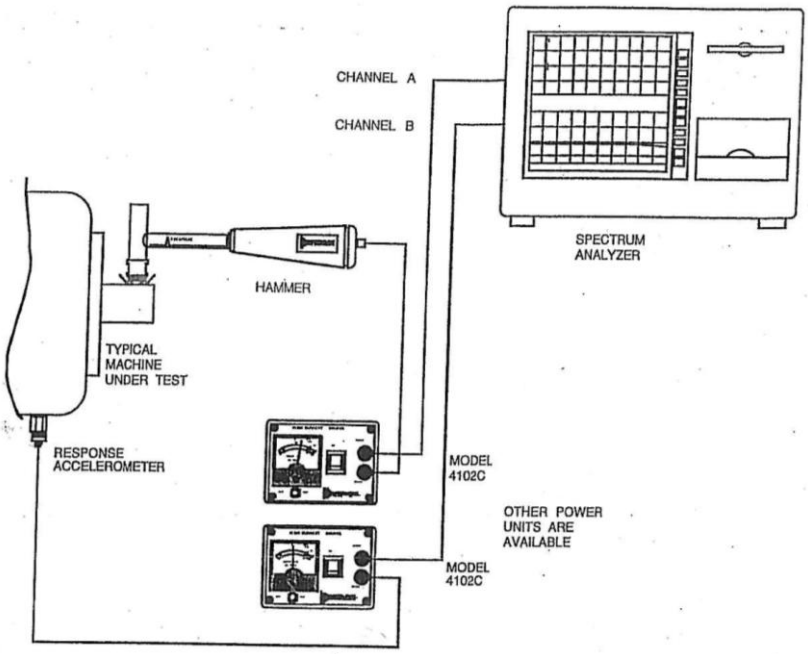

Figure 31: Typical system interconnects for measuring systems (Dytran Instruments)

4.6.1. Test procedure

It has been carried out a large number of tests with both regular and irregular waves on the truss support structure. The testing was done over a long period of time, with same procedure each day.

- Turn on the wave generator.
- Accurately adjust the water level. The water depth in front of the structure must always be 33,3cm during testing.
- Calibrate the wave gauges.
- Calibrate the analogue recorder.

4.7. Wave characteristics

The tests where run with both regular and irregular waves, with a sampling frequency 19200Hz. This means that the data where sampled at a rate of 19200 per second per recording channel. The run time of the regular waves where 10sec, and 120sec for the irregular waves.

Notation of data:

- Regular waves:
  The test series is named as ex. Mf045e270_1
  M – Miriam
  f045 – frequency f = 0,45Hz
  e270 – eccentricity e = 2,70
  _1 – first test run of this particular wave

- Irregular waves:
  The test series is named as ex. MTp185e330_1
  M – Miriam
  Tp – peak period T_p = 1,85s
  e330 – eccentricity e = 3,30
  _1 – first test run of this particular wave

- Impulse hammer:
  The test series is named as ex. Mhammer5_1
  M – Miriam
  hammer5 – pluck with impulse hammer in point 5
  _1 – first pluck in this point on the structure (see Figure 37)

4.8. Executed experiments

The table below show the tests run of regular and irregular waves with four different frequencies and several different eccentricities on the plastic truss model.

Table 3: Tests run of regular and irregular waves

Regular waves					Irregular waves				
e	f [Hz] (T [s])				e	f [Hz] (T [s])			
	0,45Hz (2,22s)	0,48Hz (2,08s)	0,51Hz (1,96s)	0,54Hz (1,85s)		0,45Hz (2,22s)	0,48Hz (2,08s)	0,51Hz (1,96s)	0,54Hz (1,85s)
120	x	x	x	x	120				x
130				x	170				x
150				x	200				x
170	x	x	x	x	230				x
180				x	260				x
185				x	280				x
190	x	x	x	x	290			x	x
195				x	300		x	x	x
200	x	x	x	x	310		x	x	x
205				x	320		x	x	x
210	x	x	x	x	330		x	x	x
215		x			340		x	x	x
220	x	x	x	x	350		x	x	x
225		x			360		x	x	x
230	x	x	x	x	370		x	x	x
235		x			380		x	x	x
240	x	x	x	x	390	x	x	x	x
245		x	x		400	x	x	x	
250	x	x	x	x	410	x	x	x	
255		x	x	x	420	x	x	x	
260	x	x	x	x	430	x	x	x	
265			x	x	440	x	x	x	
270	x	x	x	x	450	x			
275				x	460	x			
280	x	x	x	x	470	x			
290	x	x		x	480	x			
300		x			490	x			
310	x	x			500	x			
315		x							
320	x	x							
325		x							
330	x	x							
335	x								
340	x	x							
345	x								
350	x	x							
360	x								

4.9. Analysis of response

4.9.1. Single degree of freedom system

The forces acting the truss structure can be found by assuming that the structure is a single degree of freedom system (SDOF). Figure 32 shows a principle sketch of this kind of system. (Næss, 2007)

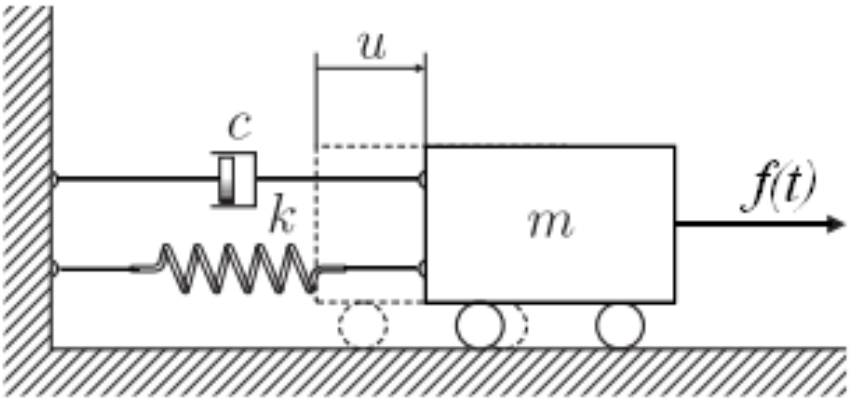

Figure 32: Principle sketch of a SDOF oscillator with linear damping (Næss, 2007)

m is the mass, *k* is the stiffness, *c* is the damping constant, *u* is the displacement and *f(t)* is the applied load. Based on Newton's second low, the dynamic equilibrium is then:

$$m\ddot{u} + c\dot{u} + ku = f(t) \tag{23}$$

The response, *u(t)*, read out from the force response diagram at testing can then be put up like this:

$$u(t) = ku = f(t) - (m\ddot{u} + c\dot{u}) \tag{24}$$

4.9.2. Eigenfrequency and damping

An eigenfrequency**,** or natural frequency, appears on the truss support structure when the structure is hit by the slamming force. If the slamming force hits the upper part of the structure, the structure can be assumed to act like a reverse pendulum and as a SDOF system. The eigenfrequency can be measured by testing.

The natural frequency of a cantilever pile can be calculated by:

$$\omega_{e,1} = 3.52\sqrt{\frac{EI}{mL^4}} \tag{25}$$

$$\omega_{e,2} = 22.03\sqrt{\frac{EI}{mL^4}} \tag{26}$$

$$\omega_{e,3} = 61.70\sqrt{\frac{EI}{mL^4}} \tag{27}$$

E is the modulus of elasticity, *I* is the area moment of inertia, *m* is the mass per unit length and *L* is the spanwise length.

The damping constant, *c*, can then be calculated by:

$$c = 2\pi\omega_e\xi \tag{28}$$

ξ is the damping ratio.

4.9.3. Suddenly applied constant force of limited duration

The limited period of time t_* of the duration of the breaking wave will impact how the system is analyzed. The time history will be given as $f(t) = 0$ for $t < 0$ and $t > t_*$, and $f(t) = f_0$=constant for $0 \leq t \leq t_*$, with maximum response u_{max}.

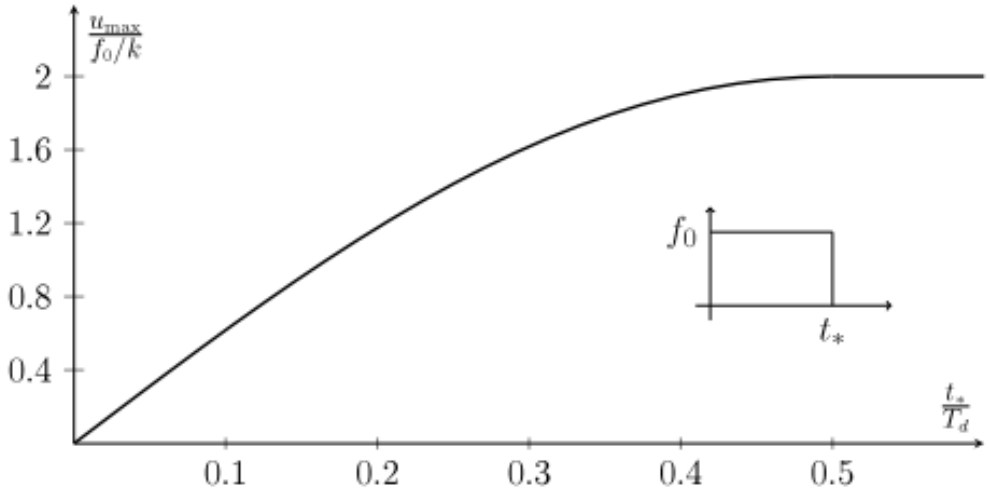

Figure 33: Maximum response to a constant impulse force of limited duration (Næss, 2007)

Figure 33 shows the response vs. $t_* = T_d/2$, where T_d is the natural period of oscillation. This is the case of a suddenly applied force of finite duration.

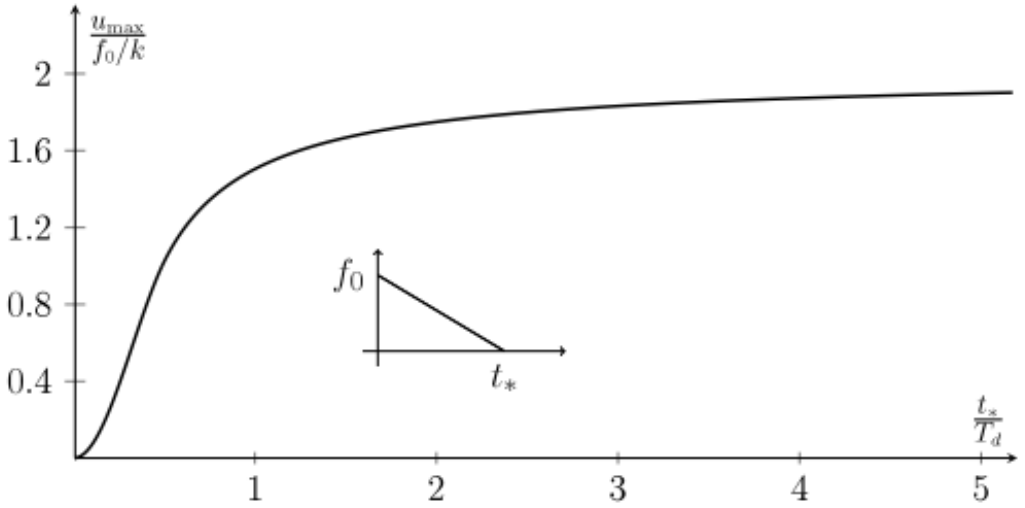

Figure 34: Maximum response to a triangular impulse force time history (Næss, 2007)

Figure 34 shows the result with a suddenly applied force that decreases linearly toward zero. This force time history will always lead to lower maximum response than the corresponding rectangular force time history, because the total impulse is smaller.

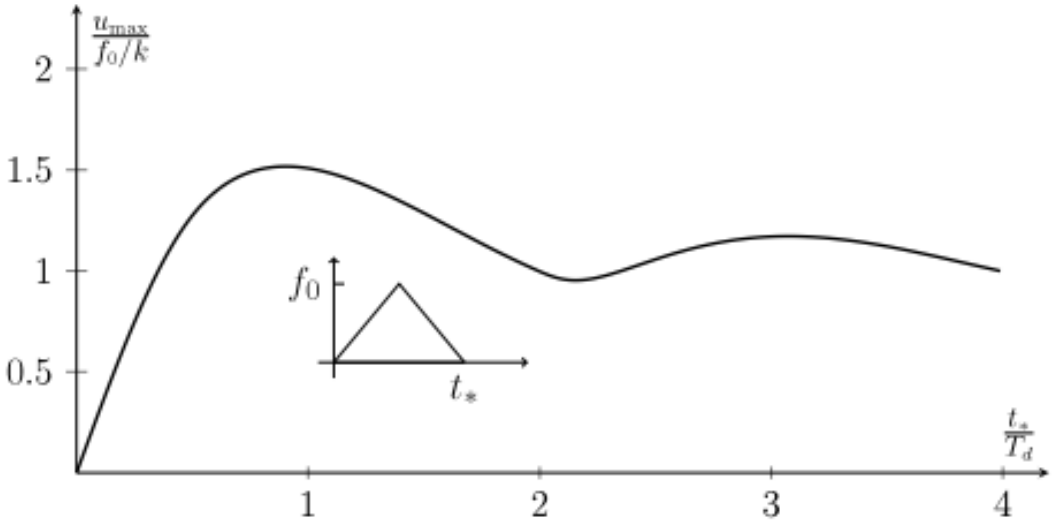

Figure 35: Maximum response to a sym. triangular impulse force time history (Næss, 2007)

Figure 35 shows the maximum response when the force time history looks like a saw-tooth. The maximum response is in this case largest when the duration of the applied force is equal to the natural period.

Figure 33, 34 and 35 shows a characteristic feature of the maximum response to load time histories of limited duration. An upper bound of the maximum response is:

$$u_{\max} = \frac{I'}{\omega_d m} \tag{29}$$

I' is the impulse load, ω_d is the damped frequency and *m* is the mass.

Hence, when the duration is short, it is not the size of the load or its time history that is important, but the impulse. (Næss, 2007)

4.9.4. The Duhamel integral

The response of a pile can be calculated by using the Duhamel integral (Næss, 2007). Assuming a general time history, *f(t)*, on the right side of Equation (23), the effect of *f(t)* on the vibration system at a point in time $t = \tau$ can be considered as the effect of an infinitesimal impulse load:

$$dI'(\tau) = f(\tau)d\tau \tag{30}$$

The corresponding response, see Figure 36, at time $t > \tau$ is given by:

$$du(t;\tau) = f(\tau)d\tau h(t-\tau) \tag{31}$$

h(t) is the impulse response function.

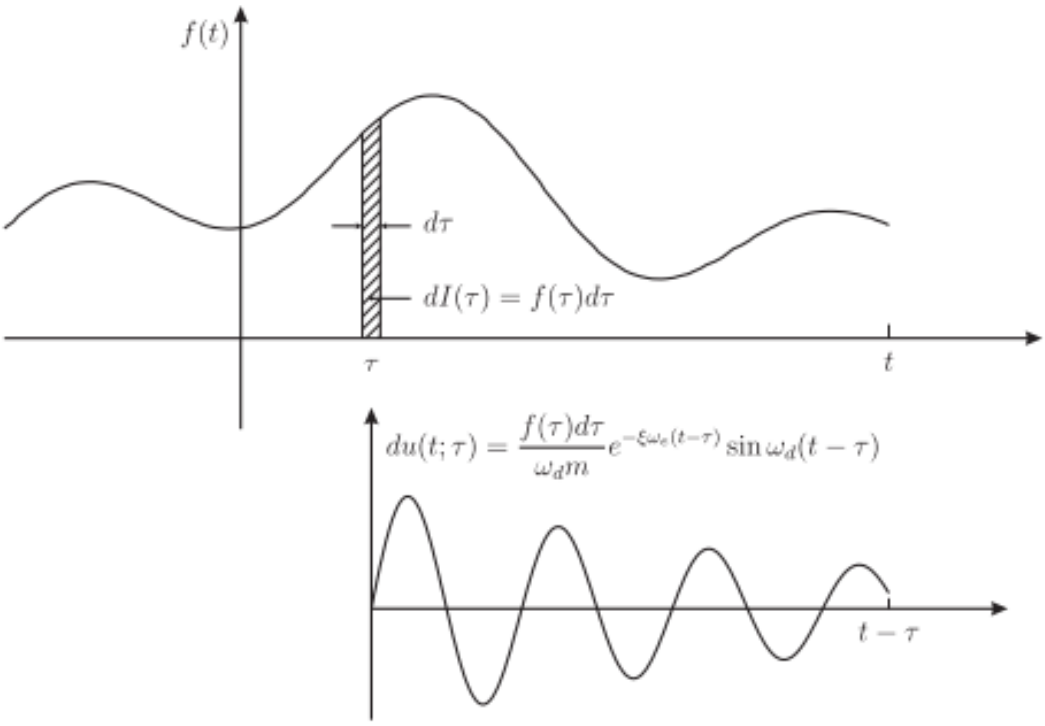

Figure 36: The response from the impulse load (Næss, 2007)

Wienke and Oumeraci (2005) and Arntsen, et al. (2011) used the Duhamel integral approach when analyzing their response force data on single piles.

The Duhamel integral cannot easily be used for analyzing the truss support structure. This is because a truss structure is too complicated. The wave is first slamming in the front of the structure, and then on the back side of the structure. (See later)

4.10. "New" method of analyzing wave slamming forces

The regular waves are analyzed by following a procedure described by Määtänen (1979), as described by Alf Tørum in APPENDIX D. Details of the filtering of the force response to obtain the wave slamming response are also shown in APPENDIX D.

The measured response force, *f(t)*, can be expanded into a Fourier integral. In case of forced vibration it will be:

$$f(t) = \frac{1}{2\pi} \int_{-\infty}^{\infty} H(\omega) S_F(\omega) e^{i\omega t} d\omega \tag{32}$$

$H(\omega)$ is the frequency response function (FRF) and $S_F(\omega)$ is the linear spectrum of the applied force.

An impulse hammer is used to find the FRF. The structure is hit by the impulse hammer several places, in the approximate location of the wave slamming resultant load. It is found from the tests run that this is approximately 17cm above still water level. The impulse force is measured by a force transducer in the tip of the hammer. The frequency response function, *H(ω)*, is obtained from the measured impulse force and the simultaneously measured response forces in the four force transducers on the structure.

The Fourier transform is the linear spectrum of the measured response force, *f(t)*:

$$H(\omega) S_F(\omega) = \int_{-\infty}^{\infty} f(t) e^{-i\omega t} d\omega \tag{33}$$

$S_F(\omega)$ can be solved from this, and the inverse Fourier transform gives the requested real wave slamming force:

$$F(t) = \frac{1}{2\pi} \int_{-\infty}^{\infty} \frac{S_F(\omega)}{H(\omega)} e^{i\omega t} d\omega \tag{34}$$

The transfer function, *H(ω)*, is a calibration factor. In our case it has been obtained by using the impulse hammer.

4.10.1. Frequency response function (FRF)

The FRF, *H(ω)*, is obtained by hitting the impulse hammer 7 different places on the structure, as shown in Figure 37. Point 1 to 6 is in the range where the plunging breaking wave usually hits the structure.

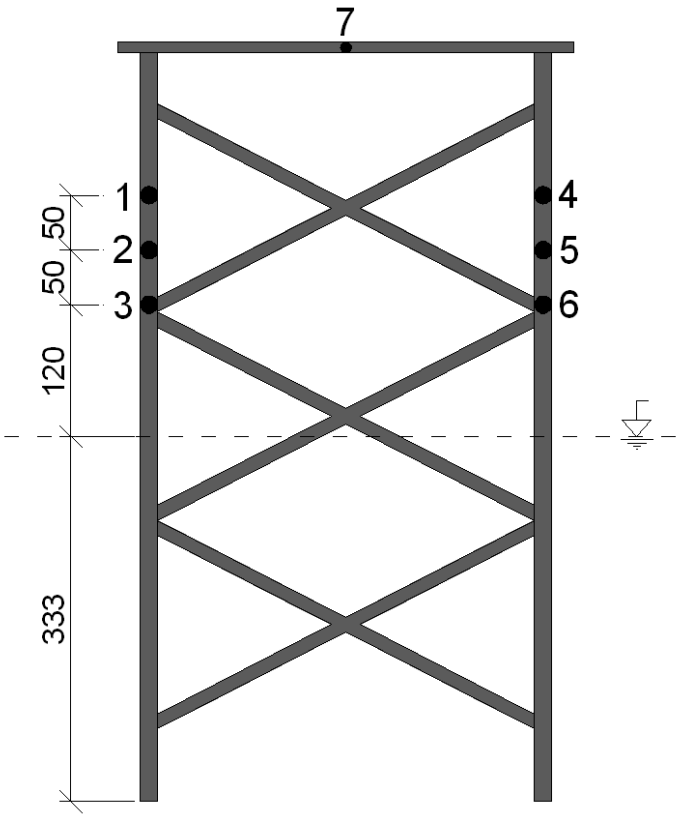

Figure 37: Places the impulse hammer is hit on the structure measures in [mm]

The structure represents a multiple degree of freedom system, but is for simplicity made into a single degree of freedom system. This is done by adding all the four force transducers into a total force response.

FRF:

$$H(\omega) = \frac{S_{Total,hammer}(\omega)}{S_{Hammer}(\omega)} \tag{35}$$

where

$$S_{Total,hammer}(\omega) = \int_{-\infty}^{\infty} f_{Total,hammer}(t) e^{-i\omega t} d\omega \tag{36}$$

and

$$S_{Hammer}(\omega) = \int_{-\infty}^{\infty} f_{Hammer}(t) e^{-i\omega t} d\omega \tag{37}$$

4.10.2. FRF applied to the wave slamming response forces

The described analysis is applied to obtain the wave slamming force for response force time series. This is a simplified analysis based on an assumption of a single degree of freedom system subjected to a total force. The response is a mixture of Morison forces and wave slamming forces. The wave slamming forces is supposed to be the high frequency part of the time trace, see APPENDIX D.

The inverse fast Fourier transform (IFFT) of $S(\omega)/H(\omega)$ has a high frequency component. This high frequency component has been filtered away by a low-pass filter, and we obtain a force time series that show the wave slamming force.

4.11. Analysis of irregular waves: Probability of plunging breakers

Reedijk, Muttray and Bergman wrote in 2009 a paper concerning risk awareness for design approach for breakwater armouring (Reedijk, et al. 2009). The probability of wave breaking on the foreshore is investigated in this paper. The method can also be used to find the probability of plunging breakers on the truss structure for irregular waves. The occurrence of plunging breakers will result in larger wave forces, and it is therefore relevant to investigate the frequency of plunging breaking waves hitting the truss structure.

Battjes (1974) and many other authors have been developed parametric surf zone models. These models are based on a Rayleigh wave height distribution in deeper water. As the waves propagate into shallow water, the models predict the distorted wave height distribution due to wave breaking. These models present the occurrence of wave breaking and the effect on the significant wave height inside the surf zone.

Goda (1975), cited in Goda (2000), proposed a parametric surf zone model that includes the effect of bottom slope. Reedijk, et al. (2009) modified this model by excluding wave set-up and surf beat, and applying a linear shoaling approach.

Reedijk, et al. (2009) applied the modified surf zone model of Goda (2000) to assess the frequency of plunging breaking waves in front of a breakwater. This model derives directly the occurrence of wave breaking, and can also be used to assess the frequency of plunging breaking waves in front of the truss structure. The breaker types are classified by Battjes (1974) as explained in section 2.2, with surf similarity parameter ξ_0 as Equation (7) shows.

Reedijk, et al. (2009) performed a large number of simulations, and determined by dimensional analysis two parameters, the breaker parameter, *B*, and the seabed slope, *tan(α)*. The breaker parameter is a dimensionless wave parameter:

$$B = \frac{H_{S,0}}{h}\left(\frac{h}{L_0}\right)^{1/4} = (H_{S,0}L_0)^{1/4}h^{-5/4} \tag{38}$$

$H_{S,0}$ is the equivalent deep water wave height (significant wave height in deep water), h is the local water depth and $L_0 = gT_p^2/(2\pi)$ is the deep water wave length.

When analyzing the results from the model testing, measured significant wave height at intermediate water, H_S, is found. This is the significant wave height at "deep" water in the wave channel.

Depth limited wave height can then be found:

$$\frac{H_S}{h} \tag{39}$$

Depth limited wave height is put in Figure 38 with the seabed slope. The breaker parameter, *B*, is then read out from this figure:

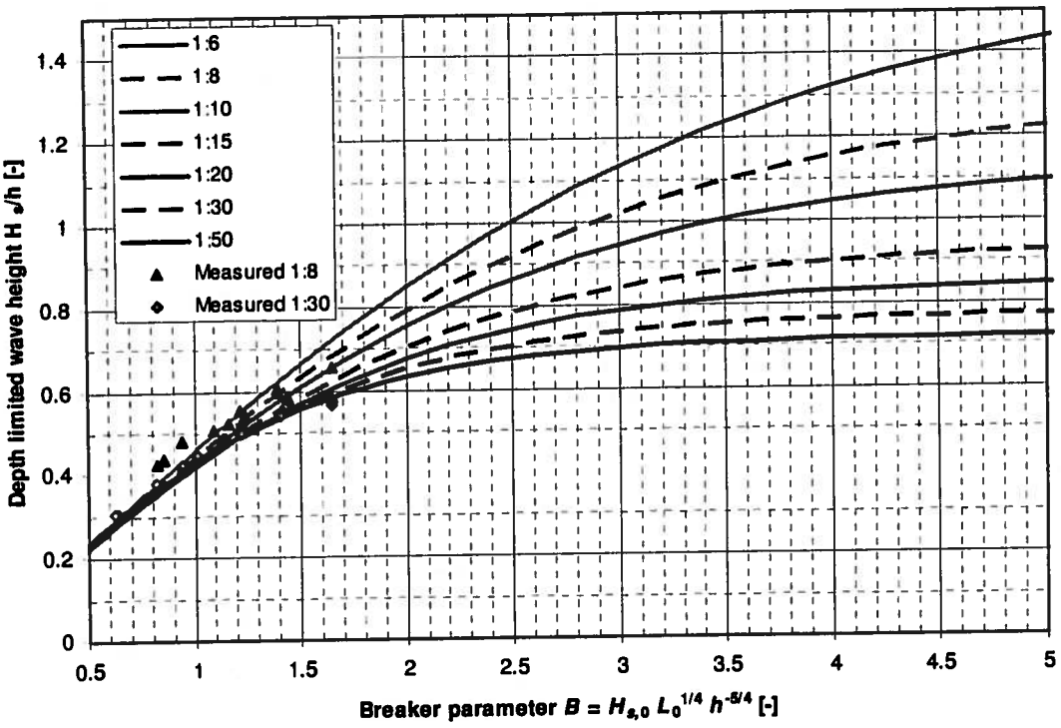

Figure 38: Significant wave height inside the surf zone Hs/h vs. B (Reedijk, et al. 2009)

The equivalent deep water wave height is then found from Equation (38):

$$H_{S,0} = \frac{B}{L_0^{1/4} \cdot h^{-5/4}} \tag{40}$$

Finally, the surf similarity parameter is found by:

$$\xi_0 = \frac{\tan\theta}{\sqrt{\frac{H_{S,0}}{L_0}}} \tag{41}$$

$tan\theta$ is the bottom slope.

For assessing the breaker types, the modified surf zone model of Goda (2000) was applied to the surf zone simulations, and the results where plotted in Figure 39. The occurrence of plunging breakers varies with the breaker parameter and the surf similarity parameter. The percentage occurrence of plunging breakers in all income waves is then found by putting in the calculated breaker parameter, B, and the surf similarity parameter, ξ_0.

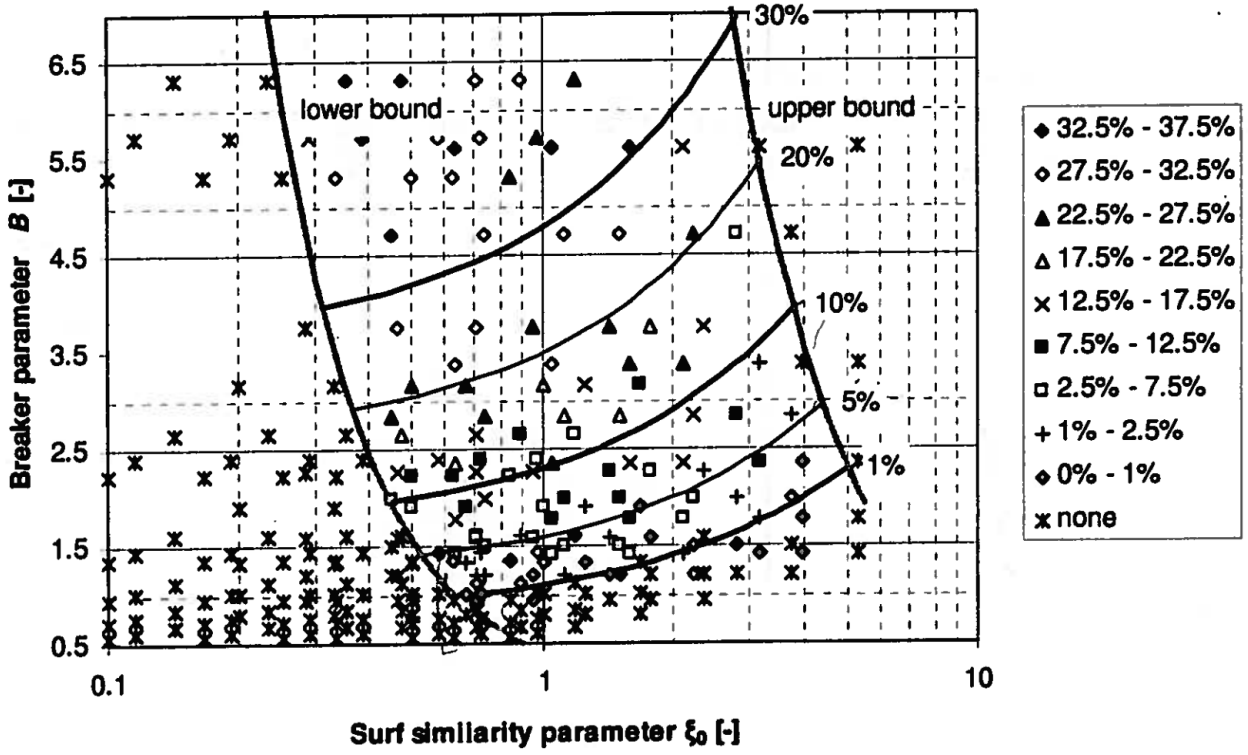

Figure 39: Probability of occurrence of plunging breakers (Reedijk, et al. 2009)

It can be seen from Figure 39 that:

- Spilling breakers are expected for $\xi_0 < 0{,}25$ to $0{,}7$
- Plunging breakers are expected in the range $0{,}25$ to $0{,}7 < \xi_0 < 3$ to 5
- Surging breakers are expected for $\xi_0 > 3$ to 5
- "Lower bound" is the transition from spilling to plunging waves
- "Upper bound" is the transition from plunging to surging waves

Example of how Figure 39 is used:
If the surf similarity parameter $\xi_0 = 1{,}0$ and the breaker parameter B = 2,5, the probability of occurrence of plunging breakers is 11%.

5. ANALYSIS OF EXPERIMENTAL RESULTS

This chapter consists of analysis of the most important results from the lab-experiments. The challenge of the data analysis is to resolve the wave slamming force from the measured response.

5.1. Maximum response

The maximum response has been recorded in the two top force transducers, transducer 3 and 4, see Figure 26 on page 23. Force transducer 3 has maximum response in most of the measurements. It is the cases specified in Table 4 that has maximum impulse. This is based on analysis of the regular waves and observation during model testing of the irregular waves.

All the data from tests of regular waves are analyzed in APPENDIX B. The slamming forces are calculated based on measured breaking wave height, H_b, and maximum surface elevation at breaking, η_b. The analysis is based on a Matlab programme developed by Alf Tørum.

A program called Wavesumm in Matlab provided by Øivind A. Arntsen is used to analyze the irregular waves. The four cases where it was observed maximum response is analyzed in APPENDIX C.

Table 4: Maximum impulse

Regular waves					Irregular waves				
e	f [Hz] (T [s])				e	f [Hz] (T [s])			
	0,45Hz (2,22s)	0,48Hz (2,08s)	0,51Hz (1,96s)	0,54Hz (1,85s)		0,45Hz (2,22s)	0,48Hz (2,08s)	0,51Hz (1,96s)	0,54Hz (1,85s)
265				x	330				x
265			x		400			x	
280		x			400		x		
270	x				490	x			

5.2. Calculated slamming forces

The slamming forces are calculated for all the tests run of regular waves in APPENDIX B. It is more complicated to calculate this force for a truss structure than for a single pile. The slamming forces are calculated by this equation:

$$F_S = \frac{1}{2}\rho C_S D_1 C_b^2 \lambda \eta_b \cdot 2 + \frac{1}{2}\rho C_S D_2 C_b^2 l \tag{42}$$

The first part of Equation (42) represent the legs of the structure and the second part the diagonal rods.

Measured values:

η_b	maximum surface elevation at breaking, see Figure 40
H_b	wave height at breaking
$l = l_1 + l_2$	length of diagonal rods impact area, see Figure 40

The breaking wave celerity is:

$$C_b = \sqrt{g(h + \eta_b)} \tag{43}$$

Constants:

$\rho = 1000 kg/m^3$	water density
$g = 9{,}81 m/s^2$	gravitational acceleration
$D_1 = 0{,}016m$	leg diameter of the truss structure
$D_2 = 0{,}012m$	diameter of diagonal rods
$\lambda_{max} = 0{,}46$	maximum curling factor (Wienke and Oumeraci, 2005)
$\lambda_{max} = 0{,}40$	maximum curling factor (Goda, et al. 1966)
$h = 0{,}333m$	local water depth
$C_S = 2\pi$	slamming factor (Wienke and Oumeraci, 2005)
$C_S = \pi$	slamming factor (Goda, et al. 1966)

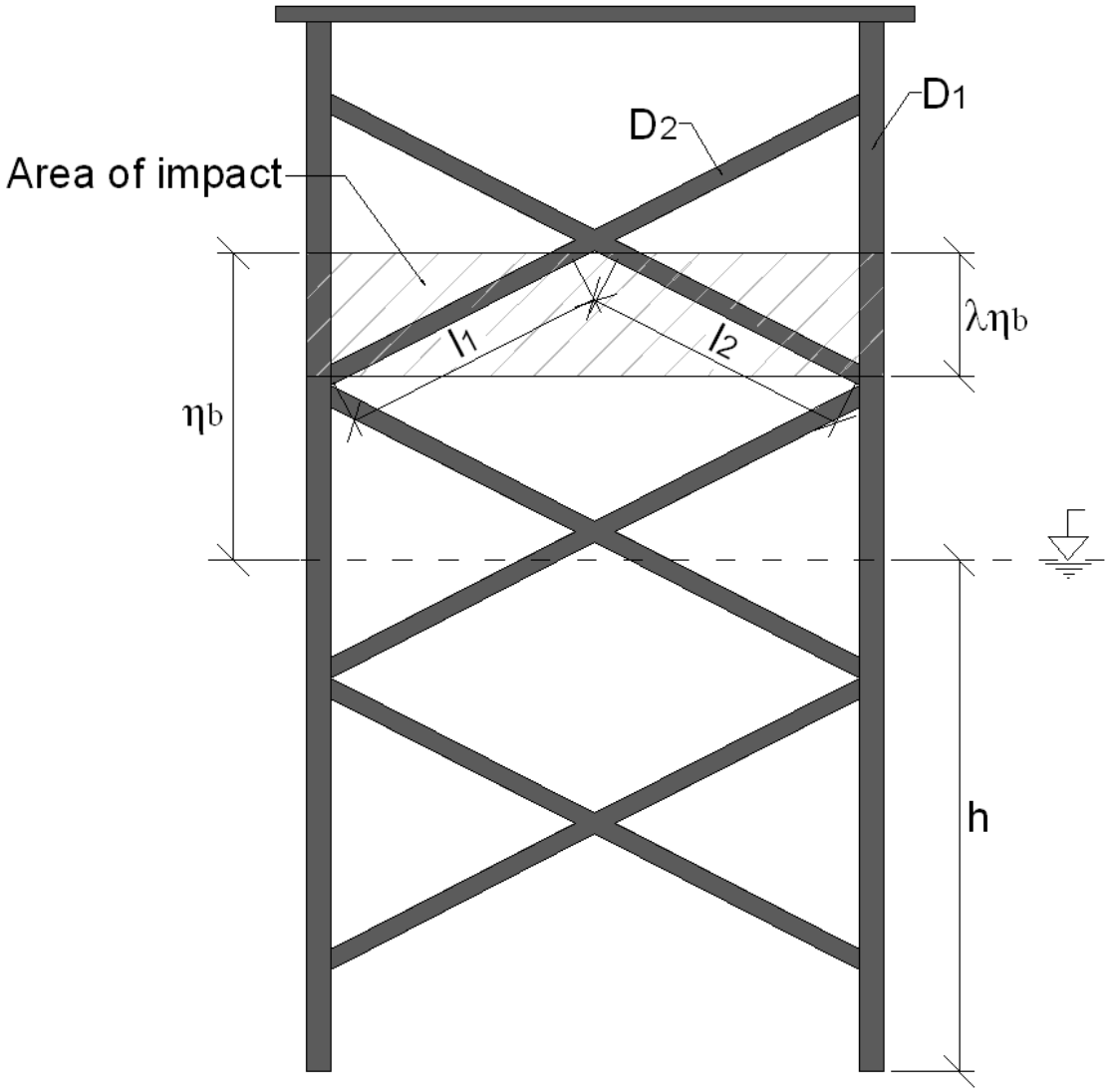

Figure 40: Definition sketch for calculation of the slamming force

5.3. Frequency response function (FRF)

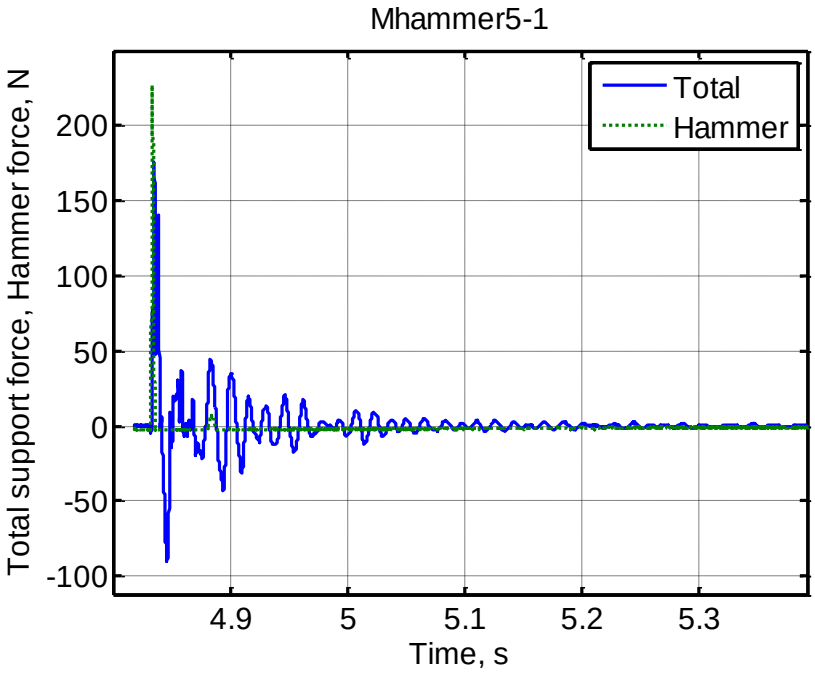

Figure 41: Impulse force and total response of the structure, Mhammer5_1

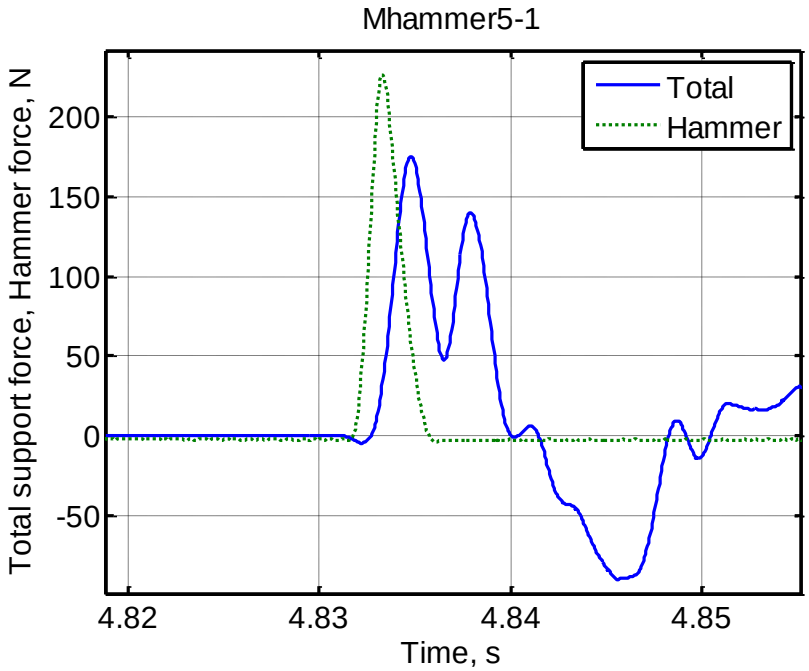

Figure 42: Expanded view: Impulse force and total response of the structure, Mhammer5_1

Figure 41 and 42 shows the impulse hammer force and the total response of the structure for the first pluck-test in point 5 on the structure; see also Figure 37 on page 35.

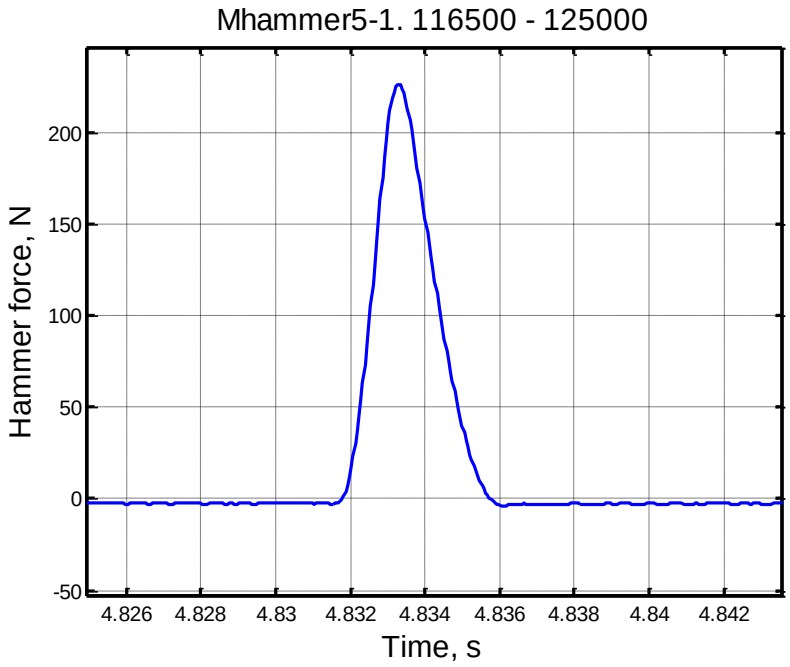

Figure 43: FRF concept used on the "Total" response force, Mhammer5_1

Figure 43 shows the frequency response function. This shows that the agreement with the original hammer force from Figure 41 and 42 is good.

Figure 42 show that the natural period of oscillation $T_d \approx 0{,}02$s.

5.4. Regular waves

5.4.1. Mf045e270_1

Frequency f = 0,45Hz
Eccentricity e = 2,70

Figure 44: Snap-shot, Mf045e270_1

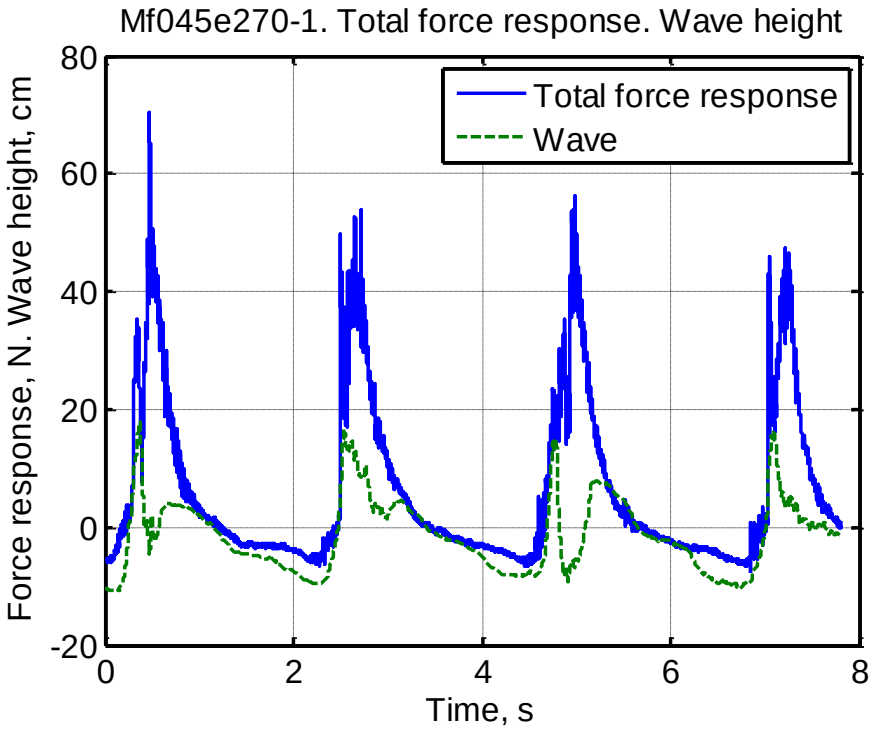

Figure 45: Total force response and wave height, Mf045e270_1

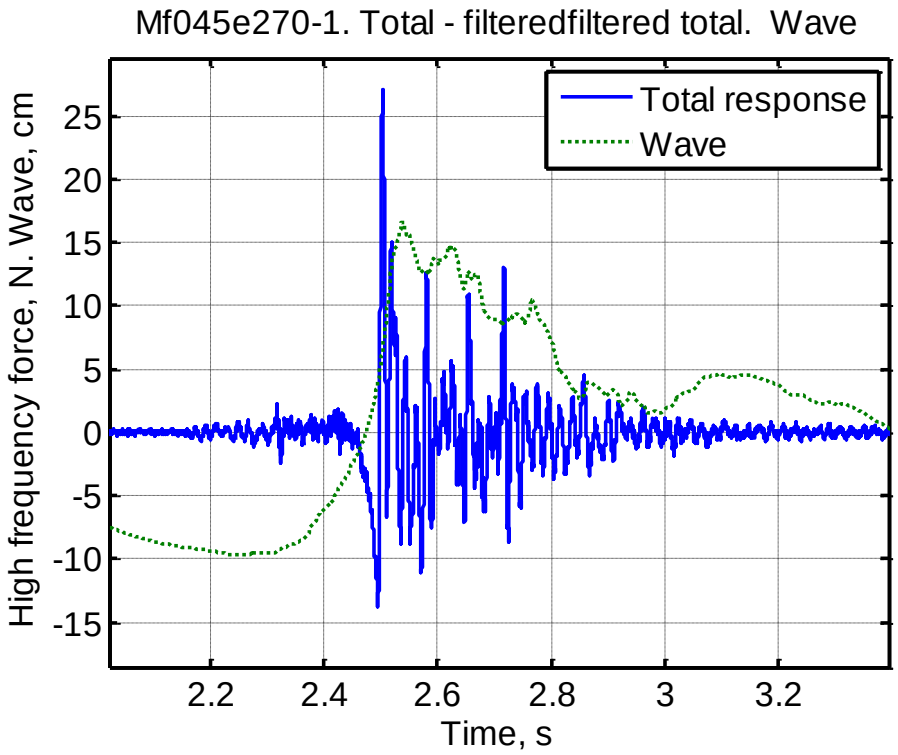

Figure 46: Total response - filteredfiltered force response and wave height, Mf045e270_1

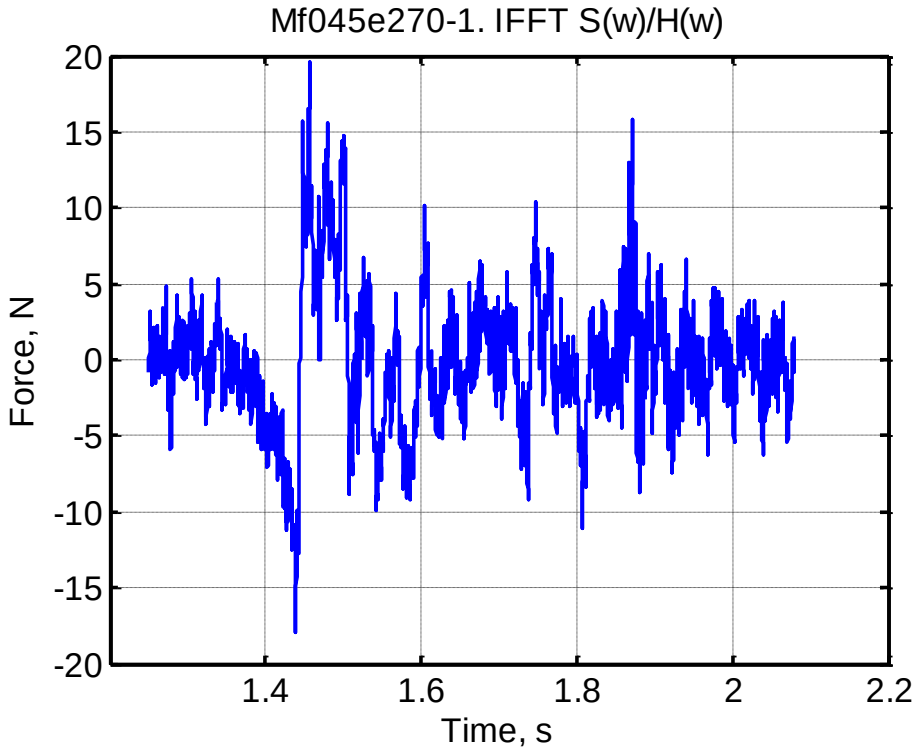

Figure 47: IFFT of S(ω)/H(ω) for the response force, Mf045e270_1

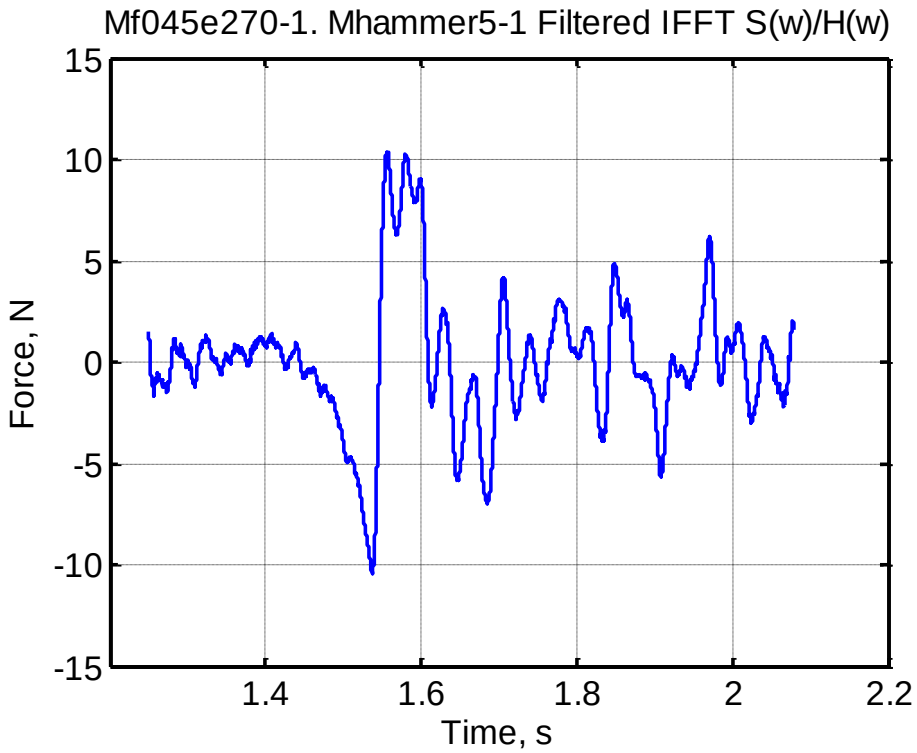

Figure 48: Low pass filtered IFFT of S(ω)/H(ω) of the response force, Mf045e270_1

Table 5: Response and force, f = 0,45Hz, e = 2,70

Response	**27,1N**
Slamming force	**10,8N**
Calculated force (Wienke and Omeraci)	**88,1N**
Calculated force (Goda)	**38,3N**

5.4.2. Mf048e280_1

Frequency f = 0,48Hz
Eccentricity e = 2,80

Figure 49: Snap-shot, Mf048e280_1

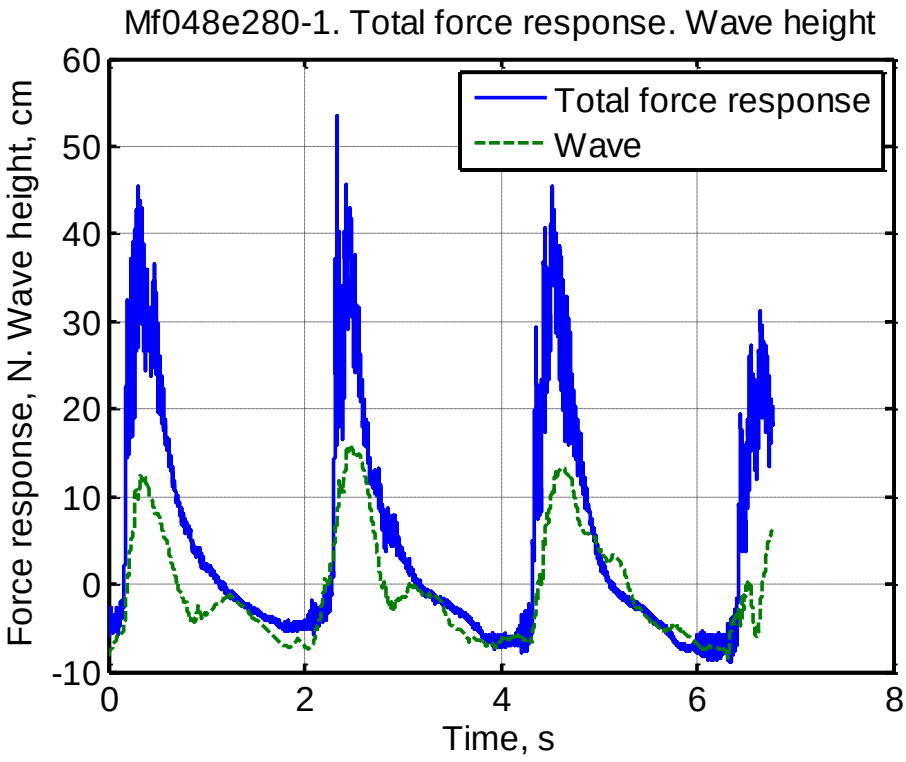

Figure 50: Total force response and wave height, Mf048e280_1

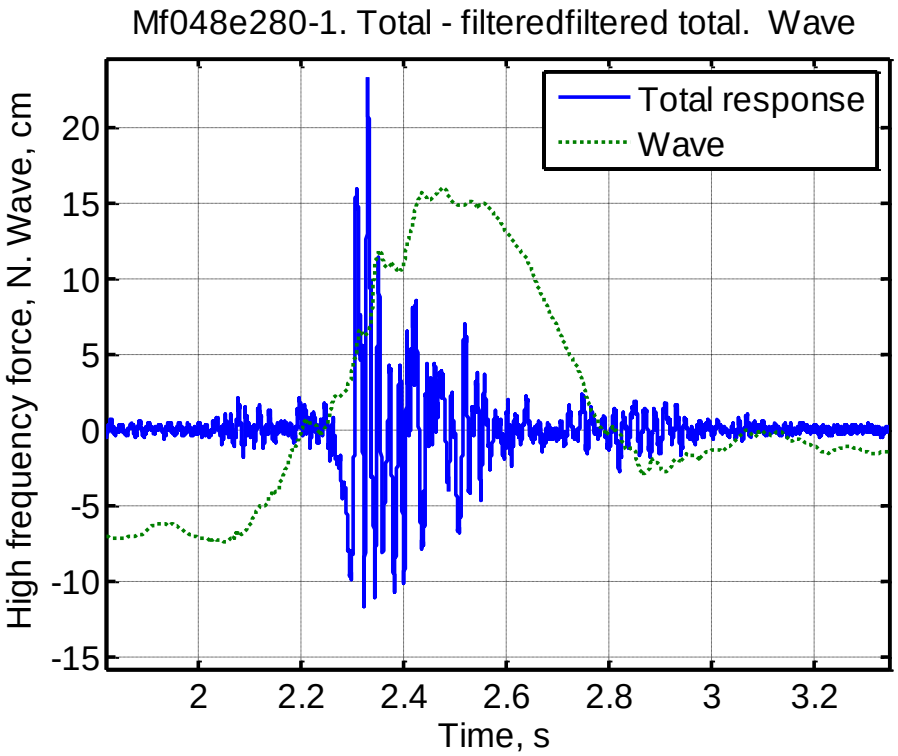

Figure 51: Total response - filteredfiltered force response and wave height, Mf048e280_1

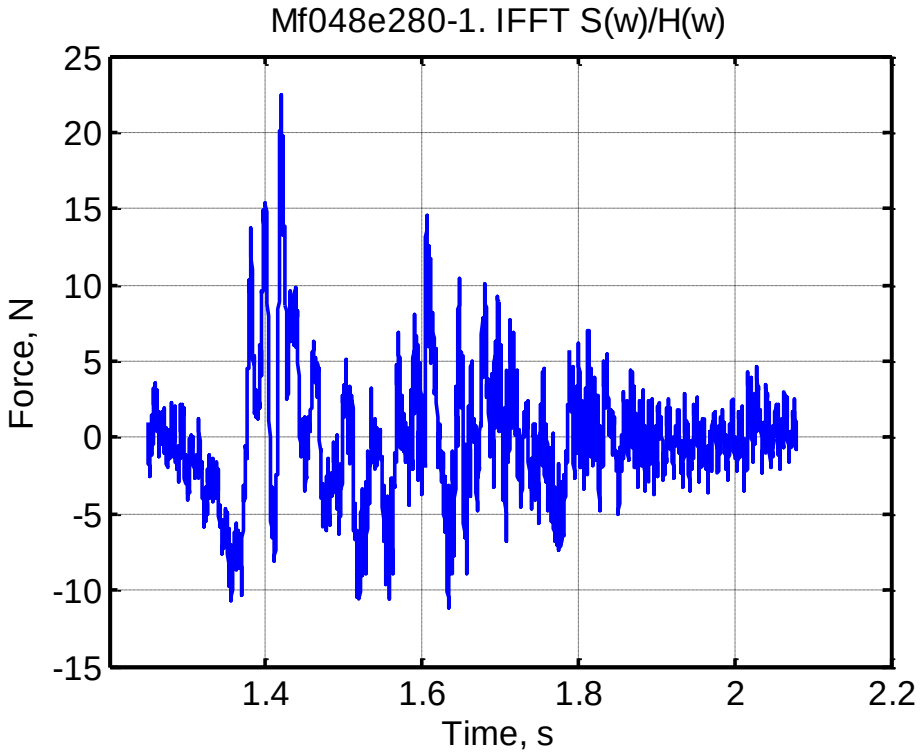

Figure 52: IFFT of S(ω)/H(ω) for the response force, Mf048e280_1

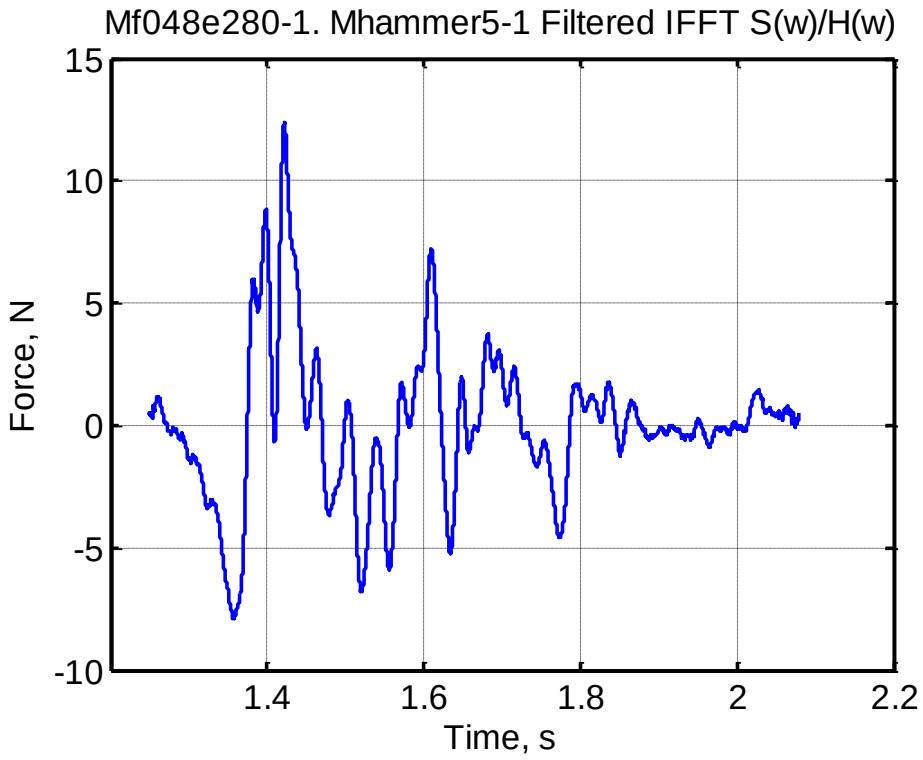

Figure 53: Low pass filtered IFFT of S(ω)/H(ω) of the response force, Mf048e280_1

Table 6: Response and force, f = 0,48Hz, e = 2,80

Response	**23,3N**
Slamming force	**12,4**
Calculated force (Wienke and Omeraci)	**83,5N**
Calculated force (Goda)	**36,0N**

5.4.3. Mf051e265_1

Frequency f = 0,51Hz
Eccentricity e = 2,65

Figure 54: Snap-shot, Mf051e265_1

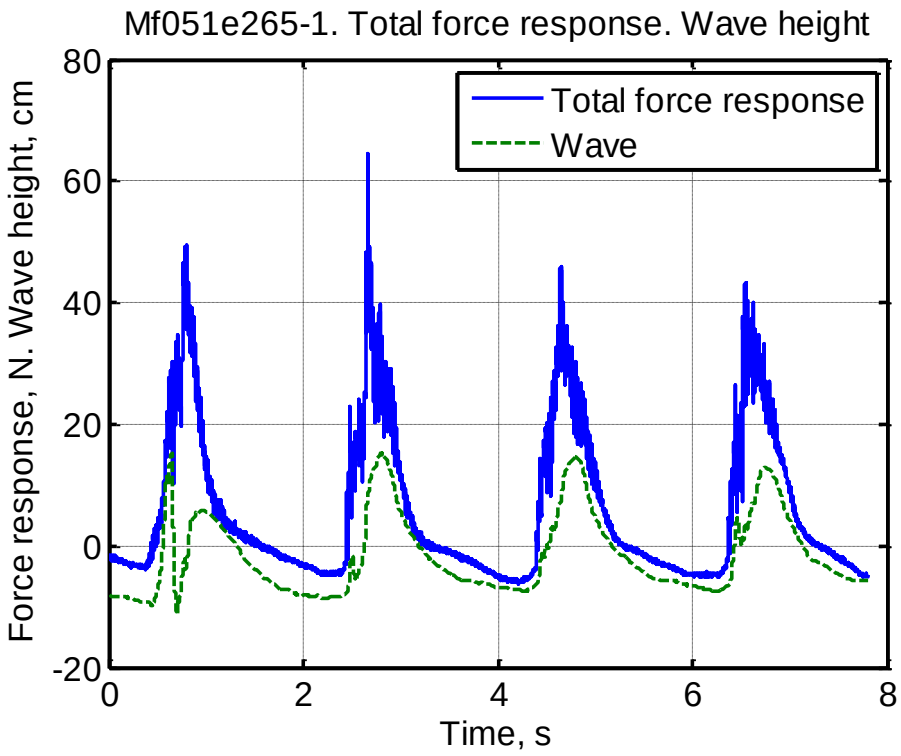

Figure 55: Total force response and wave height, Mf051e265_1

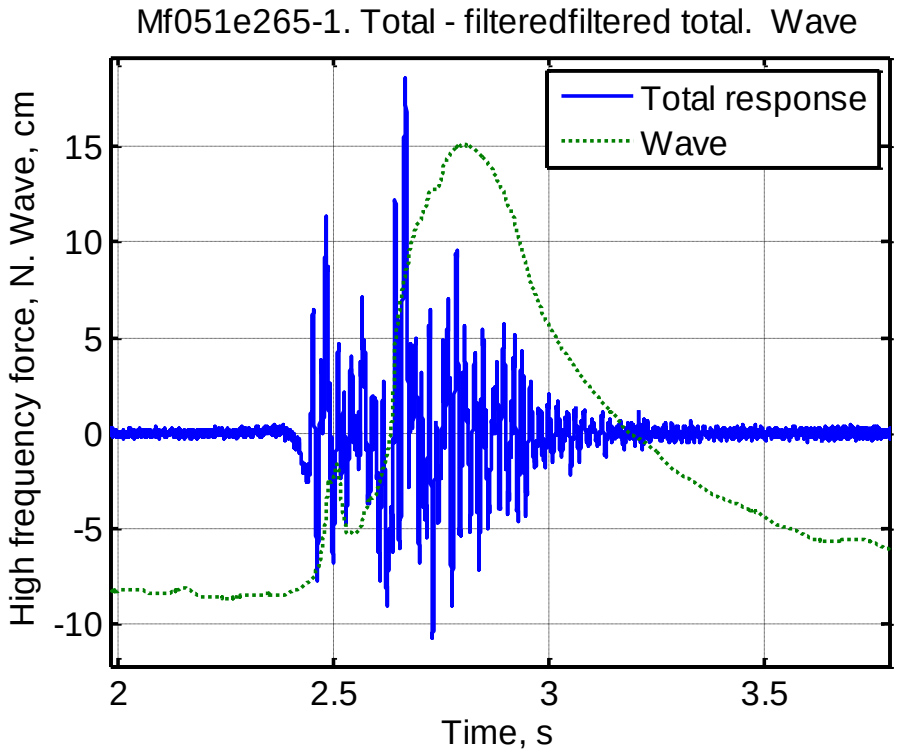

Figure 56: Total response - filteredfiltered force response and wave height, Mf051e265_1

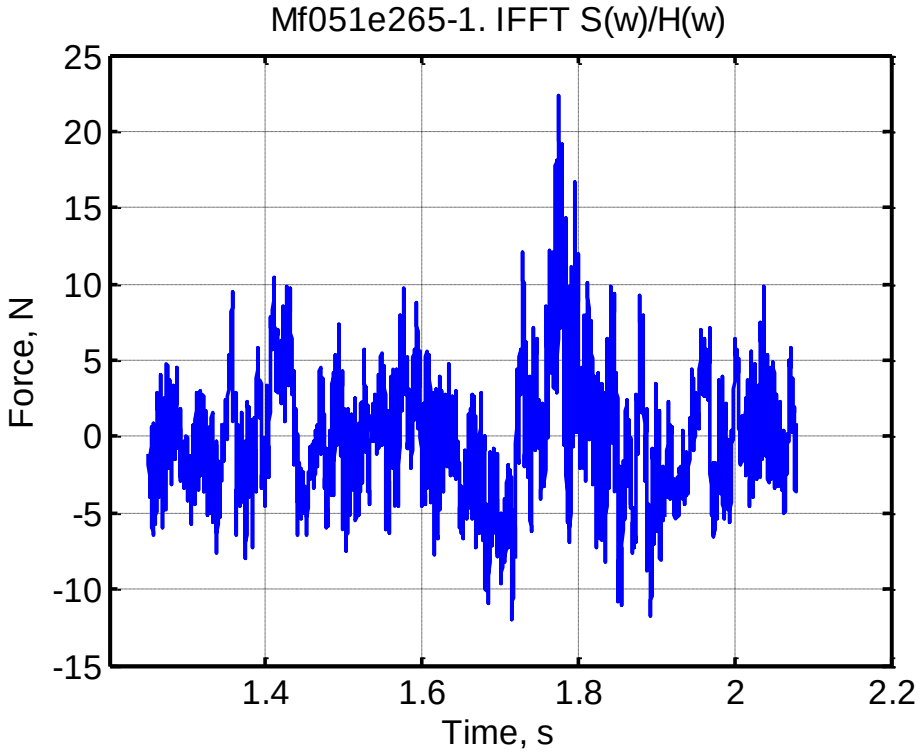

Figure 57: IFFT of S(ω)/H(ω) for the response force, Mf051e265_1

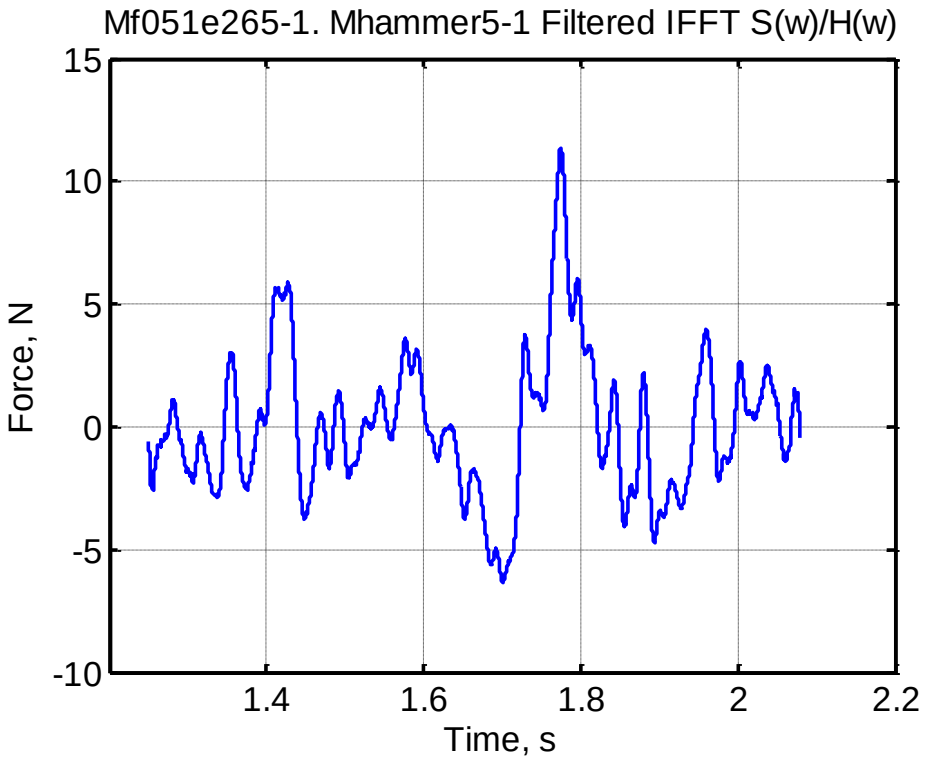

Figure 58: Low pass filtered IFFT of S(ω)/H(ω) of the response force, Mf051e265_1

Table 7: Response and force, f = 0,51Hz, e = 2,65

Response	**18,5N**
Slamming force	**11,4N**
Calculated force (Wienke and Omeraci)	**76,4N**
Calculated force (Goda)	**32,3N**

5.4.4. Mf054e2265_1

Frequency f = 0,54Hz
Eccentricity e = 2,765

Figure 59: Snap-shot, Mf054e265_1

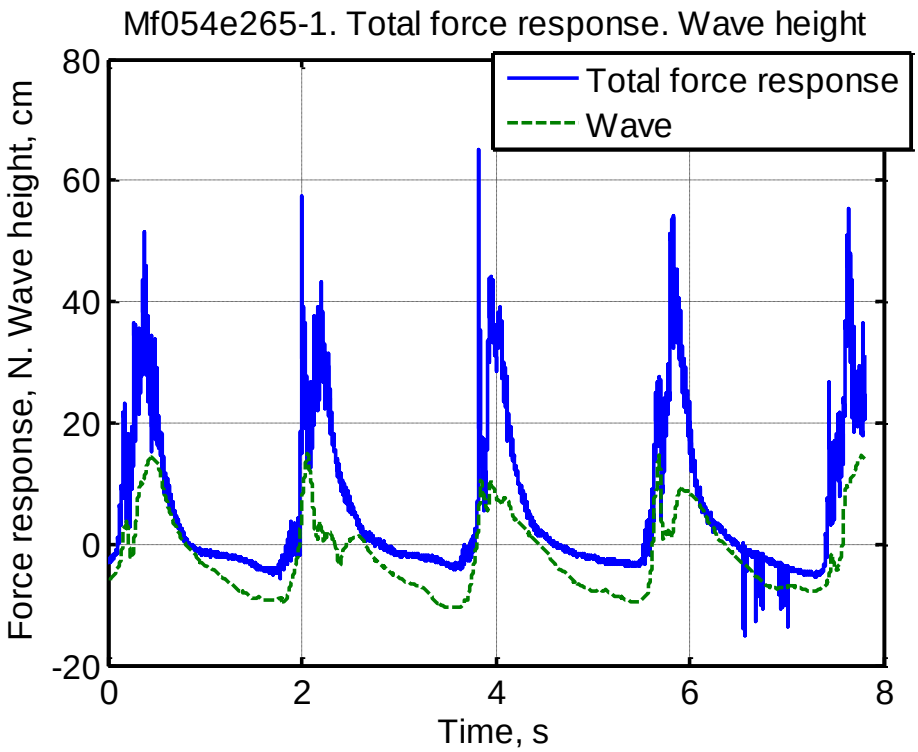

Figure 60: Total force response and wave height, Mf054e265_1

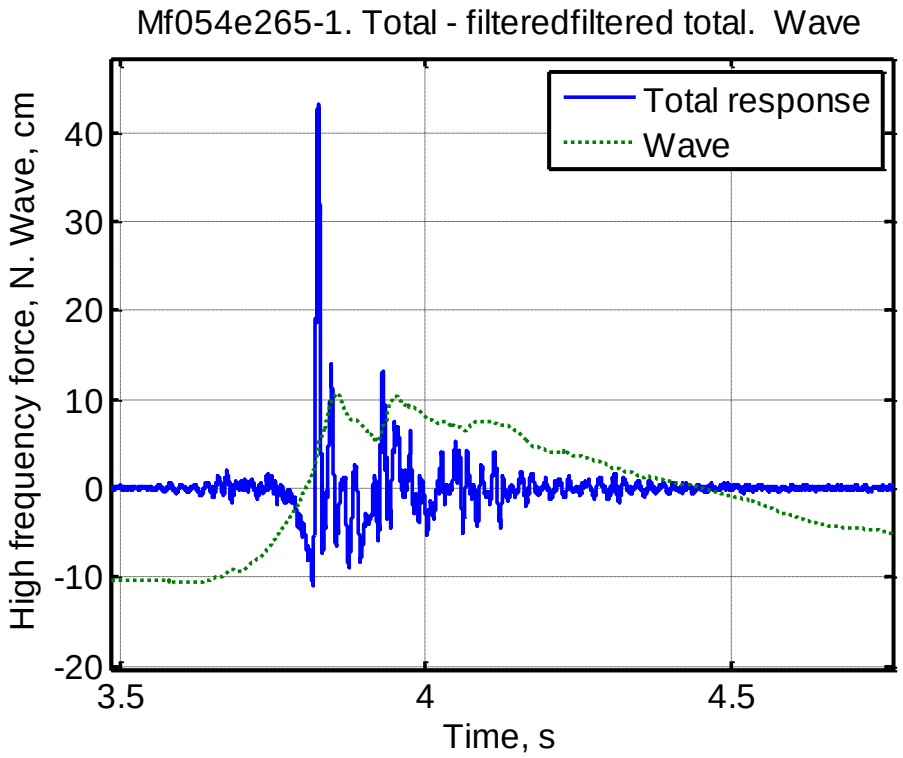

Figure 61: Total response - filteredfiltered force response and wave height, Mf054e265_1

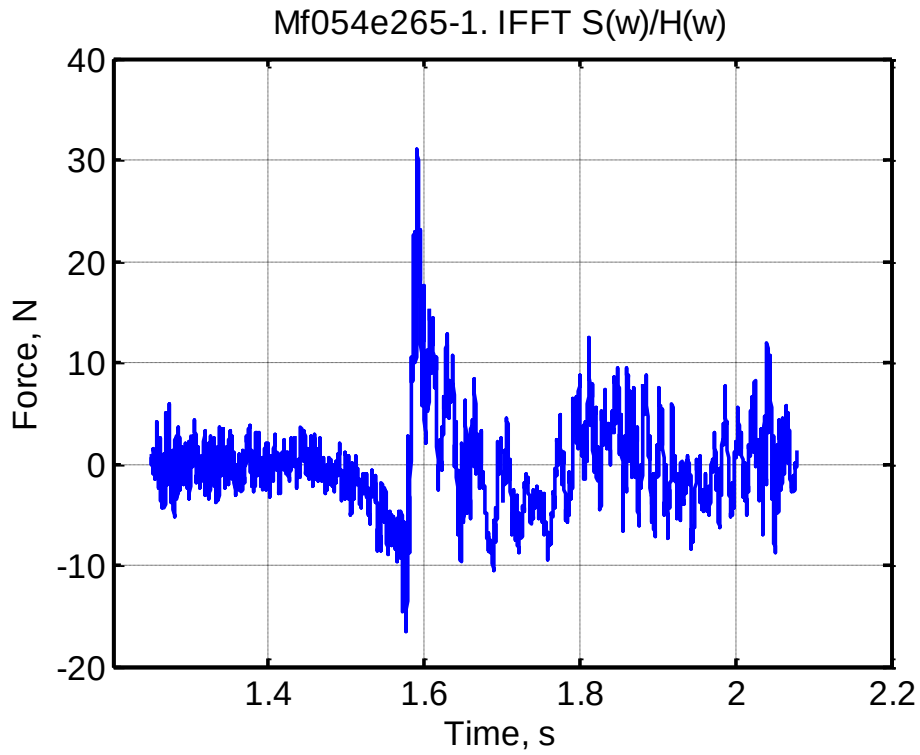

Figure 62: IFFT of S(ω)/H(ω) for the response force, Mf054e265_1

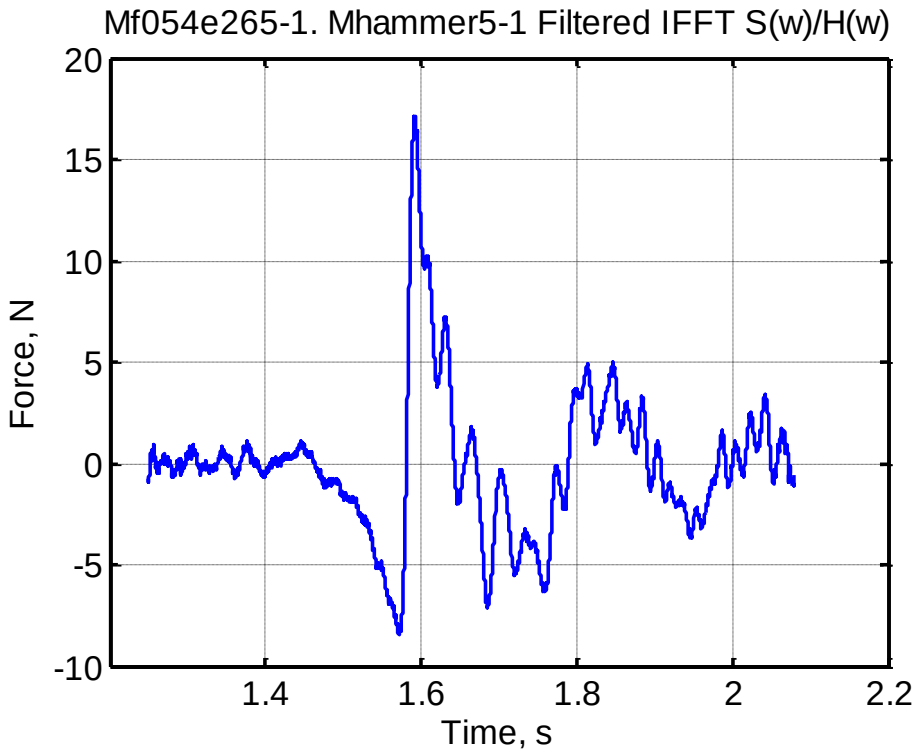

Figure 63: Low pass filtered IFFT of S(ω)/H(ω) of the response force, Mf054e265_1

Table 8: Response and force, f = 0,54Hz, e = 2,65

Response	**43,2N**
Slamming force	**17,1N**
Calculated force (Wienke and Omeraci)	**75,7N**
Calculated force (Goda)	**32,0N**

5.4.5. Comments

Figure 45, 50, 55 and 60 shows the total force response and wave height for one particular run in the four cases. The figures show that there are quite large variations of the response forces from wave to wave.

Figure 46, 51, 56 and 61 shows the total response and wave height for the maximum four cases with different frequencies. This wave slamming response is arrived from low-pass filtering the measured force response.

The inverse fast Fourier transform (IFFT) of S(ω)/H(ω) is shown in Figure 47, 52, 57 and 62.

Finally, the slamming force, which is the low-pass filtered IFFT is shown in Figure 48, 53, 58 and 63.

The hammer pluck Mhammer5_1 has been applied when the time series are analyzed.

The slamming force is about half the measured response. The calculated slamming forces are larger than the measured slamming forces. The reason for this may be scale-effects. The slamming forces are calculated for the front part of the structure. The plunging breaking wave may also hit different parts of the front section at slightly different time points, which can reduce the response forces.

From the pictures (Figure 44, 49, 54 and 59) it seems like it in reality occurs a larger crest height than measured, which will make the calculated forces larger. The measured crest height is smaller due to air entrance in the wave.

5.5. Irregular waves

5.5.1. MTp185e330_1:

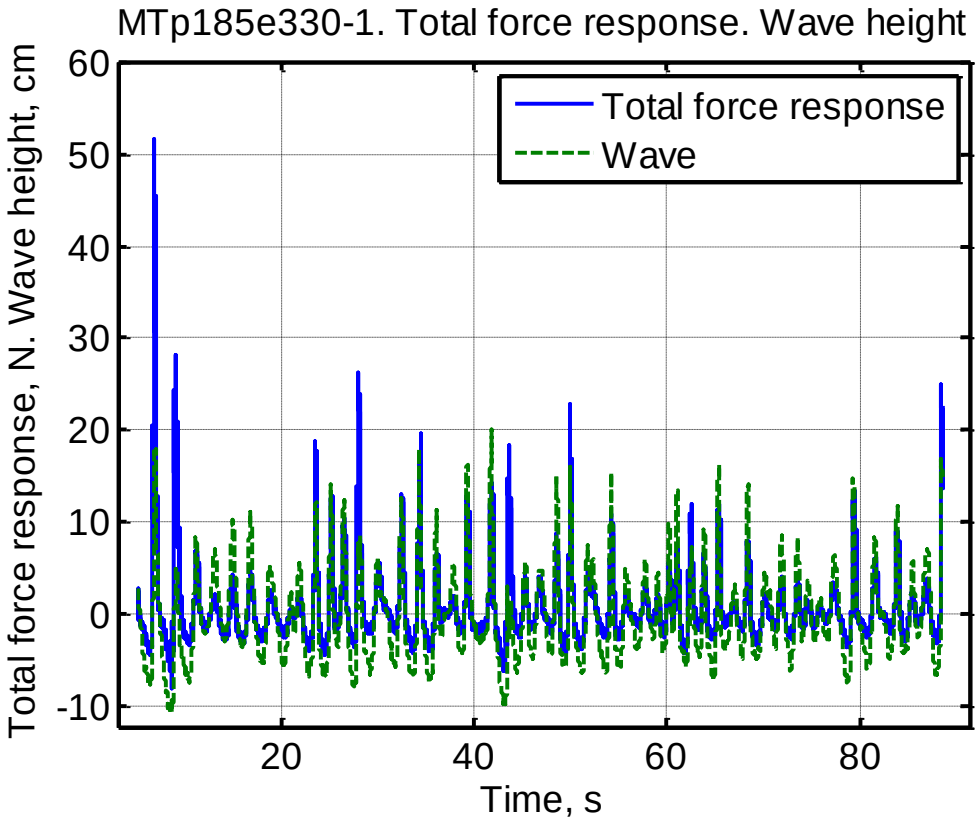

Figure 64: Time series of total force response, MTp185e330_1

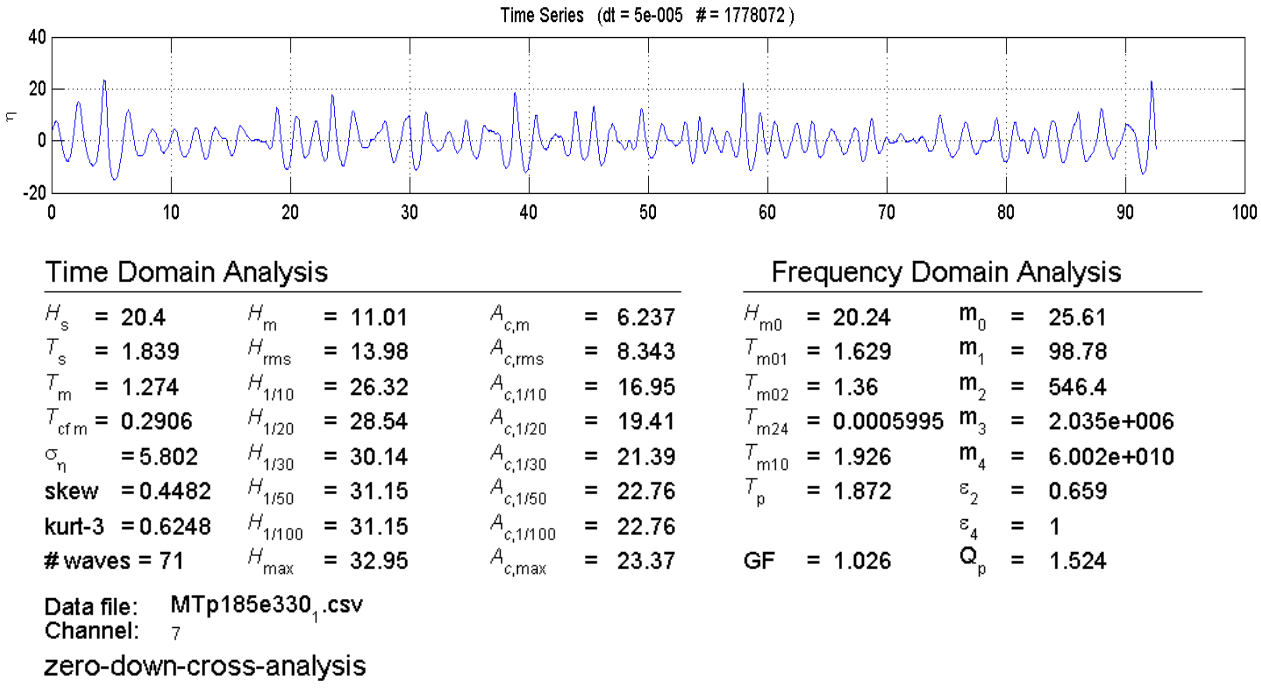

Figure 65: Time series and analysis, MTp185e330_1

Data from Figure 65:

H_S = 0,2040m	measured significant wave height at intermediate water
T_P = 1,872s	measured peak period
h = 0,333m	local water depth, water depth at the structure
g = 9,81m/s	gravitational acceleration

Deep water wave length:

$$L_0 = \frac{g}{2\pi} \cdot T_P^2 = \frac{9,81}{2\pi} \cdot 1,872^2 = 5,471m \tag{44}$$

Depth limited wave height:

$$\frac{H_S}{h} = \frac{0,2040}{0,333} = 0,61 \tag{45}$$

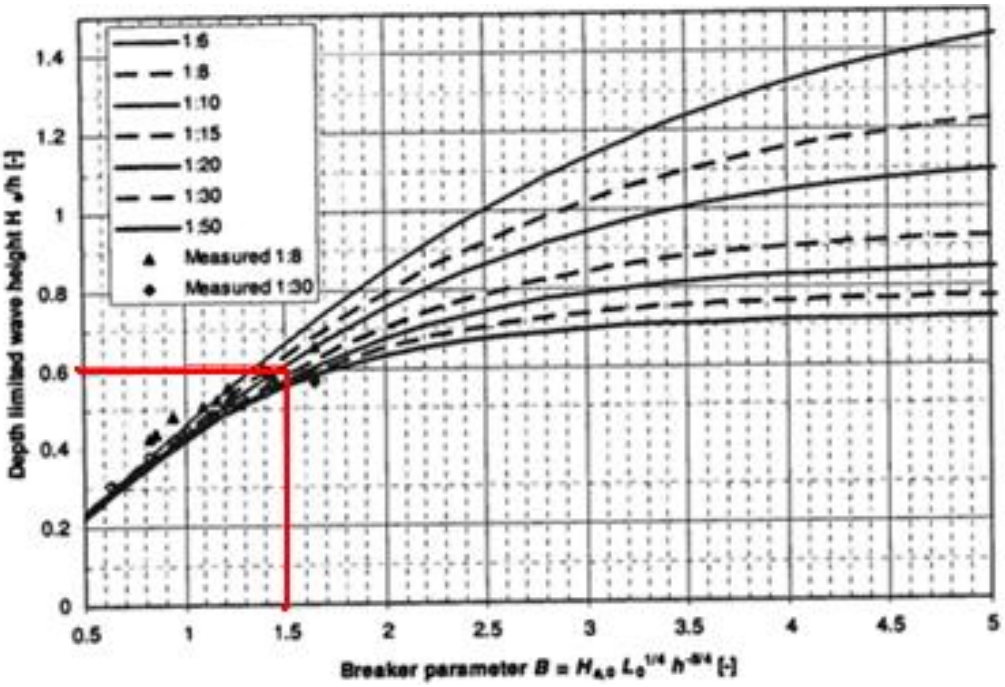

Figure 66: Significant wave height inside the surf zone Hs/h vs. B (Reedijk, et al. 2009)

From Figure 66 it is shown that the breaker parameter B = 1,5.

Significant wave height at deep water is then:

$$H_{S,0} = \frac{B}{L_0^{1/4} \cdot h^{-5/4}} = \frac{1,5}{5,417^{1/4} \cdot 0,333^{-5/4}} = 0,249m \tag{46}$$

Surf similarity parameter:

$$\xi_0 = \frac{\tan\theta}{\sqrt{\frac{H_{S,0}}{L_0}}} = \frac{0,1}{\sqrt{\frac{0,249}{5,471}}} = 0,47 \tag{47}$$

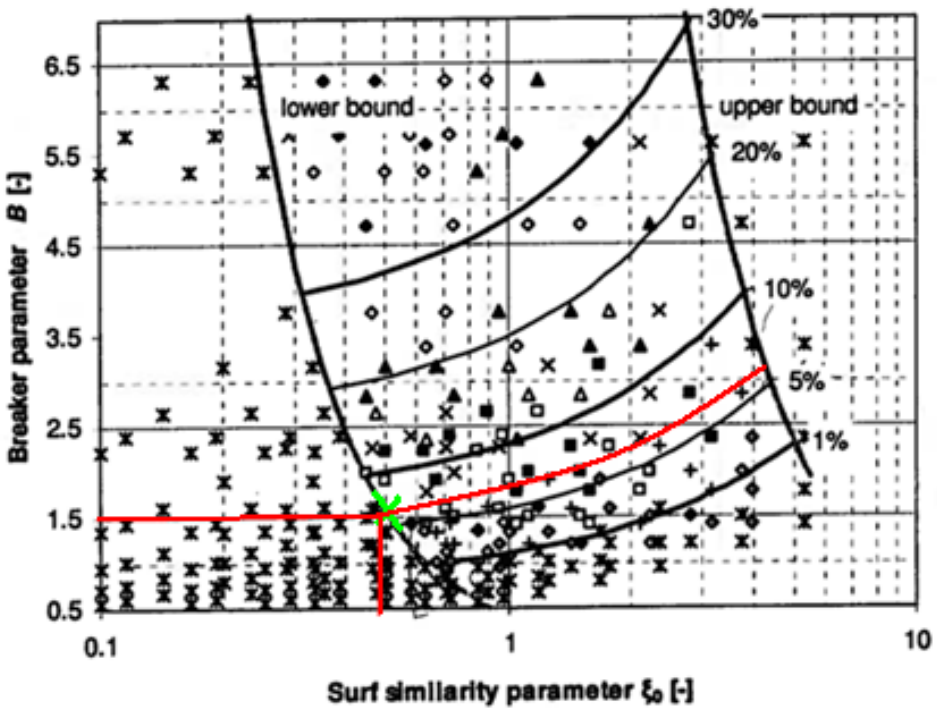

Figure 67: Occurrence of plunging breakers (Reedijk, et al. 2009)

Figure 67 shows that the probability of occurrence of spilling breaking waves in this case is about 6%.

5.5.2. MTp196e400_1:

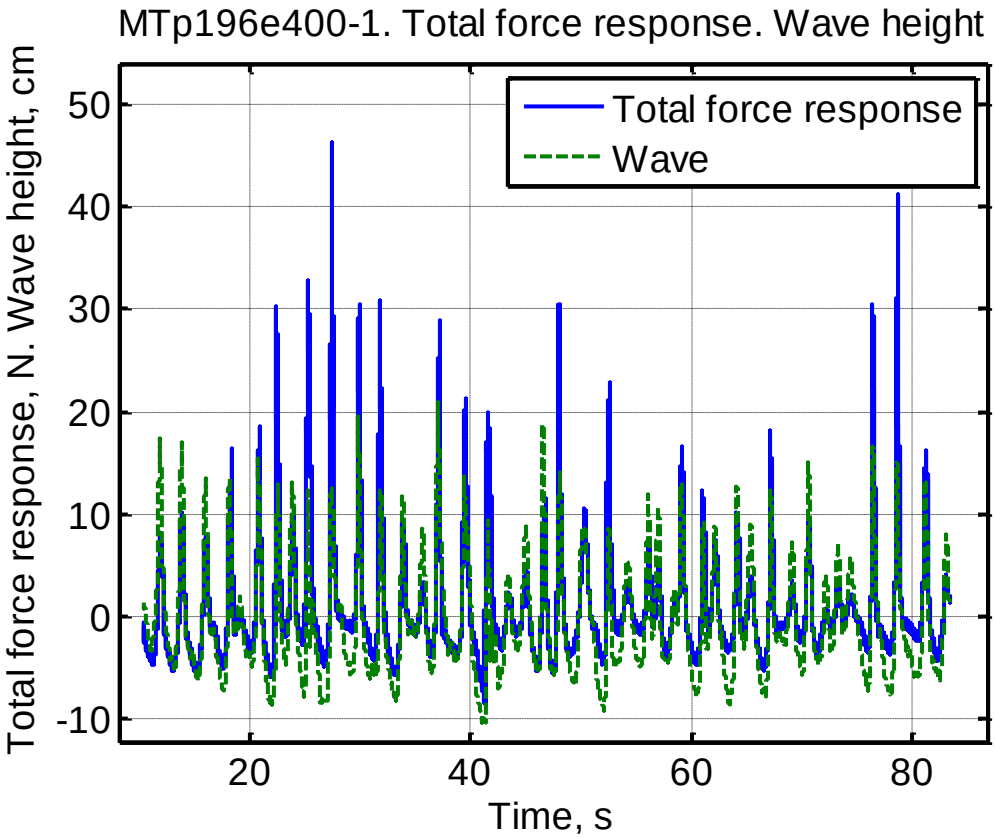

Figure 68: Time series of total force response, MTp196e400_1

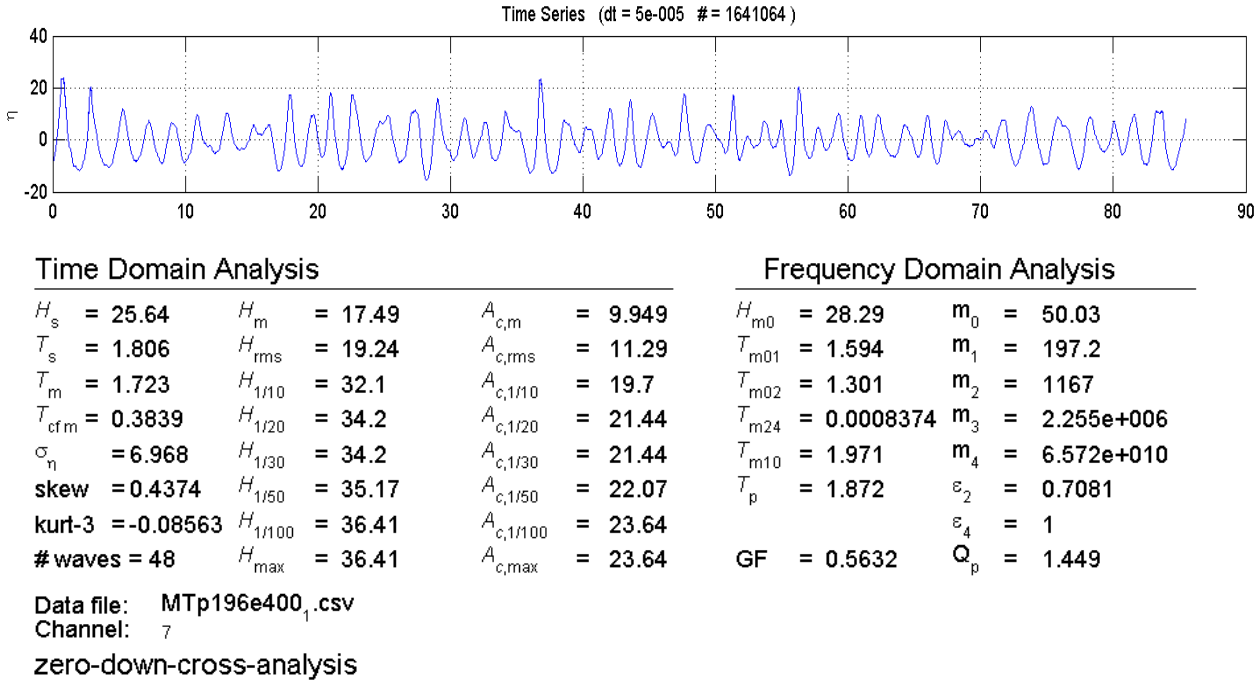

Figure 69: Time series and analysis, MTp196e400_1

Data from Figure 69:

H_S = 0,2564m	measured significant wave height at intermediate water
T_P = 1,872s	measured peak period
h = 0,333m	local water depth, water depth at the structure
g = 9,81m/s	gravitational acceleration

Deep water wave length:

$$L_0 = \frac{g}{2\pi} \cdot T_P^2 = \frac{9,81}{2\pi} \cdot 1,872^2 = 5,471m \tag{48}$$

Depth limited wave height:

$$\frac{H_S}{h} = \frac{0,2564}{0,333} = 0,77 \tag{49}$$

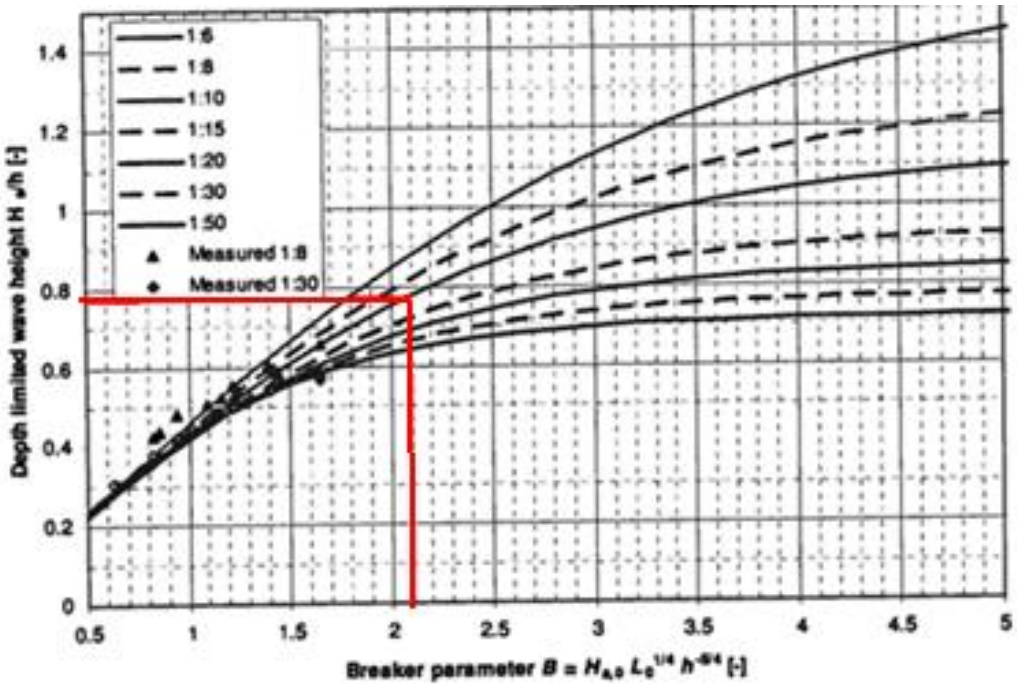

Figure 70: Significant wave height inside the surf zone Hs/h vs. B (Reedijk, et al. 2009)

From Figure 70 it is shown that the breaker parameter B = 2,1.

Significant wave height at deep water is then:

$$H_{S,0} = \frac{B}{L_0^{1/4} \cdot h^{-5/4}} = \frac{2,1}{5,417^{1/4} \cdot 0,333^{-5/4}} = 0,348m \tag{50}$$

Surf similarity parameter:

$$\xi_0 = \frac{\tan\theta}{\sqrt{\frac{H_{S,0}}{L_0}}} = \frac{0,1}{\sqrt{\frac{0,348}{5,471}}} = 0,40 \tag{51}$$

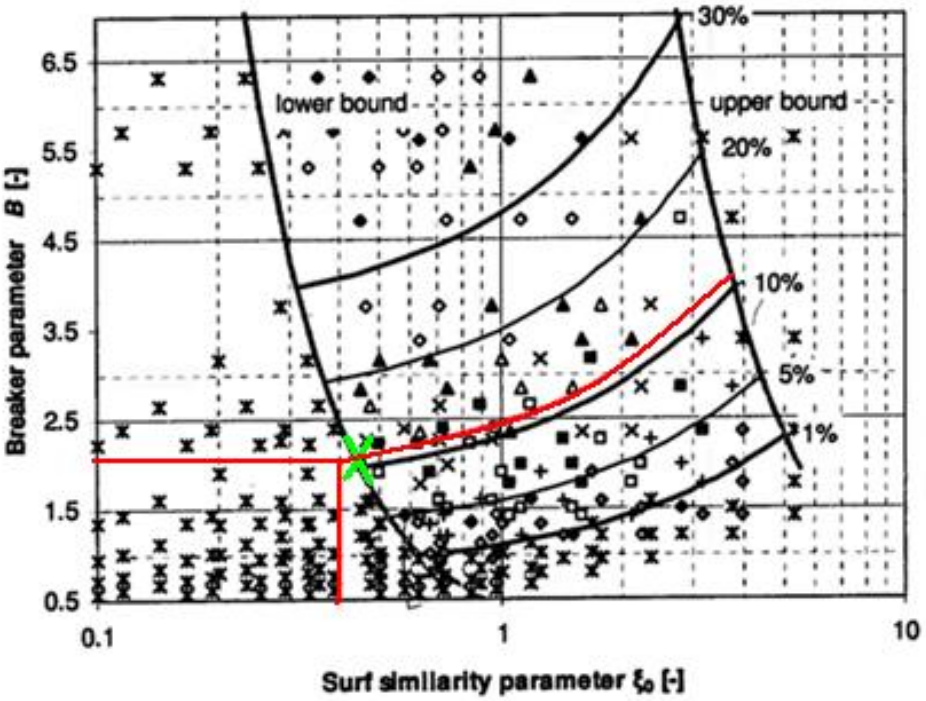

Figure 71: Occurrence of plunging breakers (Reedijk, et al. 2009)

Figure 71 shows that the probability of occurrence of spilling breaking waves in this case is about 11%.

5.5.3. MTp208e400_1:

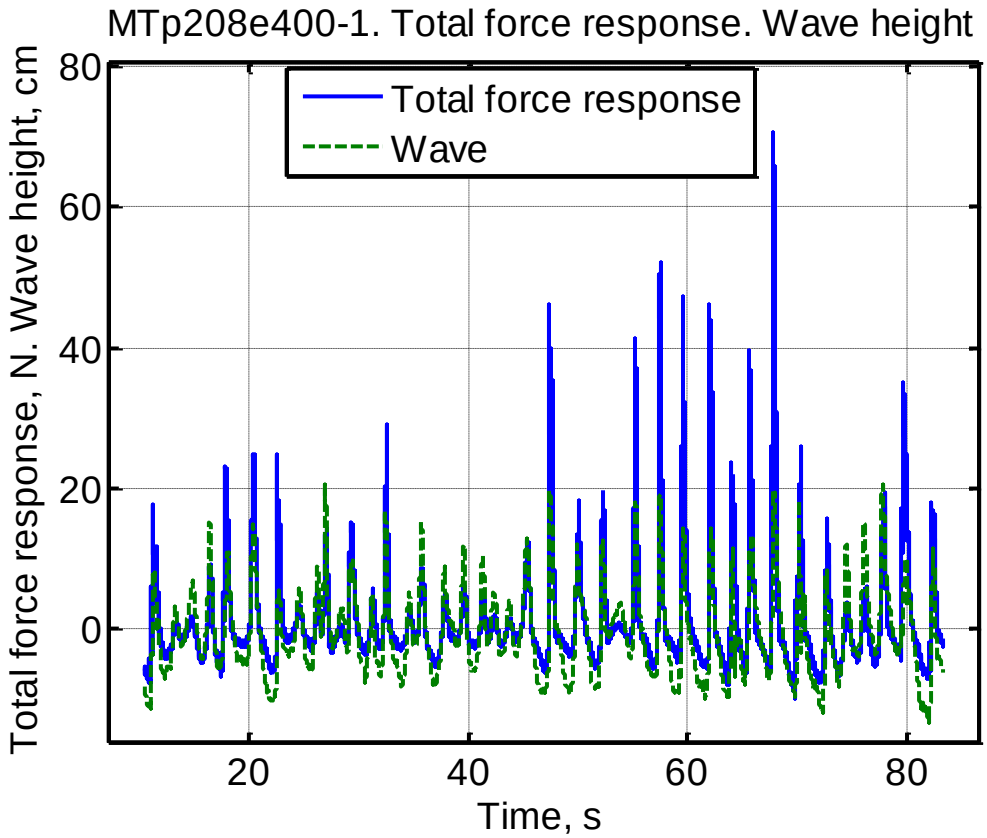

Figure 72: Time series of total force response, MTp208e400_1

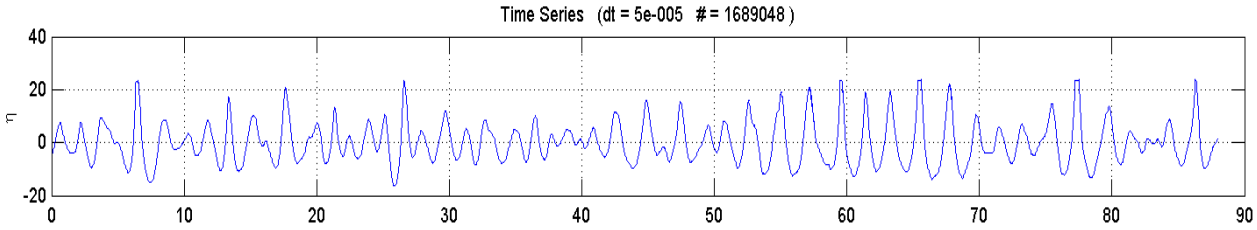

Time Domain Analysis

H_s	= 30.68	H_m	= 17.82	$A_{c,m}$	= 10.66		
T_s	= 2.014	H_{rms}	= 21.02	$A_{c,rms}$	= 13.02		
T_m	= 1.586	$H_{1/10}$	= 35.91	$A_{c,1/10}$	= 23.68		
T_{cfm}	= 0.3565	$H_{1/20}$	= 36.77	$A_{c,1/20}$	= 23.82		
σ_η	= 7.811	$H_{1/30}$	= 37.41	$A_{c,1/30}$	= 23.91		
skew	= 0.6548	$H_{1/50}$	= 38.06	$A_{c,1/50}$	= 23.99		
kurt-3	= 0.3106	$H_{1/100}$	= 38.06	$A_{c,1/100}$	= 23.99		
# waves	= 54	H_{max}	= 39.85	$A_{c,max}$	= 24		

Frequency Domain Analysis

H_{m0}	= 29.58	m_0	= 54.68
T_{m01}	= 1.75	m_1	= 196.3
T_{m02}	= 1.365	m_2	= 1158
T_{m24}	= 0.0006393	m_3	= 3.314e+006
T_{m10}	= 2.16	m_4	= 1.119e+011
T_p	= 2.016	ε_2	= 0.8021
		ε_4	= 1
GF	= 0.7662	Q_p	= 1.435

Data file: MTp208e400_1.csv
Channel: 7
zero-down-cross-analysis

Figure 73: Time series and analysis, MTp208e400_1

Data from Figure 73:

H_S = 0,3068m	measured significant wave height at intermediate water
T_P = 2,016s	measured peak period
h = 0,333m	local water depth, water depth at the structure
g = 9,81m/s	gravitational acceleration

Deep water wave length:

$$L_0 = \frac{g}{2\pi} \cdot T_P^2 = \frac{9,81}{2\pi} \cdot 2,016^2 = 6,346m \tag{52}$$

Depth limited wave height:

$$\frac{H_S}{h} = \frac{0,3068}{0,333} = 0,92 \tag{53}$$

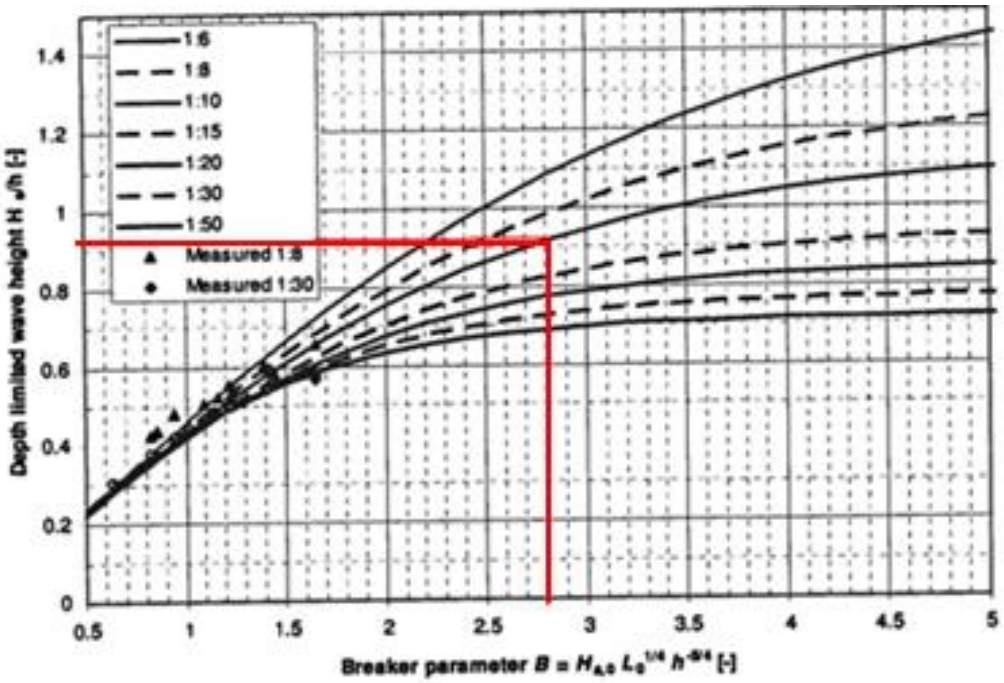

Figure 74: Significant wave height inside the surf zone Hs/h vs. B (Reedijk, et al. 2009)

From Figure 74 it is shown that the breaker parameter B = 2,8.

Significant wave height at deep water is then:

$$H_{S,0} = \frac{B}{L_0^{1/4} \cdot h^{-5/4}} = \frac{2,8}{6,346^{1/4} \cdot 0,333^{-5/4}} = 0,446m \tag{54}$$

Surf similarity parameter:

$$\xi_0 = \frac{\tan\theta}{\sqrt{\frac{H_{S,0}}{L_0}}} = \frac{0,1}{\sqrt{\frac{0,446}{6,346}}} = 0,38 \tag{55}$$

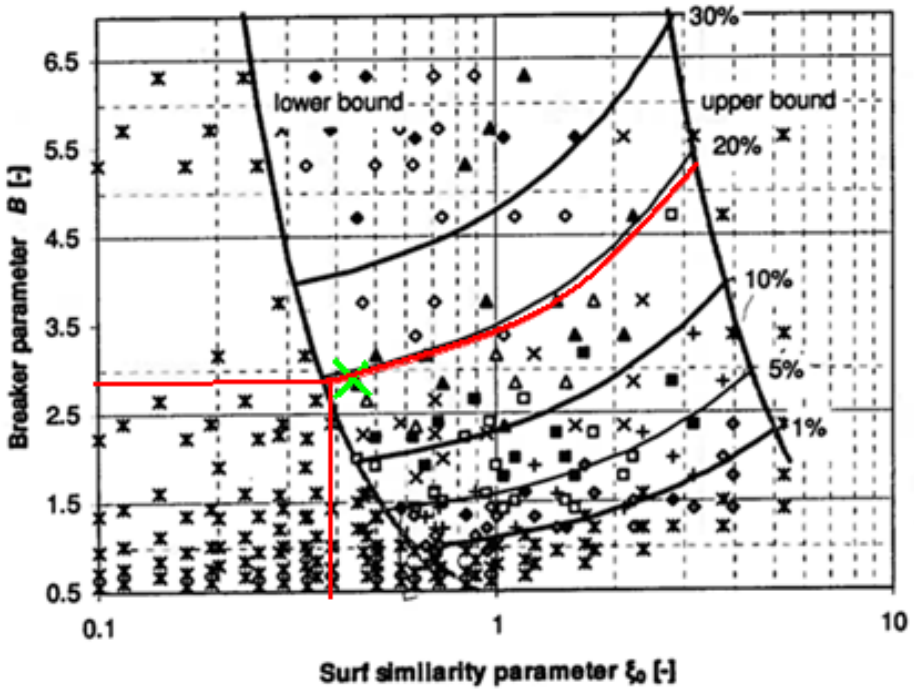

Figure 75: Occurrence of plunging breakers (Reedijk, et al. 2009)

Figure 75 shows that the probability of occurrence of plunging breaking waves in this case is about 19%.

5.5.4. MTp222e490_1:

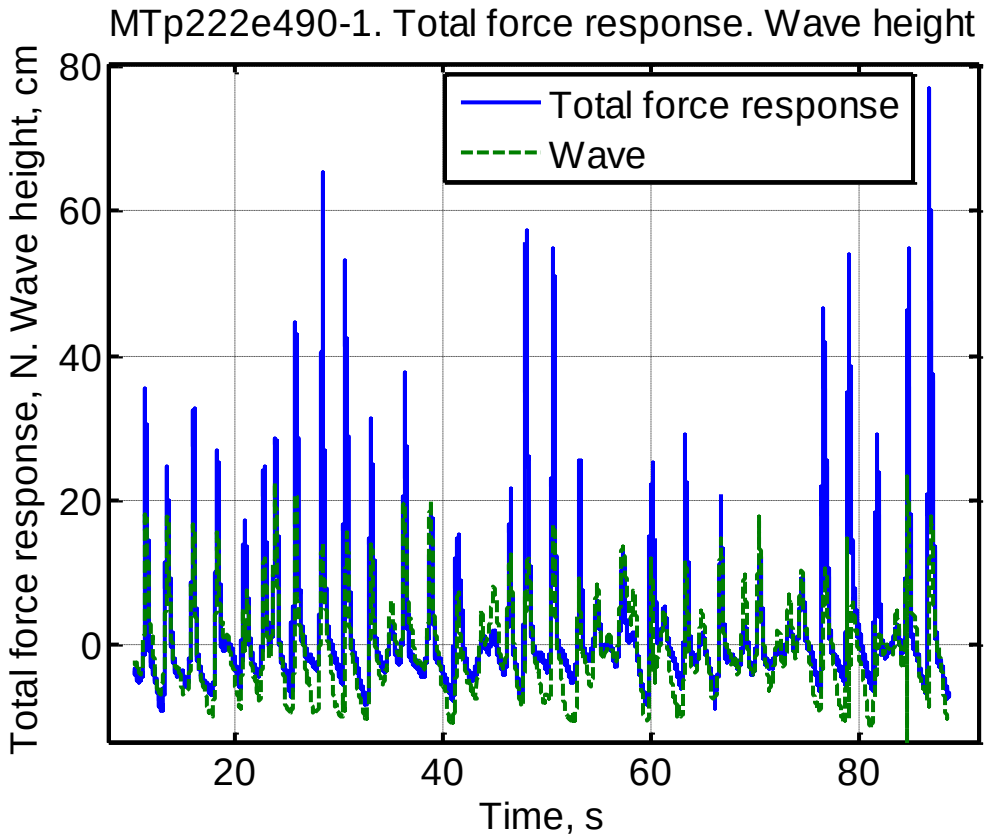

Figure 76: Time series of total force response, MTp222e490_1

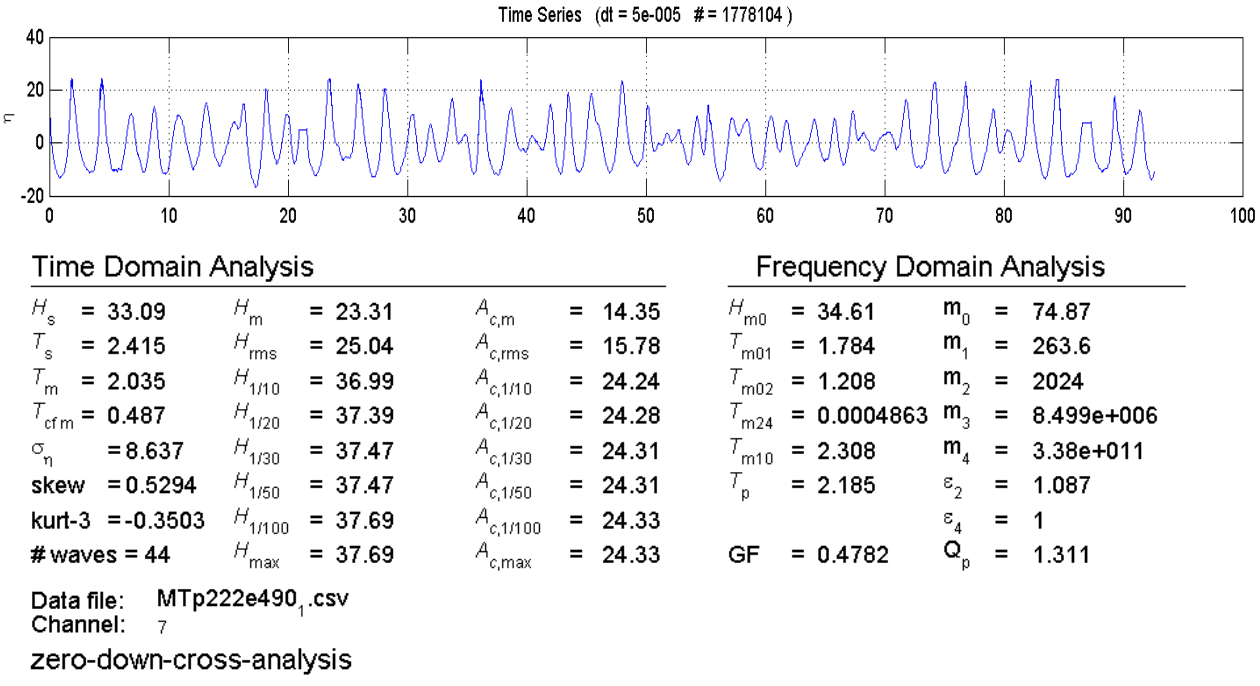

H_s	= 33.09	H_m	= 23.31	$A_{c,m}$	= 14.35	H_{m0}	= 34.61
T_s	= 2.415	H_{rms}	= 25.04	$A_{c,rms}$	= 15.78	T_{m01}	= 1.784
T_m	= 2.035	$H_{1/10}$	= 36.99	$A_{c,1/10}$	= 24.24	T_{m02}	= 1.208
T_{cfm}	= 0.487	$H_{1/20}$	= 37.39	$A_{c,1/20}$	= 24.28	T_{m24}	= 0.0004863
σ_η	= 8.637	$H_{1/30}$	= 37.47	$A_{c,1/30}$	= 24.31	T_{m10}	= 2.308
skew	= 0.5294	$H_{1/50}$	= 37.47	$A_{c,1/50}$	= 24.31	T_p	= 2.185
kurt-3	= -0.3503	$H_{1/100}$	= 37.69	$A_{c,1/100}$	= 24.33		
# waves	= 44	H_{max}	= 37.69	$A_{c,max}$	= 24.33	GF	= 0.4782

m_0	=	74.87	
m_1	=	263.6	
m_2	=	2024	
m_3	=	8.499e+006	
m_4	=	3.38e+011	
ε_2	=	1.087	
ε_4	=	1	
Q_p	=	1.311	

Figure 77: Time series and analysis, MTp222e490_1

Data from Figure 77:

H_S = 0,3309m	measured significant wave height at intermediate water
T_P = 2,185s	measured peak period
h = 0,333m	local water depth, water depth at the structure
g = 9,81m/s	gravitational acceleration

Deep water wave length:

$$L_0 = \frac{g}{2\pi} \cdot T_P^2 = \frac{9,81}{2\pi} \cdot 2,185^2 = 7,454m \tag{56}$$

Depth limited wave height:

$$\frac{H_S}{h} = \frac{0,3309}{0,333} = 0,99 \tag{57}$$

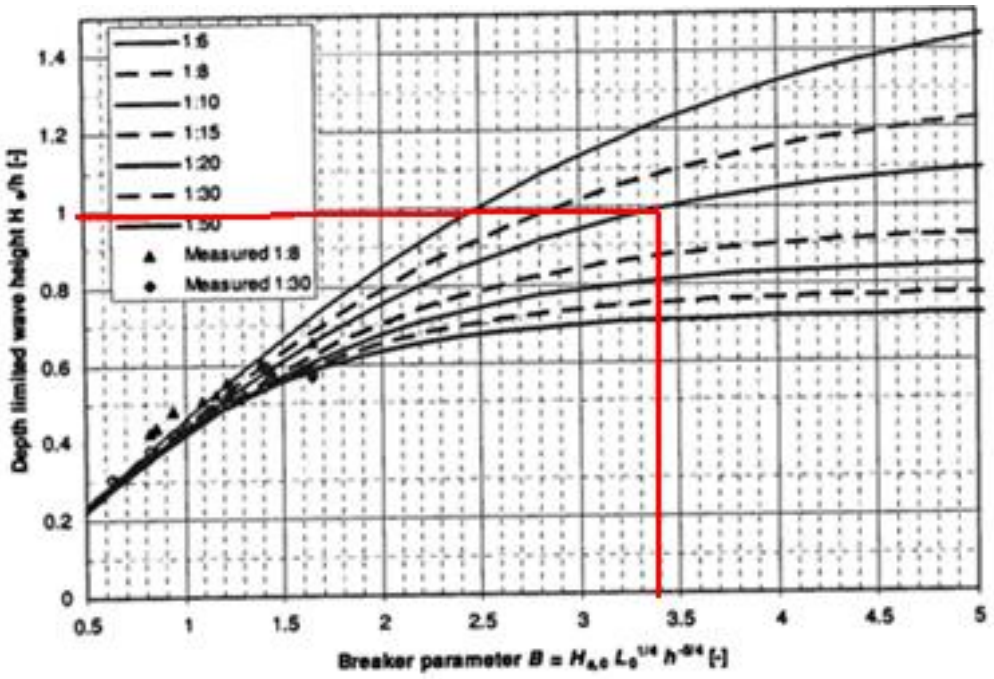

Figure 78: Significant wave height inside the surf zone Hs/h vs. B (Reedijk, et al. 2009)

From Figure 78 it is shown that the breaker parameter B = 3,4.

Significant wave height at deep water is then:

$$H_{S,0} = \frac{B}{L_0^{1/4} \cdot h^{-5/4}} = \frac{3,4}{7,454^{1/4} \cdot 0,333^{-5/4}} = 0,521m \tag{58}$$

Surf similarity parameter:

$$\xi_0 = \frac{\tan\theta}{\sqrt{\frac{H_{S,0}}{L_0}}} = \frac{0,1}{\sqrt{\frac{0,521}{7,454}}} = 0,38 \tag{59}$$

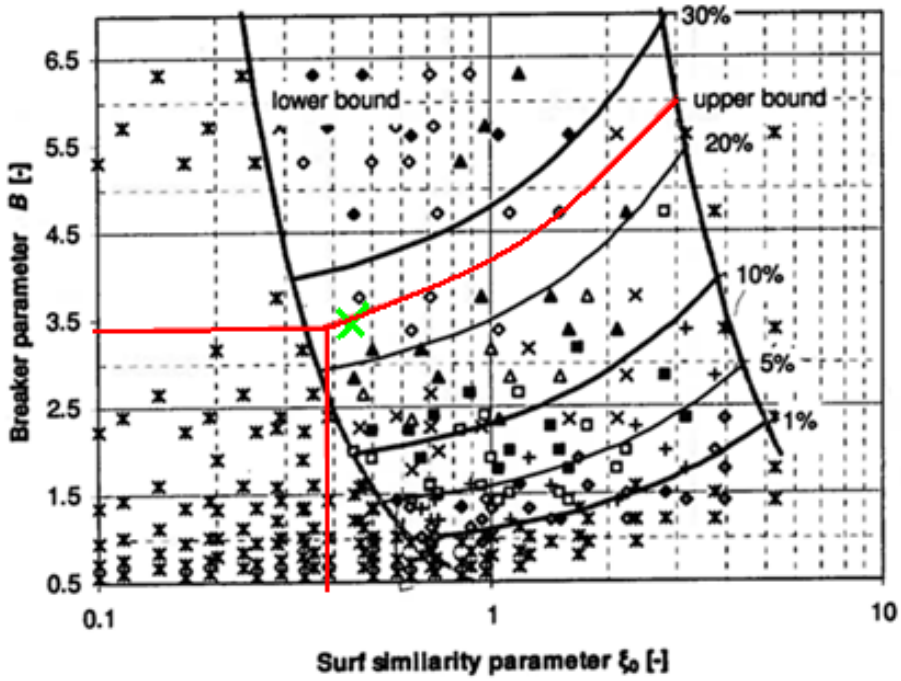

Figure 79: Occurrence of plunging breakers (Reedijk, et al. 2009)

Figure 79 shows that the probability of occurrence of plunging breaking waves in this case is about 25%.

5.5.5. Comments

Figure 65, 69, 73 and 77 show an extract from the analysis of irregular waves. The whole analysis of the four cases is in APPENDIX C.

Some of the cases are on the border between spilling breakers and plunging breakers. It is assumed that plunging breakers occur in all the cases, which was observed in all the four cases during model testing.

If another method is used to calculate significant wave height at deep water, a method described in Kysttenikk (Tørum, 1991), the results would be:

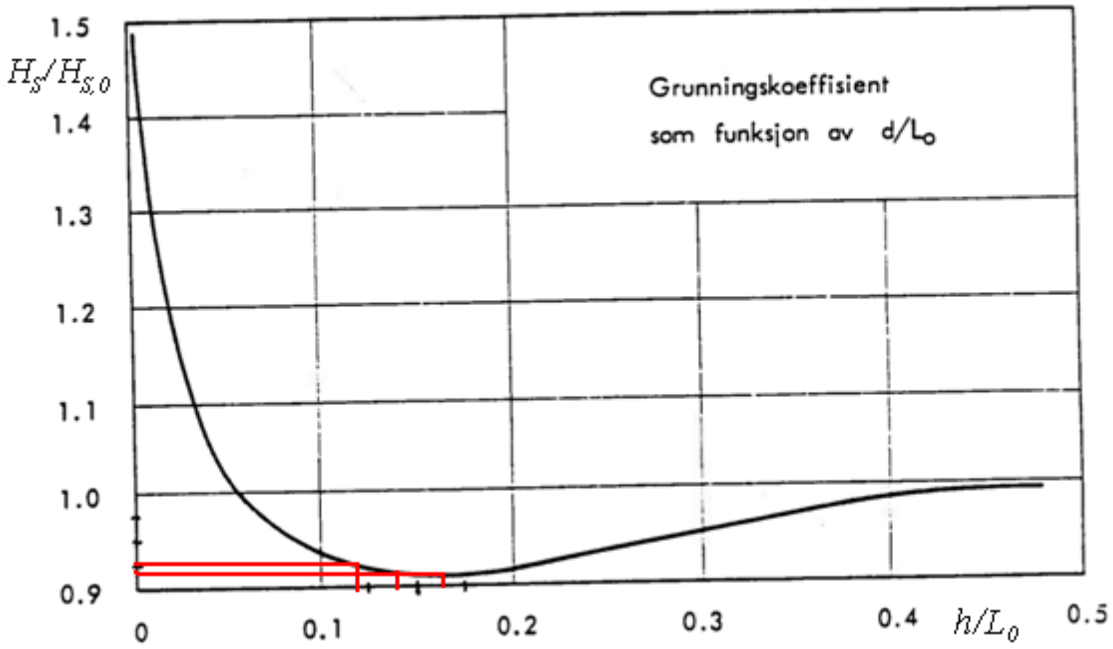

Figure 80: Priming coefficient as a function of h/L_0 (Tørum, 1991)

Figure 80 is used to find the ratio $H_S/H_{S,0}$, and then $H_{S,0}$.

- MTp185e330_1:

$$\frac{h}{L_0} = \frac{0,333}{5,471} = 0,165 \Rightarrow \frac{H_S}{H_{S,0}} \approx 0,92 \Rightarrow H_{S,0} = 0,222m \tag{60}$$

$$\xi_0 = \frac{\tan\theta}{\sqrt{\frac{H_{S,0}}{L_0}}} = \frac{0,1}{\sqrt{\frac{0,222}{5,471}}} = 0,50 \tag{61}$$

B = 1,5 (Figure 66)

⇨ The probability of occurrence of plunging breaking waves in this case is about 6%, see the green cross in Figure 67. This is within the plunging breaker area.

- MTp196e400_1:

$$\frac{h}{L_0} = \frac{0,333}{5,471} = 0,165 \Rightarrow \frac{H_S}{H_{S,0}} \approx 0,92 \Rightarrow H_{S,0} = 0,279m \tag{62}$$

$$\xi_0 = \frac{\tan\theta}{\sqrt{\frac{H_{S,0}}{L_0}}} = \frac{0,1}{\sqrt{\frac{0,279}{5,471}}} = 0,44 \tag{63}$$

B = 2,1 (Figure 70)

⇨ The probability of occurrence of plunging breaking waves in this case is about 11%, see the green cross in Figure 71. Also within the plunging breaker area.

- MTp208e400_1:

$$\frac{h}{L_0} = \frac{0,333}{6,346} = 0,142 \Rightarrow \frac{H_S}{H_{S,0}} \approx 0,92 \Rightarrow H_{S,0} = 0,333m \tag{64}$$

$$\xi_0 = \frac{\tan\theta}{\sqrt{\frac{H_{S,0}}{L_0}}} = \frac{0,1}{\sqrt{\frac{0,333}{6,346}}} = 0,44 \tag{65}$$

B = 2,8 (Figure 74)

⇨ The probability of occurrence of plunging breaking waves in this case is about 19%, see the green cross in Figure 75. Still inside the plunging breaker area.

- MTp222e490_1:

$$\frac{h}{L_0} = \frac{0,333}{7,454} = 0,121 \Rightarrow \frac{H_S}{H_{S,0}} \approx 0,93 \Rightarrow H_{S,0} = 0,356m \tag{66}$$

$$\xi_0 = \frac{\tan\theta}{\sqrt{\frac{H_{S,0}}{L_0}}} = \frac{0,1}{\sqrt{\frac{0,356}{7,454}}} = 0,46 \tag{67}$$

B = 3,4 (Figure 78)

⇨ The probability of occurrence of plunging breaking waves in this case is about 25%, see the green cross in Figure 79. Still inside the plunging breaker area.

If the method of Tørum (1991) is used to calculate the significant wave height in deep water, plunging breaking waves occurs with same probability as previous in all the four cases, as observed.

There are quite large uncertainties regarding reading error in the analyze method by Reedijk, et al. (2009), which can be the reason for that case MTp185e330_1 and MTp196e400_1 fell a bit outside the lower bound.

6. DISCUSSION

6.1. Uncertainties

6.1.1. Uncertainties in measurements

A large number of measurements have been executed, and all the tests where run as identical as possible. But there are several uncertainties in the measured results. This can be uncertainties in the equipment, in calibrations or in general human failure. An example of human failure is the calibration of the wave gauges. As explained in section 4.3, this is done by lifting and sinking the gauge ±10cm by hand. The reading is done by eye, and may therefore have some uncertainties.

The breaking wave gives some uncertainty due to air entrainment. The measured crest height seems smaller than what really occurs due to air entrance in the wave. This is seen from pictures taken in lab compared to measurements.

6.1.2. Analytical uncertainties

The procedure described by Määtänen (1979) is originally used to resolve ice forces from measured response forces on structures subjected to moving ice. The method should be applicable for wave slamming forces, but may need some adjustments.

There are quite large uncertainties regarding reading error in the method described by Reedijk, et al. (2009) for analyzing the probability of occurrence of plunging breakers in irregular waves.

6.2. Regular waves

6.2.1. Maximum response

It turned out during testing that maximum force response is given by waves that broke in front and surged against the structure, and not when the wave broke directly at the structure. The wave surged against the structure after breaking and imposed forces with a slamming character in both the top and bottom force transducers. It was smaller forces on the bottom transducers when the wave broke directly at the structure.

Figure 81: Mf048e280_1, first snap-shot of one wave

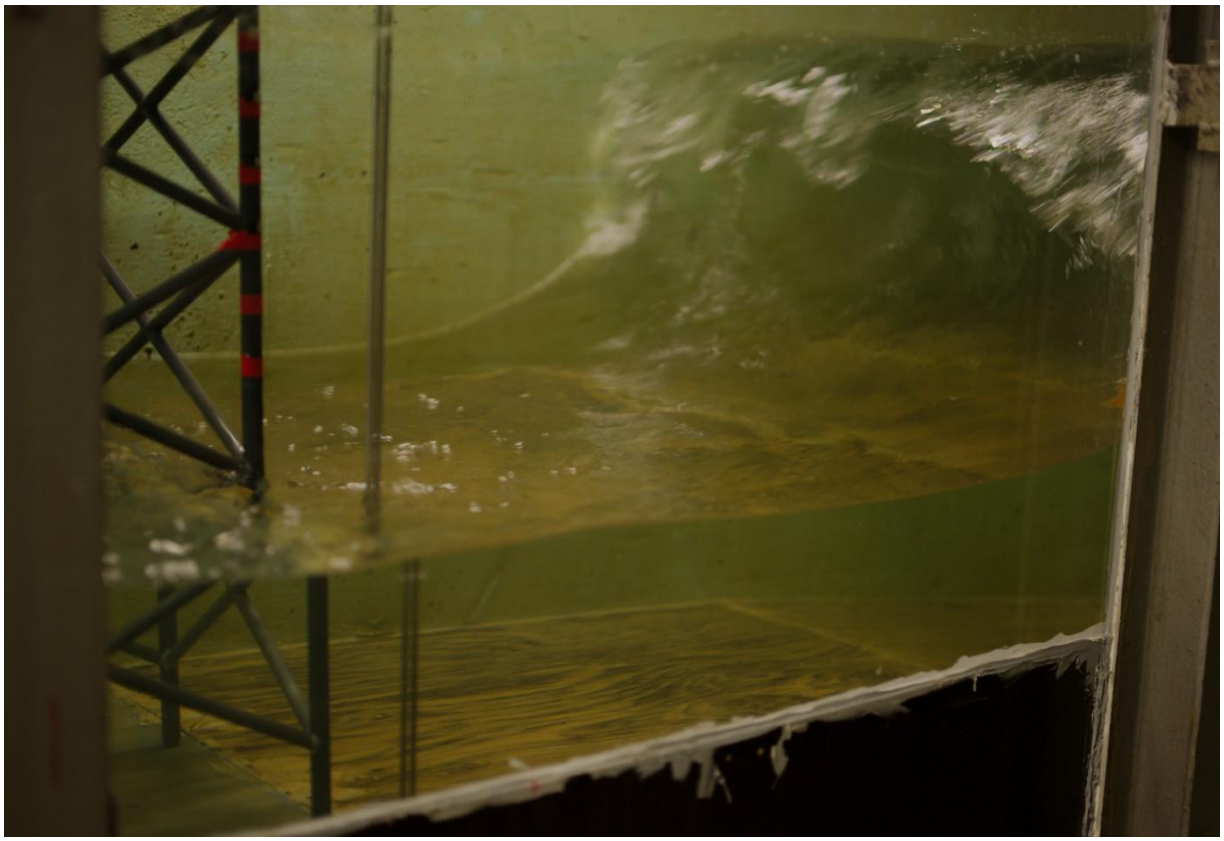

Figure 82: Mf048e280_1, second snap-shot of the same wave

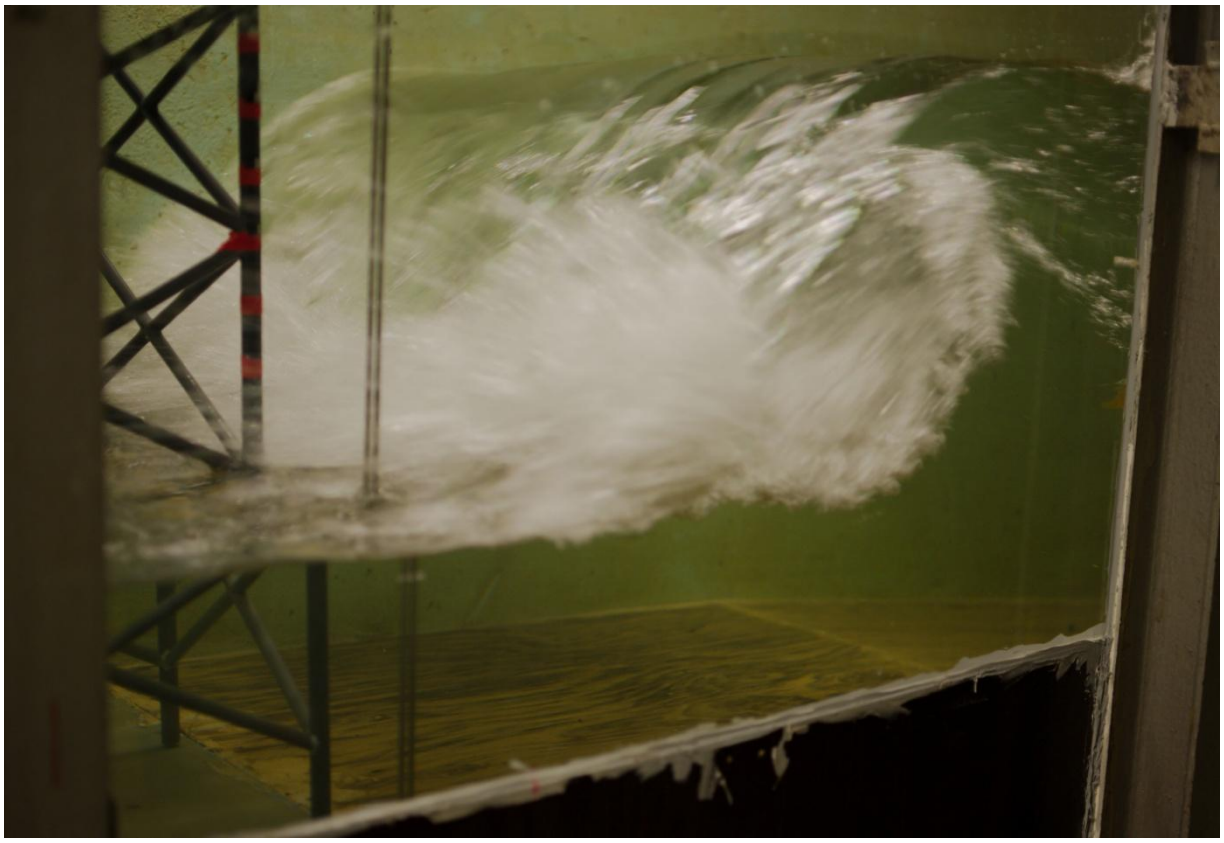

Figure 83: Mf048e280_1, third snap-shot of the same wave

Figure 84: Mf048e280_1, forth snap-shot of the same wave

Figure 81 to 84 is a series of pictures taken of a wave with frequency f = 0,48Hz and eccentricity e = 2,80. This is the wave that gave highest response within this frequency. It is clearly shown that the wave broke long before the structure, about 1,5m ahead of the structure, and surged against the structure.

6.2.2. Slamming force

Table 9: Measured and calculated slamming force

	f = 0,45Hz e = 2,70	f = 0,48Hz e = 2,80	f = 0,51Hz e = 2,65	f = 0,54Hz e = 2,65
Measured slamming force	**10,8N**	**12,4N**	**11,4N**	**17,1N**
Calculated slamming force (Wienke and Oumeraci)	**88,1N**	**83,5N**	**76,4N**	**75,7N**
Calculated slamming force (Goda)	**38,3N**	**36,0N**	**32,3N**	**32,0N**

The slamming force obtained from model testing is about half the measured response. The calculated slamming forces are larger than the measured slamming force in all four analyzed cases of regular waves, see Table 9. The reason for this may be scale effects and simultaneous hits at different points on the structure.

6.2.3. Response forces for different breaking points

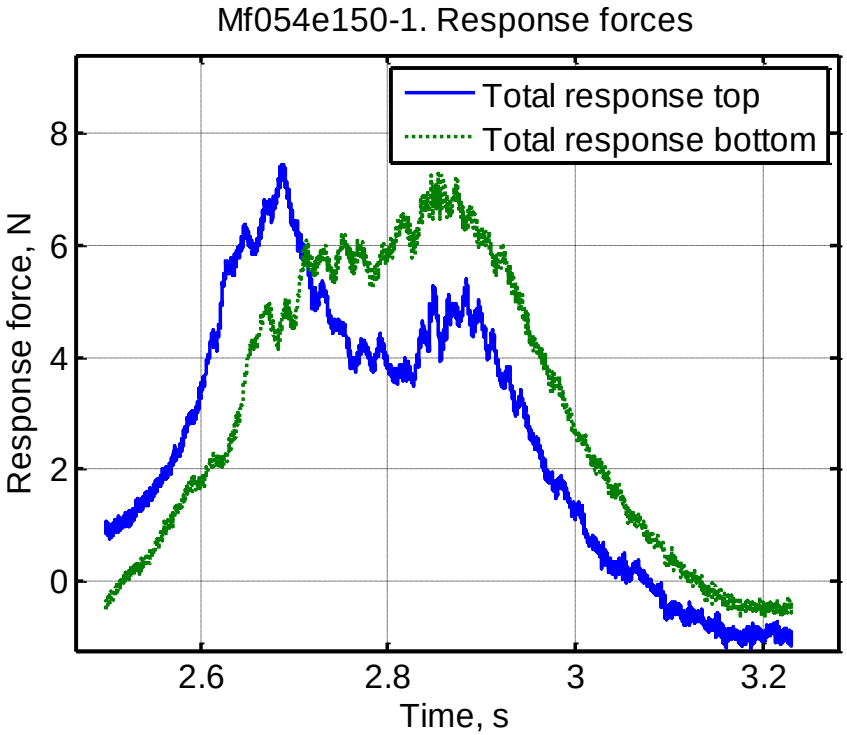

Figure 85: Total response at top and bottom force transducers, Mf054e150_1

Figure 85 shows the response forces at top and bottom of the structure for a regular wave with frequency f = 0,54Hz and eccentricity e = 1,50. This wave did not break.

Figure 86: Snap-shot, Mf054e200_2

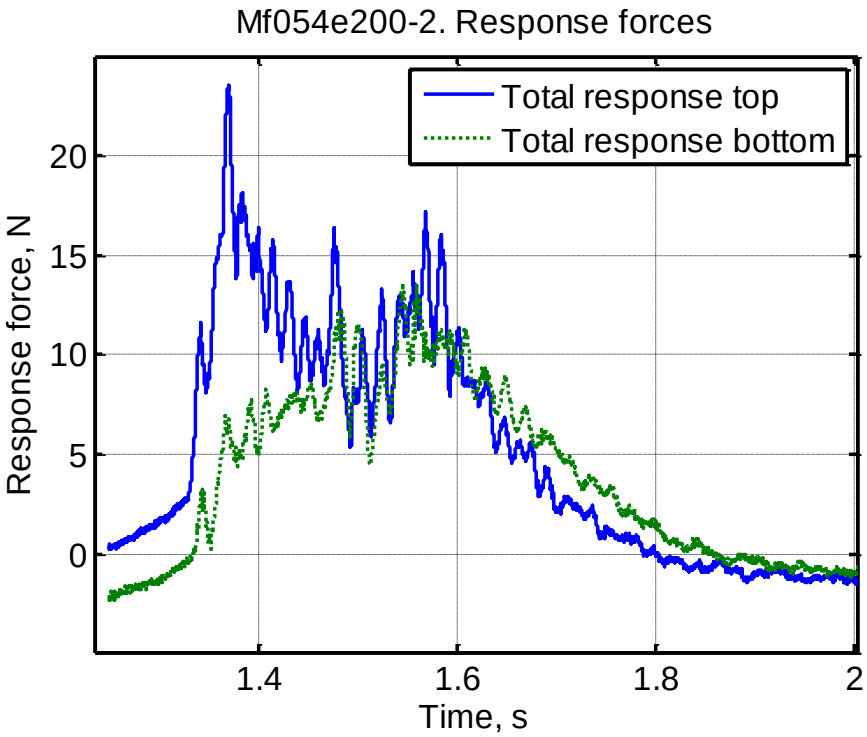

Figure 87: Total response at top and bottom force transducers, Mf054e200_2

Figure 87 shows the response forces at top and bottom of the structure for a regular wave with frequency f = 0,54Hz and eccentricity e = 2,00. This wave broke straight at the structure, as the snap-shot of the same wave in Figure 86 shows.

Figure 88: Snap-shot, Mf054e265_1

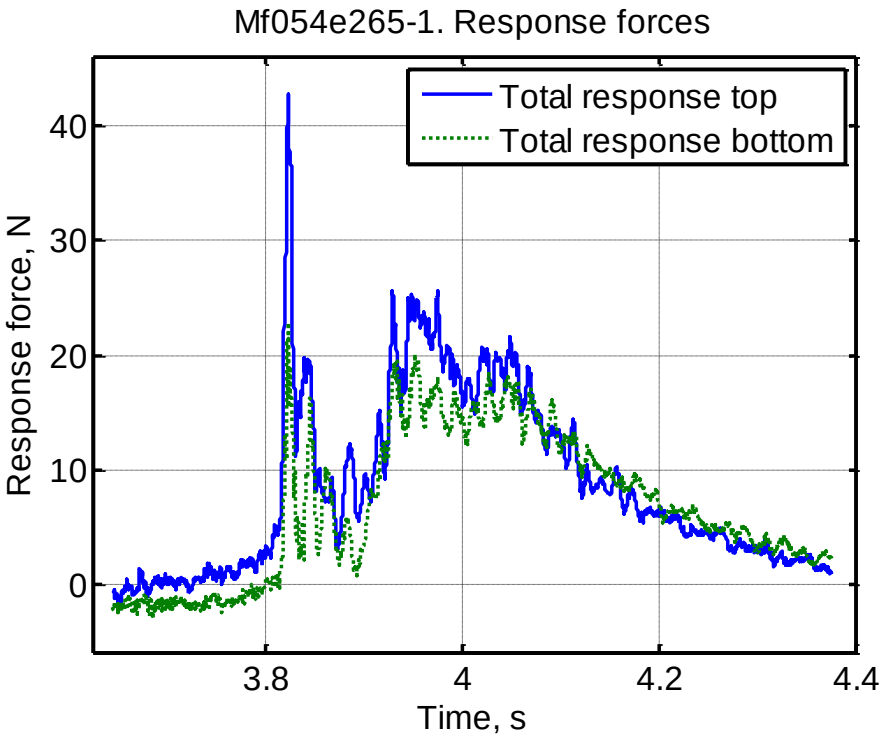

Figure 89: Total response at top and bottom force transducers, Mf054e265_1

Figure 89 shows the response forces at top and bottom of the structure for a regular wave with frequency f = 0,54Hz and eccentricity e = 2,65. This is the wave that gave largest response and slamming force within this frequency. The wave broke about 0,5m before the structure, which a snap-shot of this wave, Figure 88, shows.

Figure 90: Snap-shot, Mf054e290_1

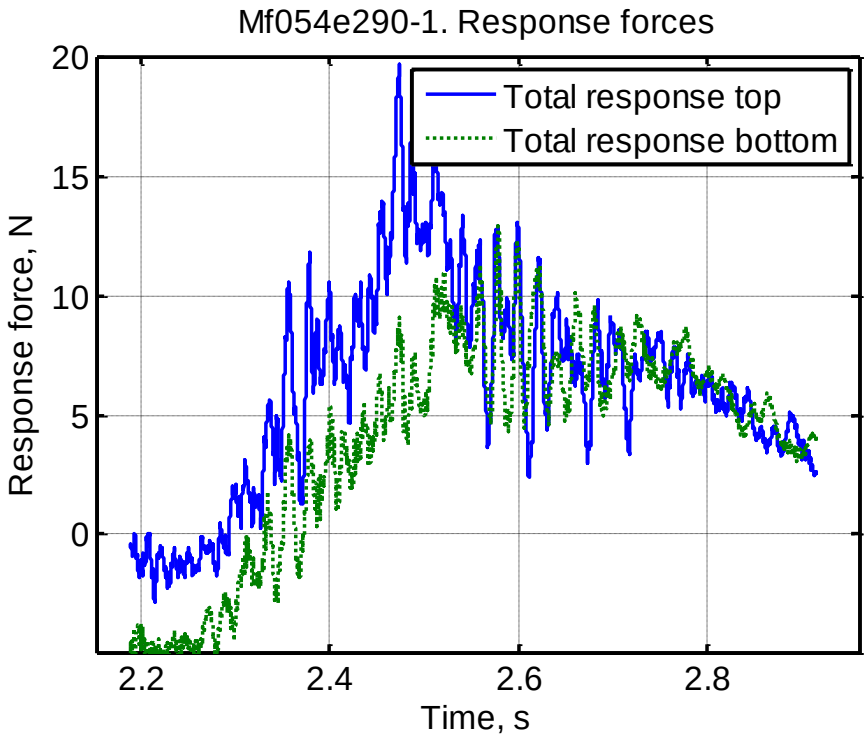

Figure 91: Total response at top and bottom force transducers, Mf054e290_1

Figure 91 shows the response forces at top and bottom of the structure for a regular wave with frequency f = 0,54Hz and eccentricity e = 2,90. This wave broke about 0,9m before the structure, as can be seen from the snap-shot of the same wave in Figure 90.

Figure 85, 87, 89 and 91 shows how the response forces at top and bottom of the structure changes for different waves with different breaking points. Total response is larger at the top transducers than at the bottom transducers when the wave broke straight at, or before the structure.

The response pattern and magnitude is quite similar at top and bottom of the structure for the non-breaking wave, but with a time-delay on the bottom transducers, see Figure 85.

It can be seen from Figure 87 and 89 that the response force is higher when the wave broke ahead of the structure then for when the wave broke directly at the structure. The surging wave, Figure 89, gives higher forces on the bottom transducers.

There are quite large variations of the response forces and wave heights from wave to wave, as shown in Figure 92.

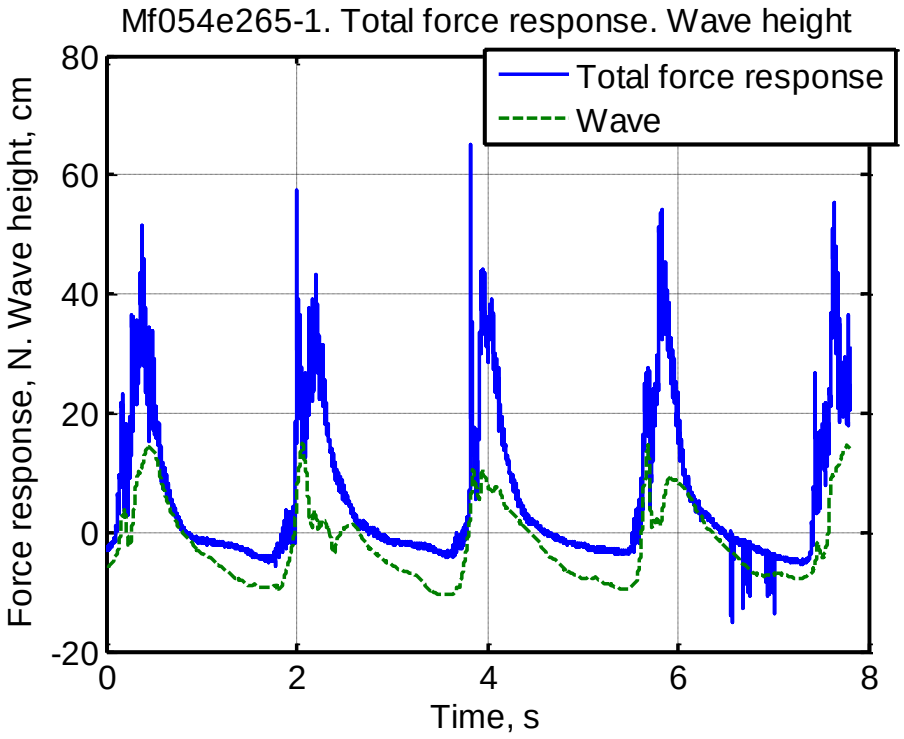

Figure 92: Total force response and wave height, Mf054e265_1

6.3. Irregular waves

6.3.1. Probability of plunging breakers

It was observed plunging breaking waves during model testing of the irregular waves.

The probability of plunging breakers is from 6-25% in the four analyzed cases. Larger wave periods gave greater possibility of plunging breakers.

There are quite large uncertainties regarding reading error in the analyze method by Reedijk, et al. (2009), which can be the reason for that some of the cases was on the border between spilling and plunging breakers.

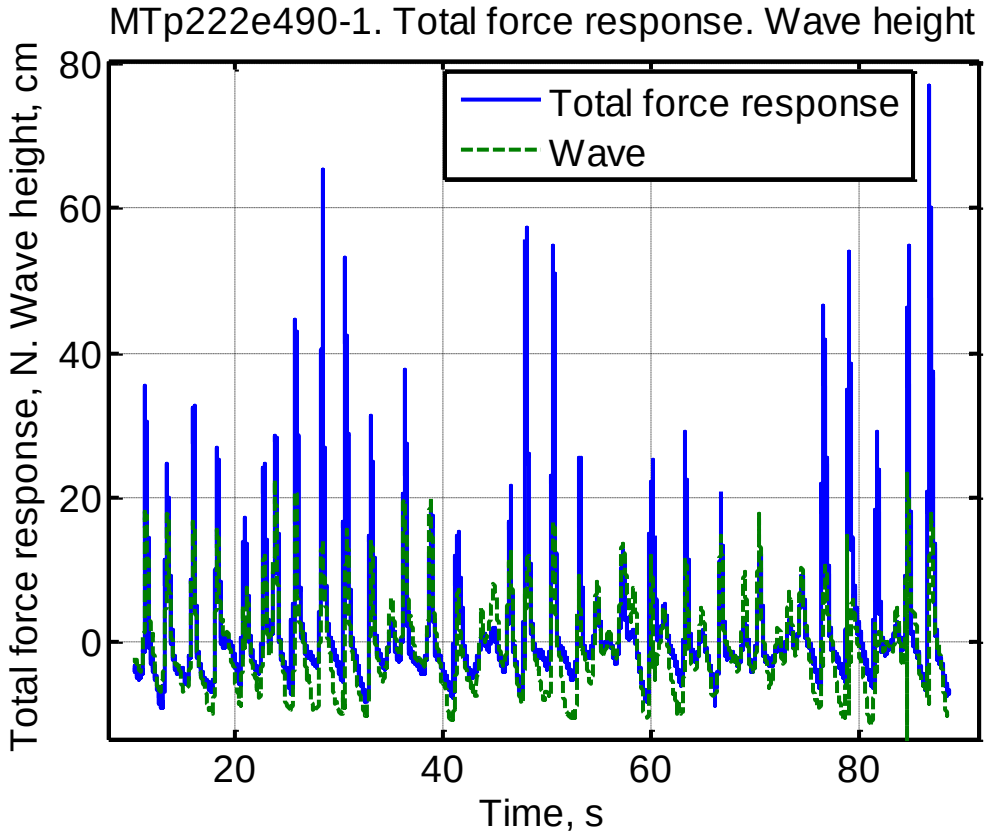

Figure 93: Time series of total force response, MTp222e490_1

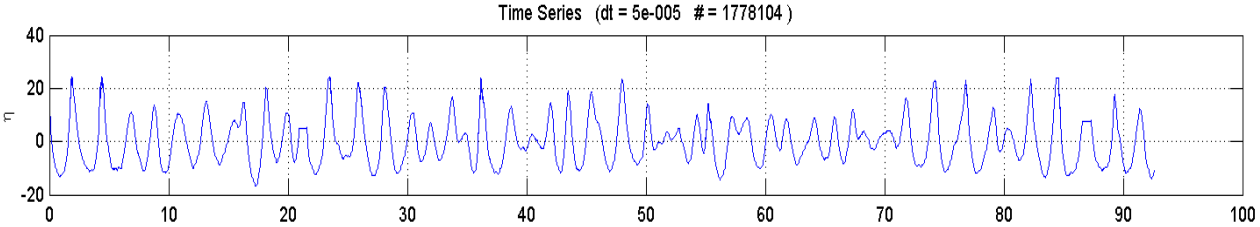

Figure 94: Time series, MTp222e490_1

Figure 93 and 94 show the time series for one specific run of irregular waves. Peak period T_P = 2,22s and eccentricity e = 4,90. The wave tops in Figure 94, the waves with a surface elevation, η, larger than $\eta \approx 20$cm, are counted to 10. This is about 24% of all the waves in this time series, ≈ 42.

From the analysis of irregular waves (see section 5.5.4), this wave-run gave a probability of plunging breakers ≈ 25%, which is corresponding well with the counting of tops on the time series.

6.4. The duration of impact

The duration of impact are calculated for the front part of the structure for all regular waves in APPENDIX B.

The values are very small:

- $\tau \approx 0{,}008$ (Wienke and Oumeraci, 2005)
- $\tau \approx 0{,}020$ (Goda, et al. 1966)

The duration of impact seems to be larger for a truss structure then for a pile. This may be because the wave hits the front part and back part at slightly different time points. The formulas for duration of impact for a pile can possibly not be used for a truss structure.

6.5. Duhamel integral

The Duhamel integral cannot easily be used for analyzing the truss support structure. This is because a truss structure is too complicated. The wave is first slamming in the front of the structure, and then on the back side of the structure.

Wienke and Oumeraci (2005) and Arntsen, et al. (2011) used the Duhamel integral approach when analyzing their response force data on single piles.

6.6. Air entrainment and scale effects

The results of previous investigation suggest that there are only minor differences between the process of air entrainment by breaking waves in freshwater and seawater. The bubble sizes are also comparable.

Previous investigation (Blenkinsopp and Chaplin, 2011) also suggest that the total volume of air entrained will scale geometrically, though pressure effects will increase with scale, but the bubble sizes will remain approximately the same at all scales. It must therefore be large differences in the temporal evolution of bubble plumes generated at model and full scale. The entrained bubble plume in breaking waves disperses much more slowly in large-scale than in small-scale. This will have the effect of significantly increasing the compressibility of the air-water mixture and will reduce the propagation speed of pressure waves.

The effect of scale may therefore impact interpretation of the results.

Since the bubble sizes of entrained air are the same at all scales, small-scale model testing may have a cushion effect. The entrained air will cushion the pressure on the structure in small-scale.

6.7. Expanded work

There have been manufactured a one-sided model; the structure is split in different parts to measure the wave forces on the individual parts. This thesis does not include testing on this model due to lack of time. This model needs to be tested to get more information about the truss structure. It should also be run tests with an additional slope.

The other hammer plucking tests should be used for further analysis. The individual response forces for each force transducer should be analyzed. The system may have to be considered as a multi degree of freedom system.

The experiments in the large wave channel in Hannover are planned to be in the spring of 2013. Some of the challenges in these tests are to resolve the slamming forces on the individual members of the truss structure.

7. CONCLUSION

Different researchers of breaking waves have agreed on the formulas used to calculate the slamming force on single piles, but have different theories on the value of the slamming, curling and duration of impact factor. This causes uncertainties in the dimension of structures exposed to these kinds of forces, and are therefore still under investigation.

Maximum force response is given by waves that broke some distance away from the truss structure and not when the wave broke directly at the structure. The wave broke ahead and surged against the structure, which imposed forces with a slamming character in both the top and bottom force transducers. It was smaller slamming forces on the bottom transducers when the wave broke directly at the structure.

The probability of plunging breakers is from 6-25% in the four analyzed cases of irregular waves. Larger wave periods give greater possibility of plunging breakers.

The slamming force obtained from model testing of the regular waves is about half the measured response. The calculated slamming forces based on both Goda, et al. (1966) and Wienke and Oumeraci (2005) are larger than the measured slamming force. It is significant air entrained in the water during the breaking process, which may influence the results differently in small-scale model testing and in reality. The reason for this may be scale effects that may impact interpretation of the results. The measured crest height is smaller than in reality due to air entrainment in the waves as well.

The use of freshwater in the model testing can be considered valid, as that there are only minor differences between the process of air entrainment by breaking waves in freshwater and seawater. The bubble sizes are also comparable.

The plunging breaking waves may hit different parts of the front section at slightly different time points, thus reducing the response force compared to a single pile.

The simplified analyzing method seems promising.

REFERENCES

Arntsen, Ø. A., Ros Collados, X., & Tørum, A. (2011). Impact forces on a vertical pile from plunging breaking waves. *Proc. of the International Conference Coastal Structures.* Shanghai.

Aune, L. (2011). *Master thesis: Bølgjeslag mot jacket på grunt vatn.* Department of Structural Engineering. Trondheim: NTNU.

Battjes, J. A. (1974). Surf similarity parameter. *14th Int. Conf. on Co. Eng., ASCE,* (pp. 69-85). Copenhagen.

Blenkinsopp, C., & Chaplin, J. (2011). Void fraction measurements and scale effects in breaking waves in freshwater and seawater. *Coastal Engineering*(58), 417-428.

Dytran Instruments, I. (u.d.). *Operating guide, Model series 5800B, Dynapulse impulse hammer with BNC connector.*

Goda, Y., Haranka, S., & Kitahata, M. (1966). Study on impulsive breaking wave forces on piles. *Port and harbour technical research institute*(6), 1-30.

HBM. (u.d.). *Force transducer, Mounting instructions.*

Holmedal, L. E. (2009). *Lecture notes in subject TBA4270 Coastal Engineering: Sediment Transport.* Department of Civil and Transport Enginnering. Trondheim: NTNU.

IEC 61400-3. (2009). International Standard: Wind turbines - Part 3: Design requirements for offshore wind turbines.

ISO 21650. (2007). International Standard: Actions from waves and currents on coastal structures.

Kamphuis, J. W. (2000). *Introduction to coastal engineering and management.* World Scientific Publishing Co. Pte. Ltd.

McCowan, J. (1894). On the Highest Wave of Permanent Type. *Phil. Mag. Ser. 5*(36), 351-358.

Morison, J., O'Brian, M., Johnson, J., & Schaaf, S. (1950). The forces exerted by surface waves on piles. *Journal of Petrolium Technology, Petrolium Transactions*(189), 149-154.

Munk, W. (1949). The Solitary Wave Theory and its Application to Surf Problem. *Ann. New York Acad. Sci.*(51), 376-423.

Määtänen, M. (1979). Laboratory tests for dynamic ice-structure interaction. *Proceedings "Port and Ocean Engineering under Arctic Conditions" (POAC).* Trondheim: Norwegian Institute of Tecknology.

Næss, A. (2007). *Lecture notes: An introduction to random vibrations.* Center for Ships and Ocean Structures. Trondheim: NTNU.

Reedijk, J. S., Muttray, M., & Bergmann, H. (2009). Risk Awareness - Key to a Sustainable Design Approach for Breakwater Armouring. *Proceedings: Coasts, Marine Structures and Breakwaters.* Edinburgh.

Ros Collados, X. (2011). *Master thesis: Impact forces on a vertical pile from plunging breaking waves.* Department of Civil and Transport Engineering. Trondheim: NTNU.

Swaragi, T., & Nochino, M. (1984). Impact forces of nearly breaking waves on a vertical circular cylinder. *Coastal Engineering in Japan*(27), 249-263.

Tanimoto, K., Takahashi, S., Kaneco, T., & Shiota, K. (1986). Impulsive breaking wave forces on an inclined pile exerted by random waves. *Proceedings of the 20th International Conferece on Coastal Engineering*, (ss. 2288-2302).

Tørum, A. (1991). *Lecture notes: Kystteknikk.* Department of Structural Engineering. Trondheim: NTH.

Tørum, A. (2011). *Industrial proposal 2.* Department of Civil and Transport Engineering. Trondheim: NTNU.

von Karman, T. (1929). *The impact on seaplane floats during landing.* National Advisory Committee for Aeronautics.

Wagner, H. (1932). Über Stoβ-und Gleitvorgänge an der Oberfläche von Flüssigkeiten. *Zeitschrift für angewandte Mathematik und Mechanic*(12), 193-215.

Wienke, J., & Oumeraci, H. (2005). Breaking wave impact forces on a vertical and inclined slender pile - theoretical and large scale model investigations. *Coastal Engineering*(52), 435-462.

LIST OF SYMBOLS

a	=	wave amplitude
c	=	damping constant
d	=	water depth
d_b	=	depth of water at breaking
du/dt	=	water particle acceleration
f(t)	=	time history
f(t)	=	measured response force
f_l	=	line force
g	=	gravitational acceleration
h	=	local water depth
h(t)	=	impulse response function
k	=	stiffness
l	=	length of diagonal rods impact area
m	=	mass per unit length
t	=	time
t_*	=	time of duration impact
u	=	water particle velocity
z	=	upward vertical direction
B	=	breaker parameter
C	=	wave celerity
C_b	=	breaking wave celerity
C_D	=	drag coefficient
C_M	=	inertia coefficient
C_S	=	slamming factor
D	=	pile diameter
D_1	=	leg diameter of the truss structure
D_2	=	diameter of diagonal rod
E	=	elastic modulus
F_D	=	drag force
F_M	=	inertia force
F_S	=	slamming force
F(t)	=	measured wave slamming force
H	=	wave height
H_b	=	breaking wave height
H_S	=	measured significant wave height at intermediate water
$H_{S,0}$	=	significant wave height at deep water

$H(\omega)$	=	frequency response function (FRF)
I	=	area moment of inertia
I'	=	impulse load
KC	=	Keulegan Carpenter number
L	=	wave length
L_{bp}	=	breaking wave length with peak period
L_0	=	wave length in deep water
L_b	=	wave length at breaking
R	=	cylinder radius
Re	=	Reynolds number
$S(\omega)$	=	linear spectrum of the applied force
T	=	wave period
T_d	=	natural period
T_P	=	measured peak period
T'	=	total duration of impact
V	=	wave celerity
η	=	surface elevation
η_b	=	maximum surface elevation at breaking
ξ	=	damping ratio
ξ_0	=	surf similarity parameter
$\rho_w=\rho$	=	water density
λ	=	curling factor
λ_{max}	=	maximum curling factor
ω	=	angular frequency
ω_e	=	natural frequency
ω_d	=	damped frequency
τ	=	time of duration impact
ν	=	kinematic viscosity
γ	=	angle

APPENDIX A

MASTER DEGREE THESIS

Spring 2012

for

Student: Miriam Zakri Aashamar

Wave slamming forces on truss support structures for wind turbines

BACKGROUND

Wind turbine foundation structures in shallow water may be prone to slamming forces from breaking waves in shallow water, typically plunging breaking waves.

Reinertsen A/S has been involved in the design of a truss support structure for wind turbines on the Thornton Bank, Belgian Coast. Plunging breaking waves has been specified for this area. Calculations show that the forces from the plunging breaking waves are governing the responses of the structure and the foundations. However, there are considerable uncertainties on the calculated plunging breaking wave forces.

A fairly large research project has been proposed, involving large scale experiments in the Large Wave Channel, Hannover, Germany. The objective of the proposed research is to obtain improved knowledge of wave kinematics and forces from waves breaking, especially wave slamming forces on truss structures through model tests on a large scale. The obtained results will be used for response analysis of a specified truss structure and the results will be compared with existing guidelines, which may consequently be improved.

TASK DESCRIPTION

The thesis work will mainly be model testing of such a structure in a wave flume using an existing 1:50 scale model of a truss structure. The test program may be changed as results are obtained. But the following tasks are envisaged: The tests will be run with regular as well as irregular waves. It is planned to split the structure in different parts to measure the wave forces on the individual parts. The bottom slope has been approximately 1:10 in the tests run by Ros (2011) and Aune (2011). However, if time permits, tests should be run also with an additional slope, say 1:30 or 1:50.

General about content, work and presentation

The text for the master thesis is meant as a framework for the work of the candidate. Adjustments might be done as the work progresses. Tentative changes must be done in cooperation and agreement with the professor in charge at the Department.

In the evaluation thoroughness in the work will be emphasized, as will be documentation of independence in assessments and conclusions. Furthermore the presentation (report) should be well organized and edited; providing clear, precise and orderly descriptions without being unnecessary voluminous.

The report shall include:

- Standard report front page (from DAIM, http://daim.idi.ntnu.no/)
- Title page with abstract and keywords.(template on: http://www.ntnu.no/bat/skjemabank)
- Preface
- Summary and acknowledgement. The summary shall include the objectives of the work, explain how the work has been conducted, present the main results achieved and give the main conclusions of the work.
- Table of content including list of figures, tables, enclosures and appendices.
- If useful and applicable a list explaining important terms and abbreviations should be included.
- The main text.
- Clear and complete references to material used, both in text and figures/tables. This also applies for personal and/or oral communication and information.
- Text of the Thesis (these pages) signed by professor in charge as Attachment 1..
- The report musts have a complete page numbering.

Advice and guidelines for writing of the report is given in: "Writing Reports" by Øivind Arntsen. Additional information on report writing is found in "Råd og retningslinjer for rapportskriving ved prosjekt og masteroppgave ved Institutt for bygg, anlegg og transport" (In Norwegian). Both are posted posted on http://www.ntnu.no/bat/skjemabank

Submission procedure

Procedures relating to the submission of the thesis are described in DAIM (http://daim.idi.ntnu.no/).

Printing of the thesis is ordered through DAIM directly to Skipnes Printing delivering the printed paper to the department office 2-4 days later. The department will pay for 3 copies, of which the institute retains two copies. Additional copies must be paid for by the candidate / external partner.

On submission of the thesis the candidate shall submit a CD with the paper in digital form in pdf and Word version, the underlying material (such as data collection) in digital form (eg. Excel). Students must submit the submission form (from DAIM) where both the Ark-Bibl in SBI and Public Services (Building Safety) of SB II has signed the form. The submission form including the appropriate signatures must be signed by the department office before the form is delivered Faculty Office.

Documentation collected during the work, with support from the Department, shall be handed in to the Department together with the report.

According to the current laws and regulations at NTNU, the report is the property of NTNU. The report and associated results can only be used following approval from NTNU (and external cooperation partner if applicable). The Department has the right to make use of the results from the work as if conducted by a Department employee, as long as other arrangements are not agreed upon beforehand.

Tentative agreement on external supervision, work outside NTNU, economic support etc.
Separate description to be developed, if and when applicable. See http://www.ntnu.no/bat/skjemabank for agreement forms.

Health, environment and safety (HSE) http://www.ntnu.edu/hse
NTNU emphasizes the safety for the individual employee and student. The individual safety shall be in the forefront and no one shall take unnecessary chances in carrying out the work. In particular, if the student is to participate in field work, visits, field courses, excursions etc. during the Master Thesis work, he/she shall make himself/herself familiar with " Fieldwork HSE Guidelines". The document is found on the NTNU HMS-pages at http://www.ntnu.no/hms/retningslinjer/HMSR07E.pdf

The students do not have a full insurance coverage as a student at NTNU. If you as a student want the same insurance coverage as the employees at the university, you must take out individual travel and personal injury insurance.

Start and submission deadlines
The work on the Master Thesis starts on January 16, 2012

The thesis report as described above shall be submitted digitally in DAIM at the latest at 3pm June 11, 2012

Professor in charge: Øivind Asgeir Arntsen
Other supervisors: Alf Tørum

Trondheim, January 16, 2012. (Revised: 23.05.2012)

Professor in charge (sign)

APPENDIX B

Regular wave analyze and calculation of all tests.

Table 10: Measured response and calculated slamming force, f = 0,45Hz

f [Hz]	T [s]	e	Response [N]	Slamming force [N]	ηb [m]	ληb [m]		Hb [m]	τ [s]		Cb [m/s]	l [m]		Slamming force [N]	
			Measured	Measured		(W&O)	(Goda)		(W&O)	(Goda)		(W&O)	(Goda)	(W&O)	(Goda)
0,45	2,22	120	0,6	0,1	0,114	0,052	0,046	0,169	0,008	0,020	2,09	0,188	0,144	54,2	21,9
0,45	2,22	170	12,9	6,4	0,185	0,085	0,074	0,256	0,008	0,019	2,25	0,314	0,284	103,6	46,1
0,45	2,22	190	22,6	9,0	0,171	0,079	0,068	0,244	0,008	0,019	2,22	0,282	0,248	91,6	40,1
0,45	2,22	200	15,1	5,9	0,182	0,084	0,073	0,254	0,008	0,019	2,25	0,302	0,272	100,0	44,4
0,45	2,22	210	16,2	7,7	0,165	0,076	0,066	0,234	0,008	0,019	2,21	0,272	0,236	87,3	37,9
0,45	2,22	220	20,8	8,3	0,136	0,063	0,054	0,214	0,008	0,020	2,14	0,212	0,176	65,7	27,8
0,45	2,22	230	17,4	5,5	0,114	0,052	0,046	0,187	0,008	0,020	2,09	0,188	0,144	54,2	21,9
0,45	2,22	240	16,7	9,8	0,169	0,078	0,068	0,252	0,008	0,019	2,22	0,282	0,248	90,8	52,4
0,45	2,22	250	23,1	10,2	0,118	0,054	0,047	0,204	0,008	0,020	2,10	0,182	0,152	54,5	23,2
0,45	2,22	260	15,7	7,9	0,191	0,088	0,076	0,270	0,008	0,019	2,27	0,324	0,296	108,1	48,4
0,45	2,22	270	27,1	10,8	0,167	0,077	0,067	0,264	0,008	0,019	2,21	0,272	0,236	88,1	38,3
0,45	2,22	280	14,2	6,8	0,209	0,096	0,084	0,318	0,007	0,018	2,31	0,364	0,344	124,3	56,8
0,45	2,22	290	14,9	7,8	0,095	0,044	0,038	0,192	0,008	0,021	2,05	0,190	0,166	48,5	21,1
0,45	2,22	310	25,5	9,0	0,107	0,049	0,043	0,222	0,008	0,020	2,08	0,198	0,164	53,6	22,6
0,45	2,22	320	20,8	10,5	0,114	0,052	0,046	0,199	0,008	0,020	2,09	0,188	0,144	54,2	21,9
0,45	2,22	330	15,5	6,7	0,182	0,084	0,073	0,284	0,008	0,019	2,25	0,302	0,272	100,0	44,4
0,45	2,22	335	19,5	9,8	0,117	0,054	0,047	0,243	0,008	0,020	2,10	0,188	0,144	55,1	22,4
0,45	2,22	340	14,7	6,8	0,168	0,077	0,067	0,359	0,008	0,019	2,22	0,282	0,248	90,4	39,6
0,45	2,22	345	21,2	7,1	0,111	0,051	0,044	0,221	0,008	0,020	2,09	0,194	0,154	54,2	22,4
0,45	2,22	350	12,3	3,6	0,226	0,104	0,090	0,321	0,007	0,018	2,34	0,394	0,380	138,7	64,2
0,45	2,22	360	12,6	2,6	0,164	0,075	0,066	0,244	0,008	0,019	2,21	0,272	0,236	86,9	37,7

Table 11: Measured response and calculated slamming force, f = 0,48Hz

f [Hz]	T [s]	e	Response [N]	Slamming force [N]	ηb [m]	ληb [m]		Hb [m]	τ [s]		Cb [m/s]	l [m]		Slamming force [N]	
			Measured	Measured		(W&O)	(Goda)		(W&O)	(Goda)		(W&O)	(Goda)	(W&O)	(Goda)
0,48	2,08	120	0,6	0,3	0,125	0,058	0,050	0,179	0,008	0,020	2,12	0,192	0,160	58,5	24,8
0,48	2,08	170	13,7	6,2	0,158	0,073	0,063	0,227	0,008	0,019	2,19	0,262	0,224	82,7	35,6
0,48	2,08	190	14,2	7,6	0,171	0,079	0,068	0,244	0,008	0,019	2,22	0,282	0,248	91,6	40,1
0,48	2,08	200	19,1	8,0	0,172	0,079	0,069	0,250	0,008	0,019	2,23	0,282	0,248	92,0	40,3
0,48	2,08	210	17,9	7,6	0,167	0,077	0,067	0,246	0,008	0,019	2,21	0,272	0,236	88,1	38,3
0,48	2,08	215	17,4	9,9	0,171	0,079	0,068	0,245	0,008	0,019	2,22	0,282	0,248	91,6	40,1
0,48	2,08	220	19,3	7,8	0,174	0,080	0,070	0,254	0,008	0,019	2,23	0,292	0,260	94,7	41,8
0,48	2,08	225	18,4	8,2	0,171	0,079	0,068	0,252	0,008	0,019	2,22	0,282	0,248	91,6	52,9
0,48	2,08	230	17,1	9,0	0,176	0,081	0,070	0,252	0,008	0,019	2,23	0,292	0,260	95,6	42,1
0,48	2,08	235	16,3	8,3	0,176	0,081	0,070	0,251	0,008	0,019	2,23	0,292	0,260	95,6	42,1
0,48	2,08	240	19,8	11,3	0,159	0,073	0,064	0,240	0,008	0,019	2,20	0,262	0,224	83,1	35,8
0,48	2,08	245	19,6	9,1	0,158	0,073	0,063	0,234	0,008	0,019	2,19	0,262	0,224	82,7	35,6
0,48	2,08	250	20,8	10,4	0,131	0,060	0,052	0,206	0,008	0,020	2,13	0,202	0,168	62,2	26,4
0,48	2,08	255	23,2	11,6	0,128	0,059	0,051	0,208	0,008	0,020	2,13	0,202	0,168	61,2	25,9
0,48	2,08	260	10,9	6,0	0,092	0,042	0,037	0,164	0,008	0,021	2,04	0,180	0,158	46,0	20,1
0,48	2,08	270	23,2	11,5	0,162	0,075	0,065	0,244	0,008	0,019	2,20	0,262	0,224	84,3	36,3
0,48	2,08	280	23,3	12,4	0,160	0,074	0,064	0,234	0,008	0,019	2,20	0,262	0,224	83,5	36,0
0,48	2,08	290	14,5	6,7	0,185	0,085	0,074	0,284	0,008	0,019	2,25	0,314	0,284	103,6	46,1
0,48	2,08	300	12,1	6,9	0,227	0,104	0,091	0,323	0,007	0,018	2,34	0,394	0,380	139,2	64,4
0,48	2,08	310	15,0	7,6	0,196	0,090	0,078	0,298	0,008	0,019	2,28	0,334	0,308	112,3	50,6
0,48	2,08	315	15,0	5,3	0,109	0,050	0,044	0,307	0,008	0,020	2,08	0,194	0,154	53,5	22,1
0,48	2,08	320	16,2	9,9	0,086	0,040	0,034	0,211	0,008	0,021	2,03	0,170	0,148	42,7	18,6
0,48	2,08	325	16,1	9,4	0,145	0,067	0,058	0,271	0,008	0,020	2,17	0,232	0,192	72,4	40,4
0,48	2,08	330	14,9	12,1	0,171	0,079	0,068	0,271	0,008	0,019	2,22	0,282	0,248	91,6	65,6
0,48	2,08	340	15,1	9,2	0,125	0,058	0,050	0,239	0,008	0,020	2,12	0,192	0,160	58,5	48,6

Table 12: Measured response and calculated slamming force, f = 0,51Hz

f [Hz]	T [s]	e	Response [N]	Slamming force [N]	ηb [m]	ληb [m]		H_b [m]	τ [s]		C_b [m/s]	l [m]		Slamming force [N]	
			Measured	Measured		(W&O)	(Goda)		(W&O)	(Goda)		(W&O)	(Goda)	(W&O)	(Goda)
0,51	1,96	120	0,6	0,1	0,114	0,052	0,046	0,165	0,008	0,020	2,09	0,188	0,144	54,2	21,9
0,51	1,96	170	8,8	2,4	0,182	0,084	0,073	0,251	0,008	0,019	2,25	0,302	0,272	100,0	44,4
0,51	1,96	190	9,4	5,4	0,173	0,080	0,069	0,241	0,008	0,019	2,23	0,292	0,260	94,3	41,6
0,51	1,96	200	15,9	7,9	0,177	0,081	0,071	0,257	0,008	0,019	2,24	0,292	0,260	96,0	42,3
0,51	1,96	210	14,9	7,3	0,171	0,079	0,068	0,235	0,008	0,019	2,22	0,282	0,248	91,6	40,1
0,51	1,96	220	15,1	5,6	0,169	0,078	0,068	0,236	0,008	0,019	2,22	0,282	0,248	90,8	39,7
0,51	1,96	230	15,3	7,2	0,172	0,079	0,069	0,243	0,008	0,019	2,23	0,282	0,248	92,0	40,3
0,51	1,96	240	16,8	6,9	0,167	0,077	0,067	0,239	0,008	0,019	2,21	0,272	0,236	88,1	50,5
0,51	1,96	245	18,0	5,9	0,180	0,083	0,072	0,252	0,008	0,019	2,24	0,302	0,272	99,1	44,0
0,51	1,96	250	18,1	6,6	0,171	0,079	0,068	0,251	0,008	0,019	2,22	0,282	0,248	91,6	40,1
0,51	1,96	255	15,6	8,2	0,165	0,076	0,066	0,243	0,008	0,019	2,21	0,272	0,236	87,3	37,9
0,51	1,96	260	13,8	6,1	0,185	0,085	0,074	0,261	0,008	0,019	2,25	0,314	0,284	103,6	46,1
0,51	1,96	265	18,5	11,4	0,151	0,069	0,060	0,238	0,008	0,019	2,18	0,242	0,200	76,4	32,3
0,51	1,96	270	9,4	4,0	0,072	0,033	0,029	0,151	0,009	0,021	1,99	0,140	0,124	34,2	15,0
0,51	1,96	280	7,5	3,1	0,149	0,069	0,060	0,237	0,008	0,019	2,17	0,242	0,200	75,7	32,0

Table 13: Measured response and calculated slamming force, f = 0,54Hz

f [Hz]	T [s]	e	Response [N]	Slamming force [N]	ηb [m]	ληb [m]		Hb [m]	τ [s]		Cb [m/s]	l [m]		Slamming force [N]	
			Measured	Measured		(W&O)	(Goda)		(W&O)	(Goda)		(W&O)	(Goda)	(W&O)	(Goda)
0,54	1,85	120	0,7	0,2	0,122	0,056	0,049	0,175	0,008	0,020	2,11	0,182	0,152	55,8	23,7
0,54	1,85	130	1,0	0,4	0,143	0,066	0,057	0,201	0,008	0,020	2,16	0,232	0,192	71,7	30,3
0,54	1,85	150	1,6	0,6	0,166	0,076	0,066	0,227	0,008	0,019	2,21	0,272	0,236	87,7	38,1
0,54	1,85	170	9,8	5,7	0,156	0,072	0,062	0,224	0,008	0,019	2,19	0,252	0,212	80,1	34,2
0,54	1,85	180	11,0	5,6	0,162	0,075	0,065	0,236	0,008	0,019	2,20	0,262	0,224	84,3	36,3
0,54	1,85	185	11,0	5,5	0,169	0,078	0,068	0,234	0,008	0,019	2,22	0,282	0,248	90,8	39,7
0,54	1,85	190	15,4	8,4	0,176	0,081	0,070	0,245	0,008	0,019	2,23	0,292	0,260	95,6	42,1
0,54	1,85	195	11,8	6,5	0,179	0,082	0,072	0,251	0,008	0,019	2,24	0,302	0,272	98,7	43,8
0,54	1,85	200	12,8	5,9	0,178	0,082	0,071	0,253	0,008	0,019	2,24	0,302	0,272	98,3	43,6
0,54	1,85	205	13,6	5,6	0,182	0,084	0,073	0,247	0,008	0,019	2,25	0,302	0,272	100,0	44,4
0,54	1,85	210	13,8	5,9	0,180	0,083	0,072	0,247	0,008	0,019	2,24	0,302	0,272	99,1	44,0
0,54	1,85	220	12,0	5,8	0,163	0,075	0,065	0,245	0,008	0,019	2,21	0,272	0,236	86,5	37,6
0,54	1,85	230	16,1	11,1	0,114	0,052	0,046	0,188	0,008	0,020	2,09	0,188	0,144	54,2	21,9
0,54	1,85	240	20,0	8,8	0,147	0,068	0,059	0,215	0,008	0,019	2,17	0,232	0,192	73,2	30,9
0,54	1,85	250	15,6	7,5	0,132	0,061	0,053	0,214	0,008	0,020	2,14	0,192	0,160	60,8	25,9
0,54	1,85	255	18,9	8,1	0,092	0,042	0,037	0,187	0,008	0,021	2,04	0,180	0,158	46,0	20,1
0,54	1,85	260	19,0	10,2	0,163	0,075	0,065	0,235	0,008	0,019	2,21	0,272	0,236	86,5	37,6
0,54	1,85	265	43,2	17,1	0,149	0,069	0,060	0,245	0,008	0,019	2,17	0,242	0,200	75,7	32,0
0,54	1,85	270	18,6	8,2	0,155	0,071	0,062	0,235	0,008	0,019	2,19	0,252	0,212	79,8	34,0
0,54	1,85	275	16,8	9,1	0,112	0,052	0,045	0,230	0,008	0,020	2,09	0,194	0,154	54,5	22,5
0,54	1,85	280	11,9	4,4	0,087	0,040	0,035	0,189	0,008	0,021	2,03	0,170	0,148	43,0	18,7
0,54	1,85	290	12,3	5,2	0,154	0,071	0,062	0,243	0,008	0,019	2,19	0,252	0,212	79,4	33,9

APPENDIX C

Irregular wave analyze of the four cases with maximum observed response.

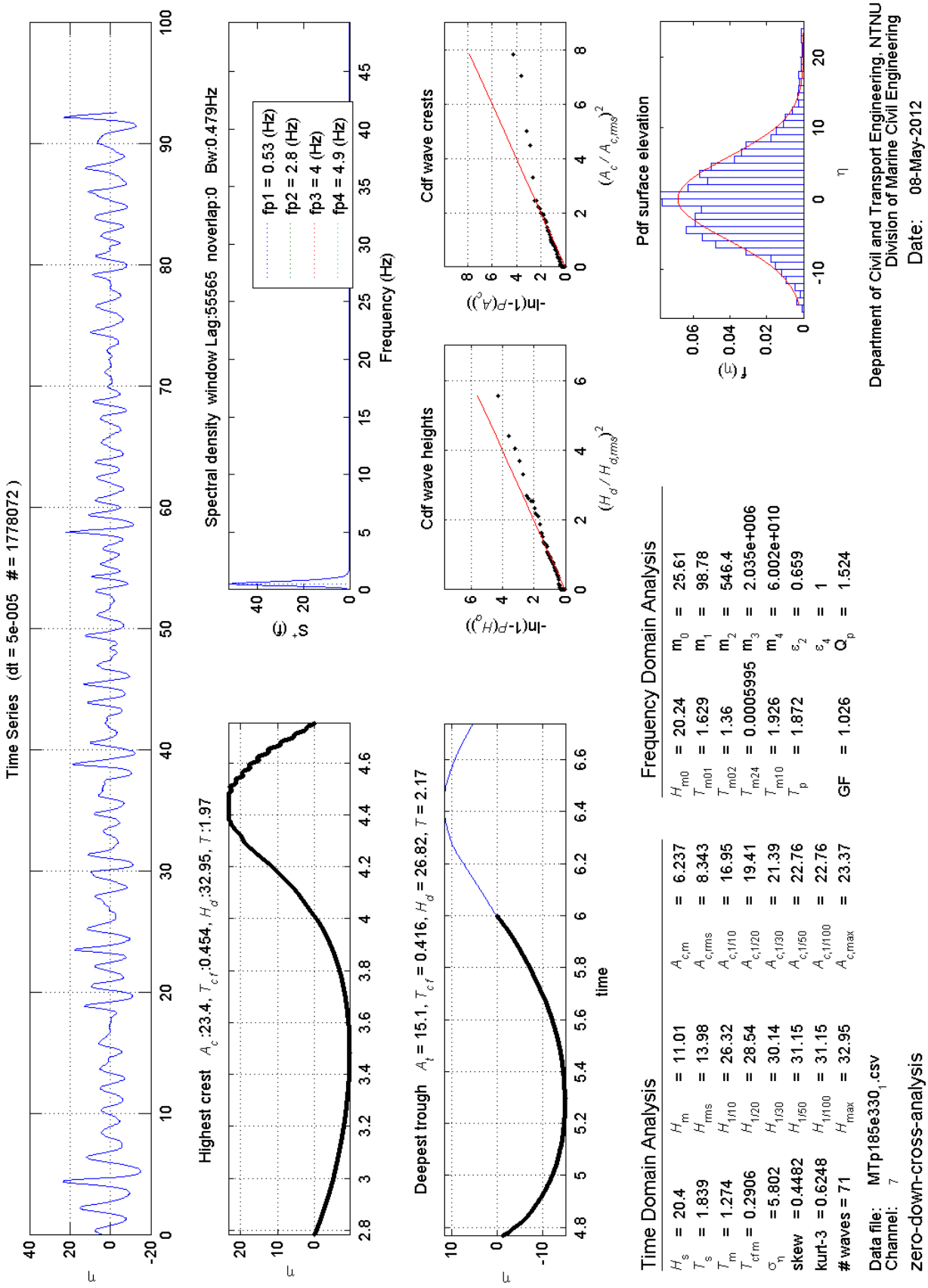

Figure 95: Analysis of irregular waves, MTp185e330_1

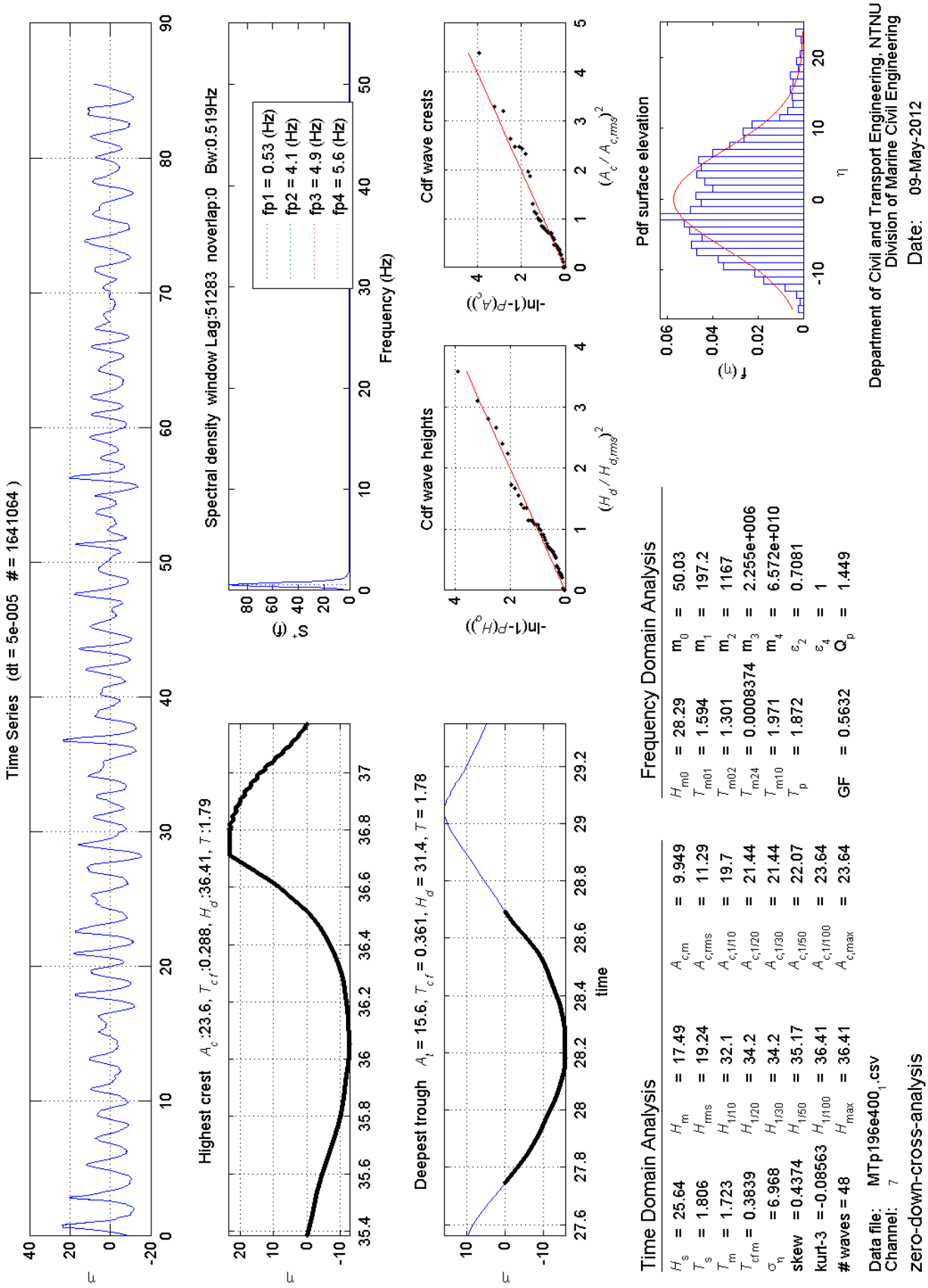

Figure 96: Analysis of irregular waves, MTp196e400_1

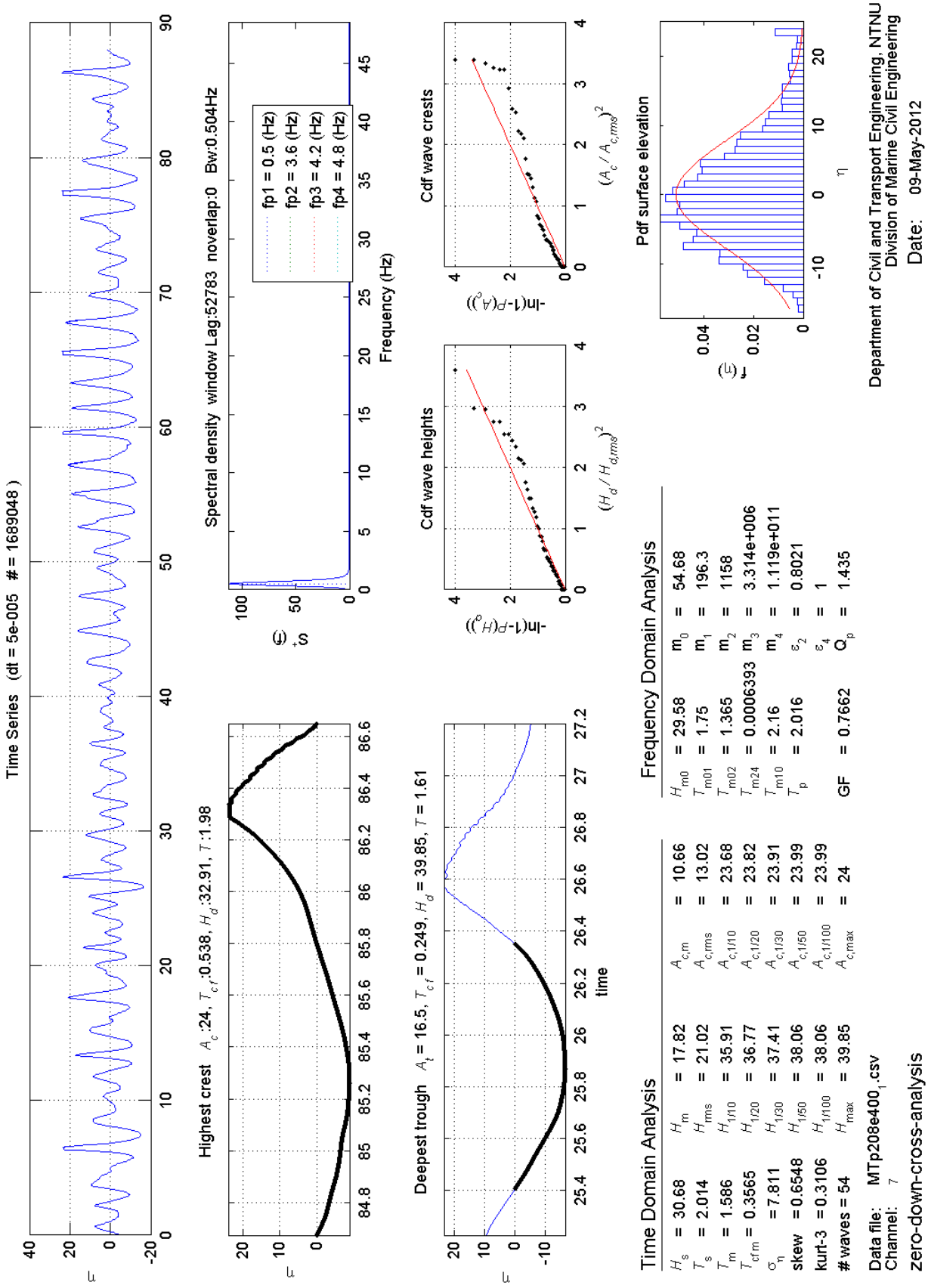

Figure 97: Analysis of irregular waves, MTp208e400_1

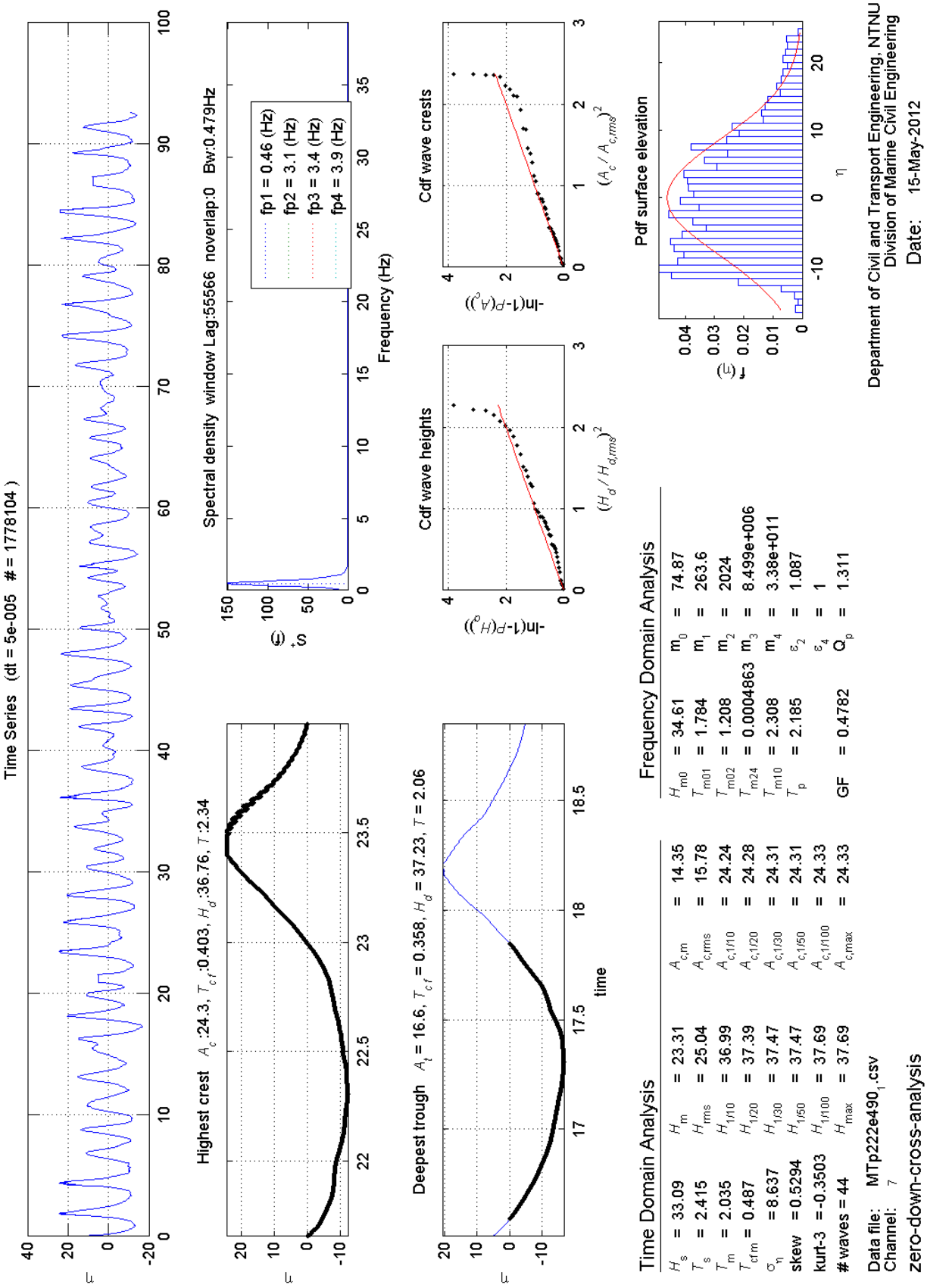

Figure 98: Analysis of irregular waves, MTp222e490_1

APPENDIX D

Preliminary

ANALYSIS OF FORCE RESPONSE DATA FROM TESTS ON A MODEL OF A TRUSS STRUCTURE SUBJECTED TO PLUNGING BREAKING WAVES

By

Alf Tørum

Norwegian University of Science and Technology
Department of Civil and Transport Engineering

22 May 2012

TABLE OF CONTENT

1. GENERAL

Wave forces from non-breaking waves on a slender vertical pile are commonly calculated according to the Morison equation,

$$dF = dF_D + dF_M = 0.5\rho_w C_D D u|u|dz + \rho_w C_M \frac{\pi D^2}{4}\frac{\partial u}{\partial t}dz \qquad (1)$$

where ρ_w is the mass density of water, C_D is the drag coefficient, C_M is the inertia coefficient, D is the pile diameter, u is the water particle velocity and t is time.

If the waves break against the pile, Figure 3, a slamming force may occur on part of the pile, $\lambda\eta_b$. The total force is then

$$F = F_D + F_M + F_s \qquad (2)$$

The slamming force is commonly written as:

$$F_s = 0.5\rho_w C_s D C_b^2 \lambda\eta_b \qquad (3)$$

where C_s is a slamming force factor, C_b is the breaking wave celerity (the water particle velocity is set equal to the wave celerity at breaking), λ is the curling factor which indicates how much of the wave crest is active in the slamming force, Figure 3. The nature of the slamming force is indicated in Figure 4. The slamming force has a short duration, τ_p, but high intensity. The duration of the slamming force is somewhere in the range τ_p = 0.20 D/C_b – $0.5D/C_b$.

The force - time history is given differently by different researchers. Figure 4 shows the most used force – time histories. The most recent force – time history is the one marked "own model" by Wienke and Oumeraci (2005). In Figure 5, t = time, V = water velocity, R = cylinder radius, f_1 = line force, ρ = mass density of water

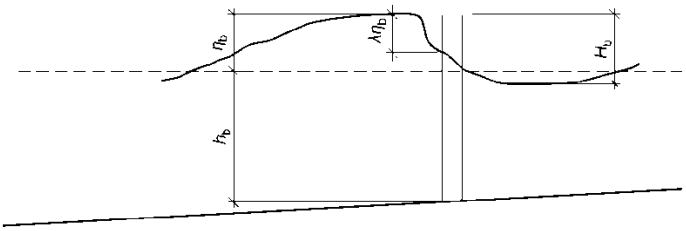

Figure 3. Breaking wave leading to possible slamming force.

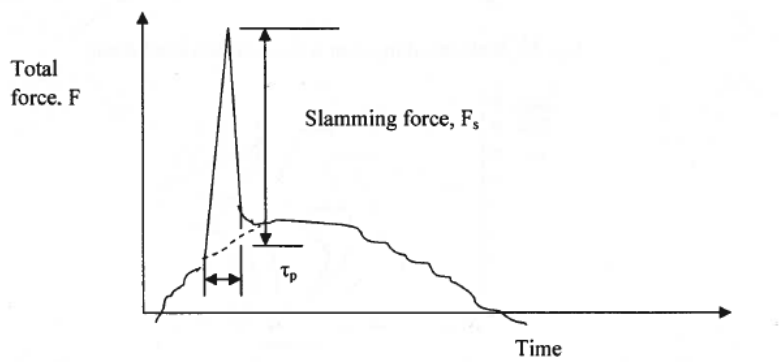

Figure 4. The nature of the slamming force.

C_s was set to $C_s = \pi$ by Goda et al. (1966). They obtained λ-values of approximately λ = 0.4. Different values of C_s have later been obtained by different researchers, but $C_s = \pi$ has frequently been used. One of the latest investigations on wave slamming forces on cylinders in a large model scale set-up has been carried out by Wienke and Oumeraci (2005). They set, on theoretical grounds, $C_s = 2\pi$ and obtained values of λ as shown in Figure 6 for different inclination of the pile. Note that since $C_s = 2\pi$, the results of Wienke and Oumeraci (2005) give approximately twice the slamming force compared to Goda (1966).

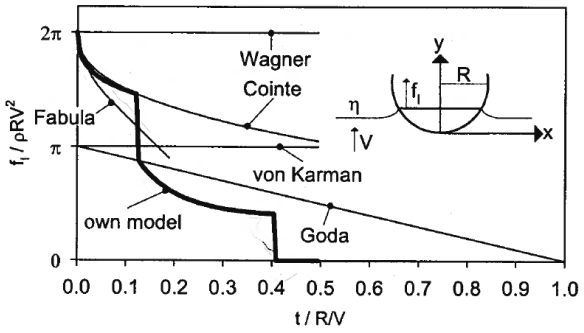

Figure 5. Different time histories of the line force. T=time, R=cylinder radius, V=cylinder velocity. Wienke and Oumeraci (2005).

All previous tests, except those by Wienke and Oumeraci (2005), have been carried out at a fairly small scale with cylinder diameters typically 5 – 10 cm in diameter. Wienke and Oumeraci (2005), carried out tests in a large wave flume with a cylinder with diameter 0.70 m, water depths approximately 4 m and with wave heights up to 2.8 m. They used "artificial breaking waves" in the sense that they programmed the wave generator to generate plunging waves in "deep" water at or very close to the cylinder in "deep" water.

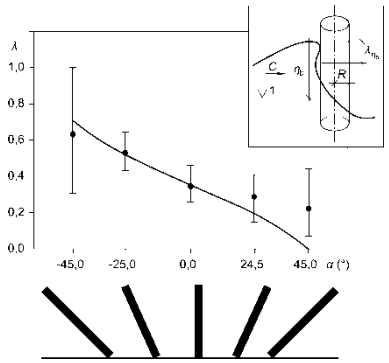

Figure 6. Curling factor vs. pile inclination. Wienke and Oumeraci (2005).

Currently new investigations are being carried out by Professor Oumeraci, Leichweiss Institut für Wasserbau, University of Braunschweig, Germany, and one of his PhD students, on slamming forces on a single pile in depths were waves break (plunging) due to depth limitations. (Personal communication between Hocine Oumeraci and Alf Tørum)

Ros (2011), Arntsen et al. (2011) carried out tests on wave slamming forces on a single pile. Figure 7 shows the test pile, where local force responses were measured at different

elevations. Figure 8 shows a time series of the responses from one of the tests. Although the waves are so-called regular there is considerable variation of the response from wave to wave. The reason for this is not exactly known, but it may be due to small variations in the front slope from wave to wave and seems to be inherent scatter in such tests.

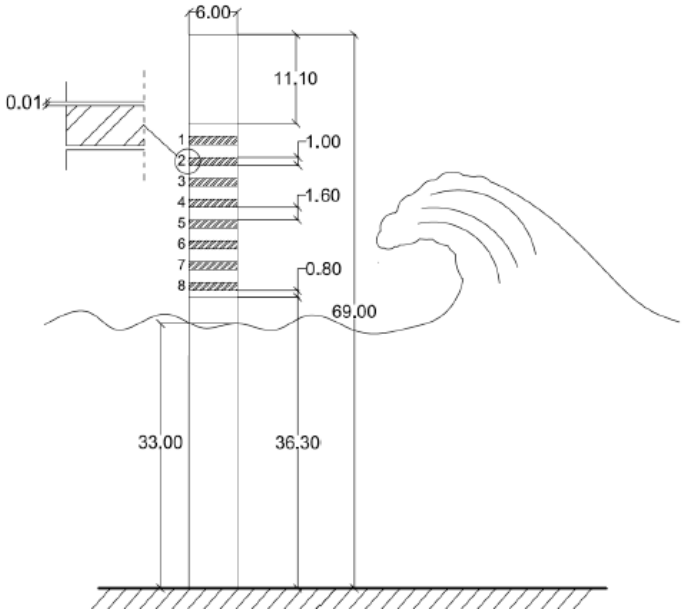

Figure 7. Instrumented cylinder (dimensions in cm). The striped zones represent the force transducers (rings). The gap between each transducer measures 0.01 cm.

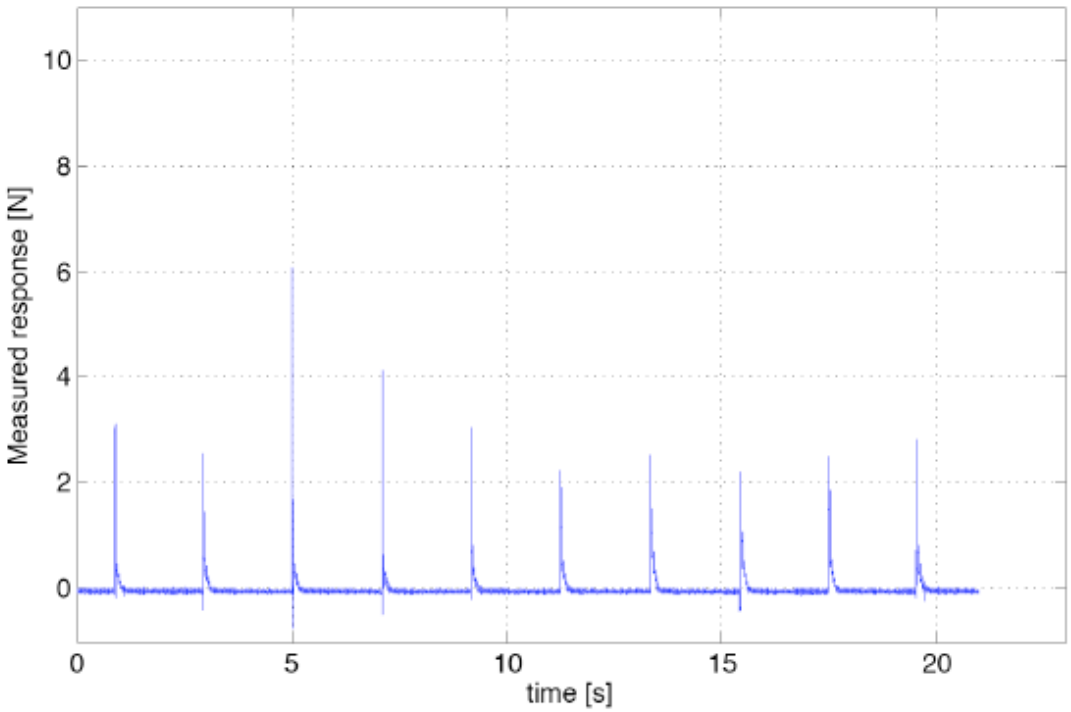

Figure 8. Measured response at the third transducer from above, Figure 8, for regular waves.

Ros (2011), Arntsen et al. (2011) obtained force intensities along the pile as shown in Figure 9. Similar triangular force intensities was also obtained by Sawaragi and Nochino (1984) and Tanimoto et al. (1986), which is in contradiction to the assumption of a uniform force intensity as assumed by Goda et al. (1966) and by Wienke and Oumeraci (2005).

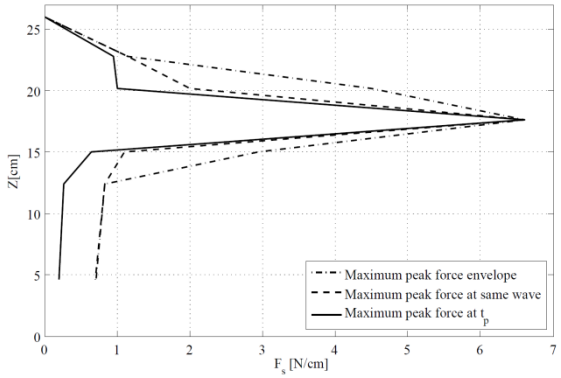

Figure 9. Slamming force intensity F_s along the pile. T = 2.2 s and H = 28 cm. Z = 0 is at the still water line. t_p: maximum peak force intensity instant.

Table 1 show comparison between the results of the slamming forces from plunging breaking waves obtained on the 6 cm diameter single pile used by Ros (2011) and the results of different researchers. Table 1 show that the results of Wienke and Oumeraci (2005) give the highest slamming force. The Wienke and Oumeraci (2005) method was based on large scale tests in the Large Wave Flume on a pile with diameter 0.70 m and with wave heights in the flume of approximately 2.5 m. The reason why Wienke and Oumeraci (2005) obtained higher forces is not clear, but it could be due to scale effects?

Table 1. Comparison on the test set-up used by Ros (2011).

Calculated total forces based on different studies				
Study	**C_s-value**	**λ_{max}**	**Vertical force distribution**	**Total slamming force, N**
Wienke and Oumeraci (2005)	**2π**	**0.46**	**Uniform**	**88**
Goda (1966)	**π**	**0.40**	**Uniform**	**39**
Sawaragi and Nochino (1986)	**π**	**0.90**	**Triangular**	**44**
Tanimoto et al. (1986)	**π**	**0.66**	**Triangular**	**32**
Ros (2011)	**4.3**	**0.67**	**Triangular**	**36.**

2. TESTS ON MODEL TRUSS STRUCTURE

Miriam Aashamar has, as part of her Master thesis, carried out tests on wave forces on a model truss structure as shown in Figure 10 and Figure 11. I have in this note looked briefly into more details of the responses that measured.

The model scale was 1:50 in relation to water depth, e.g. the model water depth was 32.0 cm, corresponding to 16 m prototype values. The width of the wave flume is 1.00 m. The wave forces/responses were measured by two force transducer at the top of the structure and two force transducers at the bottom. The waves were measured at two locations: 1. Some distance ahead of the model structure in 90 cm water depth in the wave flume, and 2. Half way between the wave flume wall and one of the front legs of the structure, Figure 10. It has to be born in mind that the wave measurements at the location of wave breaking may be somewhat uncertain because of air entrained in the water due to the wave breaking.

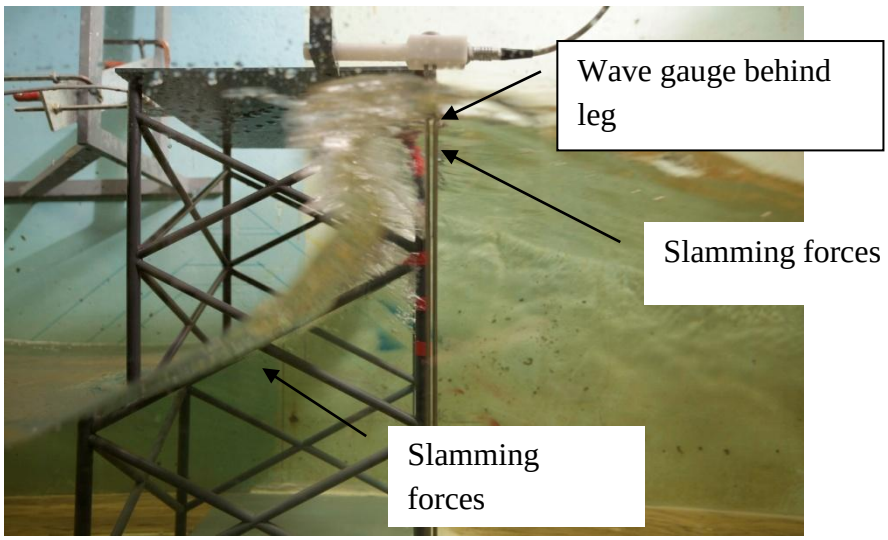

Figure 10. 1:50 scale model of truss support structure for wind turbines.

The wave slamming forces have a short duration and what is usually recorded are the force responses since there will be some dynamic effects due to the stiffness of the force measuring system and the model support structuies. The challenge of the data analysis is to resolve the wave impact force from the measured responses.

Figure 21 shows results of pluck tests by plucking of the structure with an impulse hammer (see later). The maximum response is for the sum of all the four force transducers. The pluck tests reveal that the natural period of oscillation is approximately T = 0.02 s.

For a one-degree-of-freedom system the response is depending on the form of the impulse and the ratio between the duration of the impact impulse and the natural period of oscillations of

the system. Figure 3 shows ratio between the response and the force for different impulse forms.

The duration of the impact is set differently by different researchers, but is in the range

$$t_1 = (0.25 - 0.5)\frac{D}{C_b} \tag{4}$$

where D = pile diameter, C_b is the celerity of the breaking wave. In our case (the 1:50 scale model) C_b = 2.1 m/s. Aune (2011). The vertical legs have a diameter of D = 0.016 m. This gives t_1 in the range t_1= 0.0019s- 0.0038 or t_1/T in the range t_1/T = 0.038 – 0.076. If we assume a triangular pulse the response will be somewhere in the range 0.15 – 0.3 of the force according to Figure 12. We will come back to this issue under Chapter 3.

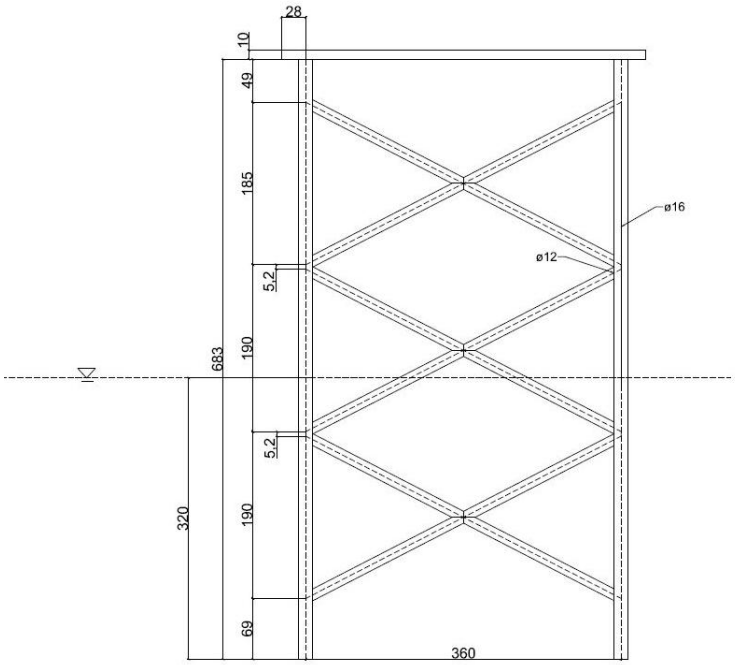

Figure 11. Model truss structure. Dimensions in mm. The structure has the same apperance from all four sides.

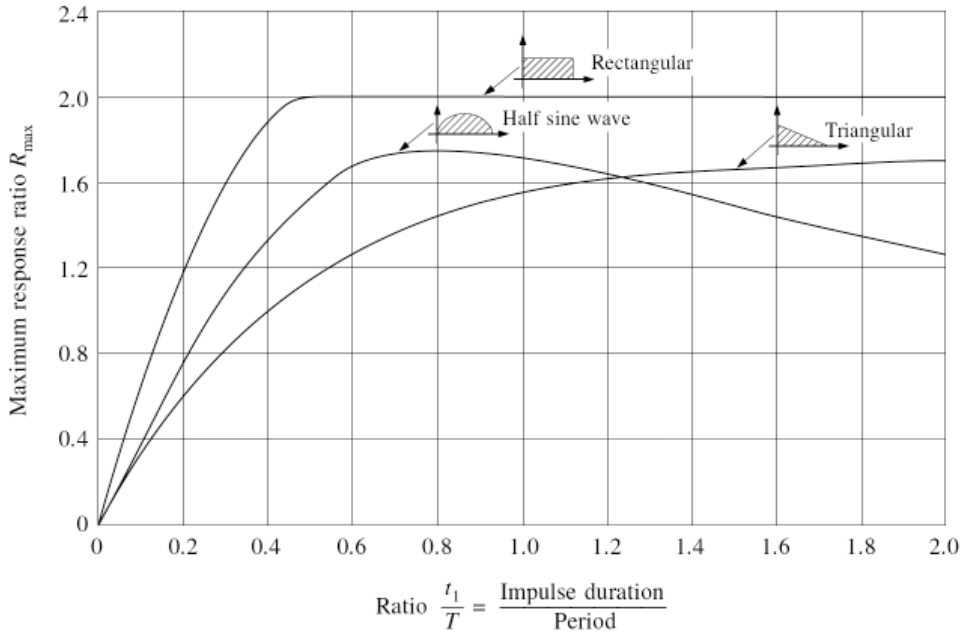

Figure 12. Ratio between response and force for a one-degree-of-freedom system as a function of impulse duration and natural period of oscillation.

Wienke and Oumeraci (2005) carried out tests on wave slamming forces from plunging breaking waves on a 0.70 m diameter single pile in the Large Wave Channel in Hannover, Figure 13.

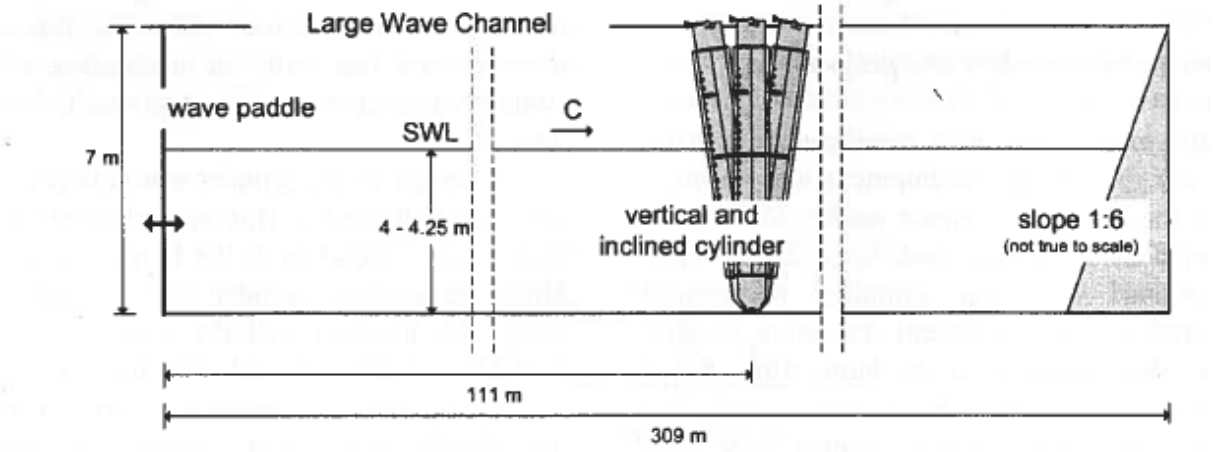

Figure 13. Test set-up, Wienke and Oumeraci (2005).

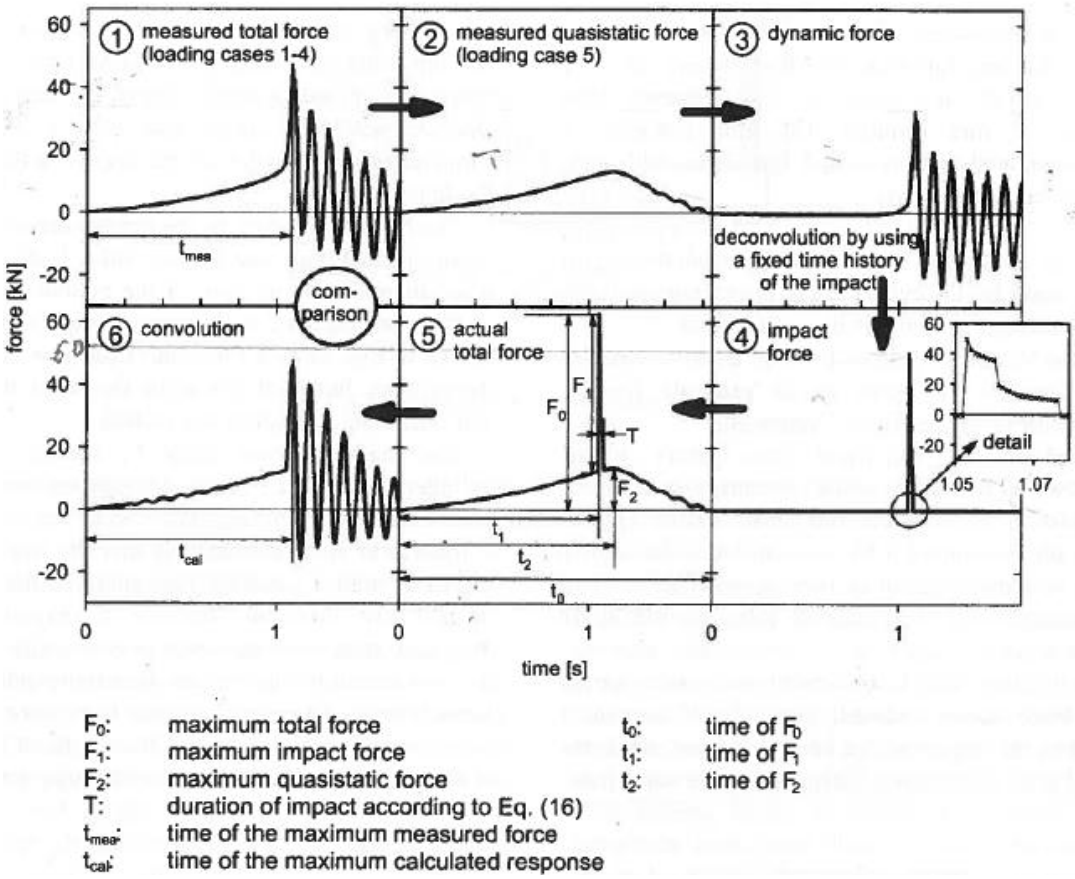

Figure 14. The six steps of the wave force analysis procedure by Wienke and Oumeraci (2005).

Figure 14 shows the steps in their wave force analysis procedure. 1. This is the recorded force response signal. 2. This is the measured Morison force from a wave slightly below wave breaking height. 3. Shows the measured response – the Morison force from 2, e.g. the dynamic part of the response. 4. From 3. to 4. De-convolution (Duhamel integral) has been applied and the wave slamming force has been obtained, In 5 the total wave force has been obtained as a sum 2+4. Finally this force has been applied to the pile and the response result, 6, is compared to the measured response.

Ros (2011), Arntsen et al. (2011) applied basically the same approach as Wienke and Oumeraci (2005).

The force response data from the tests on the model structure, Figure 10, has a different appearance than the forces response data on a single cylinder. Figure 15 shows an example of the total force and the wave height for one particular run, while Figure 16 shows a time expansion of the same time series for t = 1.25s – 2.08s. Total force means that the force responses of all four force transducers have been added together. The sampling frequency was 19200 Hz (19200 samples per second). The response is a mixture of Morison forces and wave slamming forces. The high frequency part of the time trace, Figure 16, is supposed to be due to the wave slamming forces.

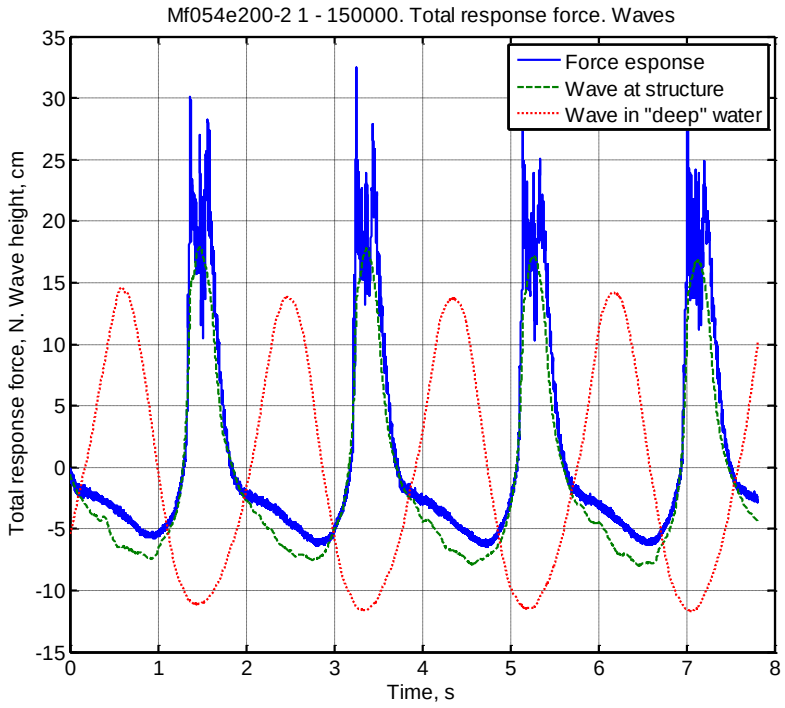

Figure 15. Total force response for the time series Mf054e200-2 and waves at the structure and in "deep" water.

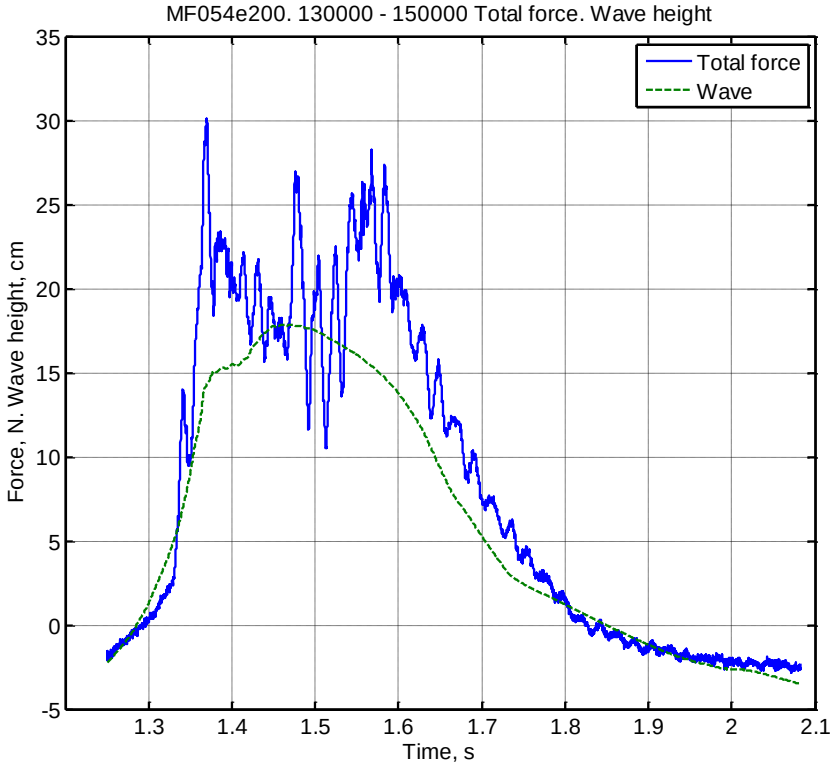

Figure 16. Force response data for tests with regular waves with frequency 0.54 Hz or wave period T = 1.85 s. (prototype T_p = 13.1 s). The wave height was approximately 0.22 m. Air entrapped in the water during wave breaking influences to some extent the wave measurements.

It is certainly not so easy to analyze the data from the truss structure as it is from the tests on a single cylinder, e.g. Wienke and Oumeraci (2005). When testing a single cylinder the highest response occur at the first response, e.g. Figure 14, and thereafter there is a damped oscillation of the structure. In our case there are also indications of smaller response forces in the beginning of the force response time series before the maximum slamming response force occurs, Figures 15 and 16. The reason for this is not precisely known, but there might be slamming forces against the several bracings, as also indicated in Figure 10. In Figure 16 we also see two marked areas at time points approximately 1.35 s and 1.55 s. This indicates that the front section/panel is first hit and then rear section/panel.

Our main interest is the wave slamming forces. Wienke and Oumeraci (2005) carried out tests with almost breaking waves and considered the forces then measured as the Morison forces, Figure 5, "Measured quasistatic force". They then deducted this Morison force from the measured response force and arrived at the slamming force response from the plunging breaking waves.

We used another approach to arrive at the wave slamming response, namely by low pass filtering the measured force response, Figure 17. We have first filtered the response force, deduced this filtered force from the total force response. The thus obtained high frequency response was the again filtered and deducted from the previous obtained high frequency response. It is this "double filtered" response force that are shown in Figure 17 and again in Figure 18.

We have therefore adopted another approach to arrive at the wave slamming force from the wave slamming response force.

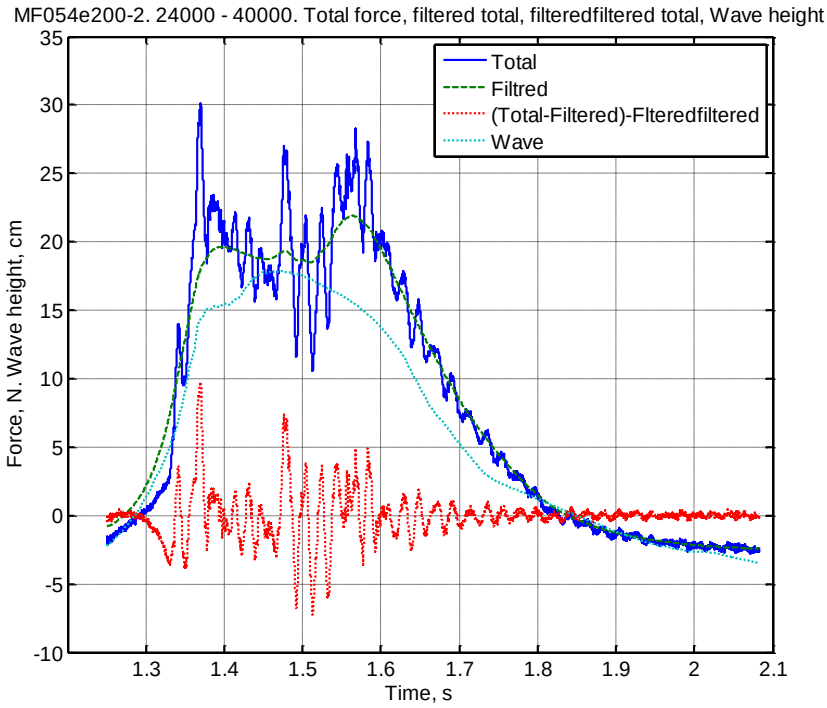

Figure 17. Total force response, filtered force response, high frequency part of the response and wave height.

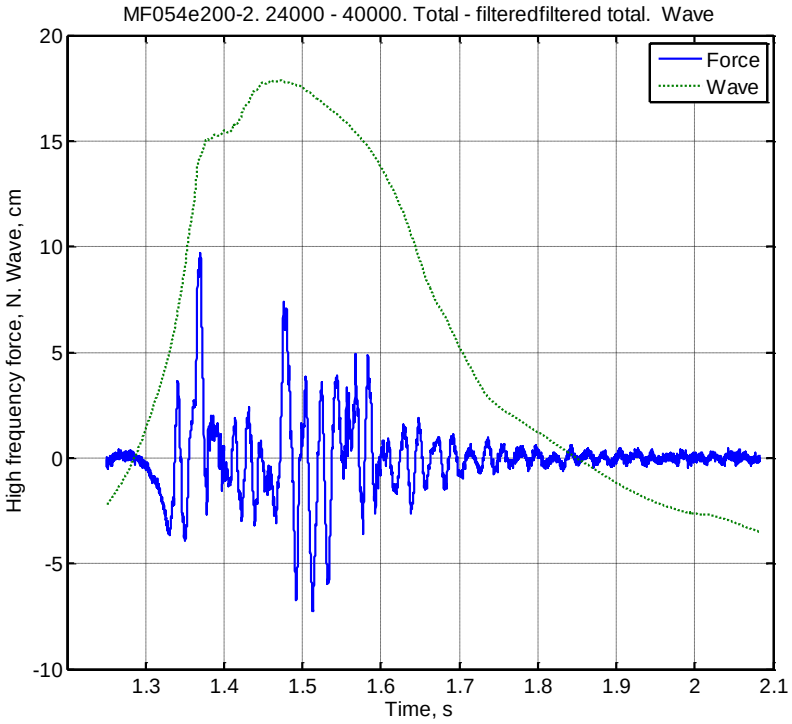

Figure 18. Filteredfiltered force response and wave.

3. A "NEW" METHOD OF ANALYSING WAVE SLAMMING FORCES

3.1. General on the "new" method.

We will follow a procedure as described by Määtänen,(1979). Prof. Määttänen used and still uses this method currently in advising PhD students at IBAT, NTNU, resolving ice forces from measured response forces on structures subjected to ice forces. But the method should also be applicable for wave slamming loads. The method is different from the method used by Wienke and Oumeraci (2006) when analyzing wave slamming forces on single piles. The wave slamming response of a truss structure is, as we have seen, more complicated than on a single pile.

The measured response force f(t) can be expanded into Fourier integral – extension of Fourier series expansion - and in case of force vibration will be:

$$f(t) = \frac{1}{2\pi}\int_{\infty}^{\infty} H(\omega)S_F(\omega)e^{i\omega t}d\omega \qquad (5)$$

where H (ω) is the transfer function and S_F (ω) is the linear spectrum (not power spectrum) of the forcing function.

The transfer function in our case will obtained by pluck tests on the structure with an impulse hammer, Figure 18. Normally pluck tests are carried out by plucking the structure at several locations. However, in this case we know from previous tests, Arntsen et al. (2011), the approximate location of the wave slamming resultant load. Plucking was therefore be carried out at and in the vicinity of the location of the resultant force, or approximately 17 cm above still water level (SWL), Figure 9. The impulse hammer measures the impulse force by a force transducer in the tip of the hammer. From the measured impulse force and from the simultaneously measured response forces in the four force transducers, the transfer function H(ω) is obtained. The Fourier transform for Eq. (5) gives

$$H(\omega)S_F(\omega) = \int_{\infty}^{\infty} f(t)e^{-i\omega t}d\omega \qquad (6)$$

which is the linear spectrum of the measured force f(t). From this $S_F(\omega)$ can be solved an d the inverse Fourier transform gives the requested real wave slamming force:

$$F(t) = \frac{1}{2\pi}\int_{\infty}^{\infty} \frac{S_f(\omega)}{H(\omega)}e^{i\omega t}d\omega \qquad (7)$$

Although the above equations look complicated, they can be easily solved by programs in e.g. Matlab. We have used the Matlab environment.

The method is also applied in modal testing.

3.2. Frequency response function (FRF).

The transfer function H(ω) is a calibration factor. In our case it has been obtained by using the impulse hammer as shown in Figure 18.

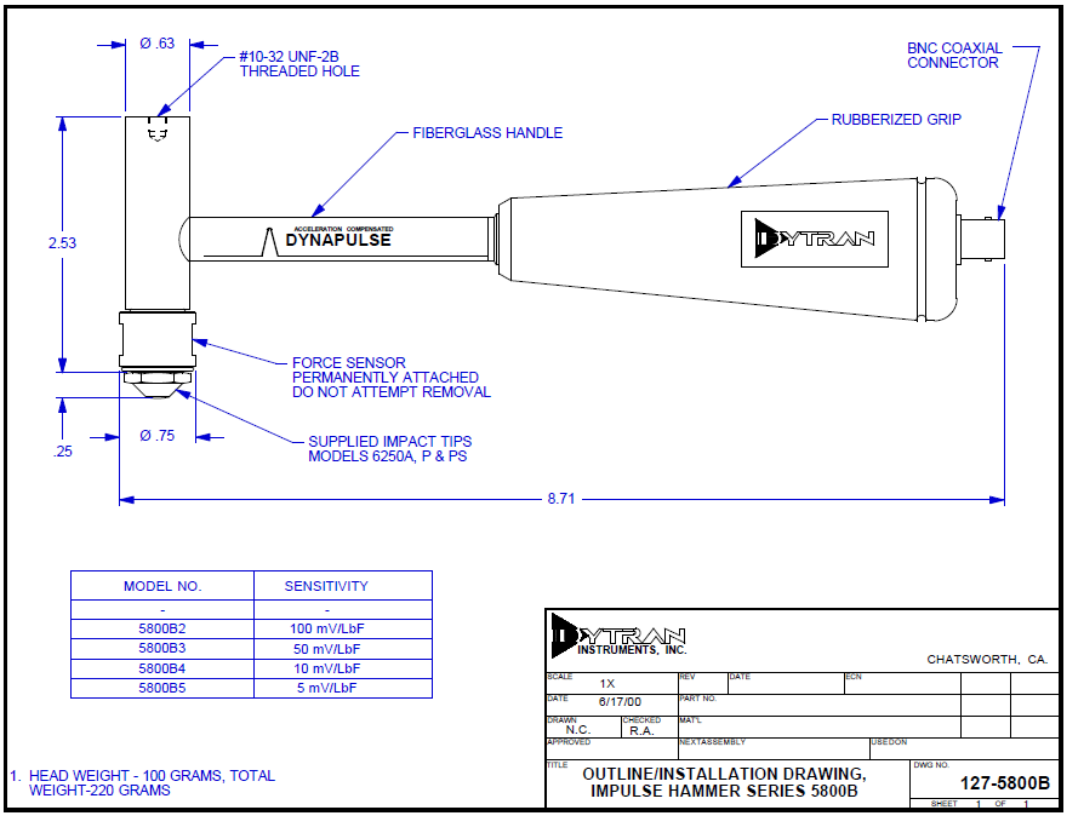

Figure 19. Impulse hammer.

We plucked the structure at 7 locations: At each corner column: Approximately 12, 17 and 22 cm above still water level. In addition in the middle of the top plate as indicated in Figure 19. For each plucking point several plucks were made.

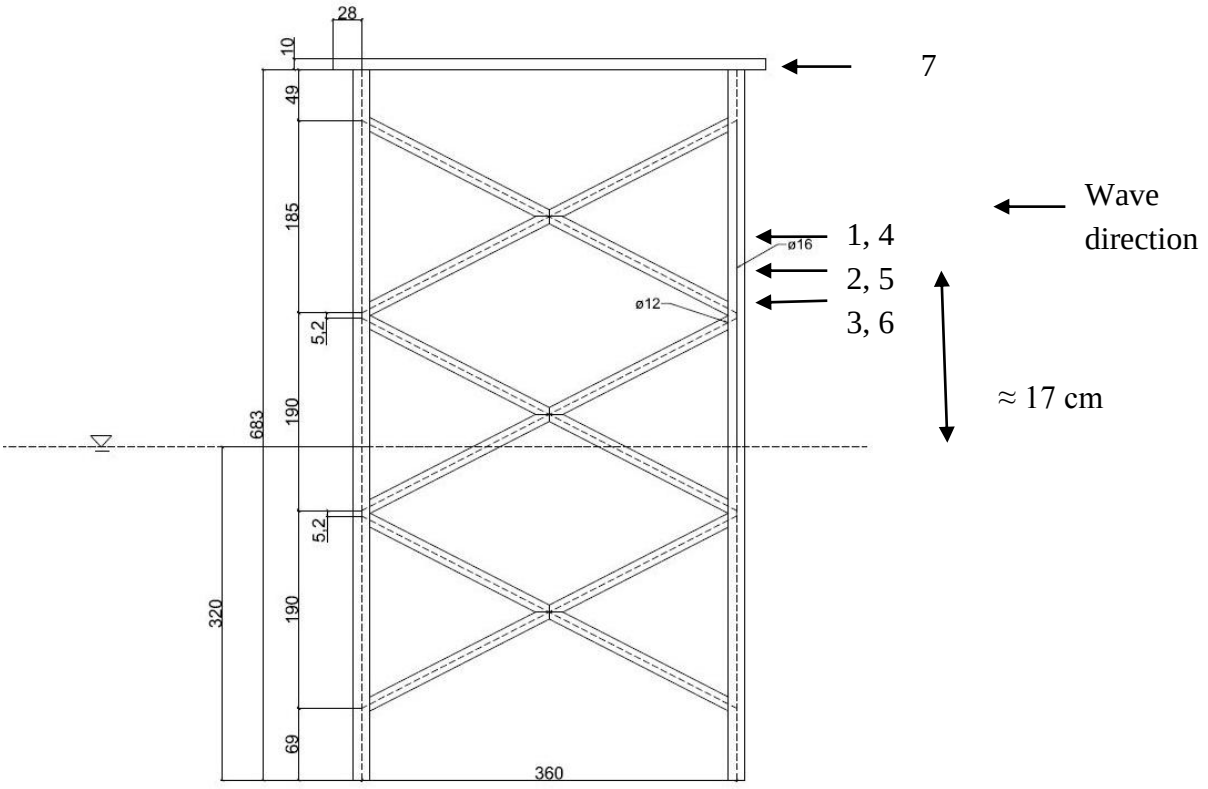

Figure 20. Approximate location of the impuls hammer hits. Points 1,2 and 3 are on the vertical leg closest to the viewer, Figure 10, while points 4, 5 and 6 are on the rear vertical leg. Points 2 and 5 are located at the level of the maximum wave slamming force, Ros (2011), Arntsen et al. (2011).

Our model structurer represents a multiple degree of freedom structure. We have however, for simplisity and to test if the analysis procedure gives reasonable results, made the structure into a single degree of freedom structure by adding all the four force transducers into a total response force. We have further taken the results of only one pluck test.

Figure 21 shows the impuls hammer force and the total response of the structure for one particular pluck testys. The total response is the sum of all the four force transducers.

Figure 22 shows a smaller time window of the impuls hammer force and the total response of the structure.

The FRF is now:

$$H(\omega) = \frac{S_{Total,hammer}(\omega)}{S_{Hammer}(\omega)} \qquad (8)$$

where

$$S_{Total,hammer}(\omega) = \int_{-\infty}^{+\infty} f_{Total,hammer}(t) e^{-i\omega t} d\omega \quad (9)$$

and

$$S_{Hammer}(\omega) = \int_{-\infty}^{+\infty} f_{Hammer}(t) e^{-i\omega t} d\omega \quad (10)$$

We have tested the transfer funcion by applying it to the $Total_{hammer}$ response, using Eq. (10), where $S_f(\omega) = S_{Total,hammer}((\omega)$. The result is shown in Figure22. The agreemengt wkith the "original" hammer force, Figure 21, is good.

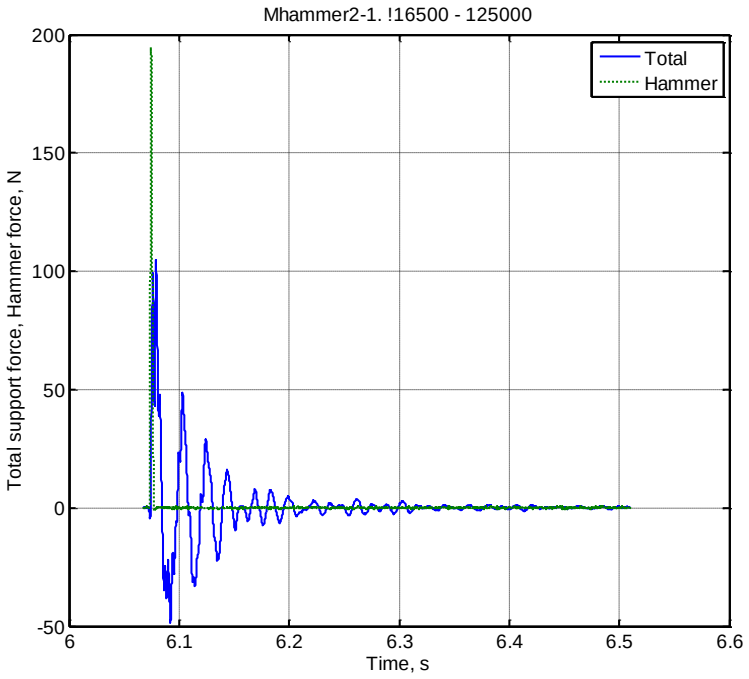

Figure 21. The impuls hammer force and the total response of the structure.

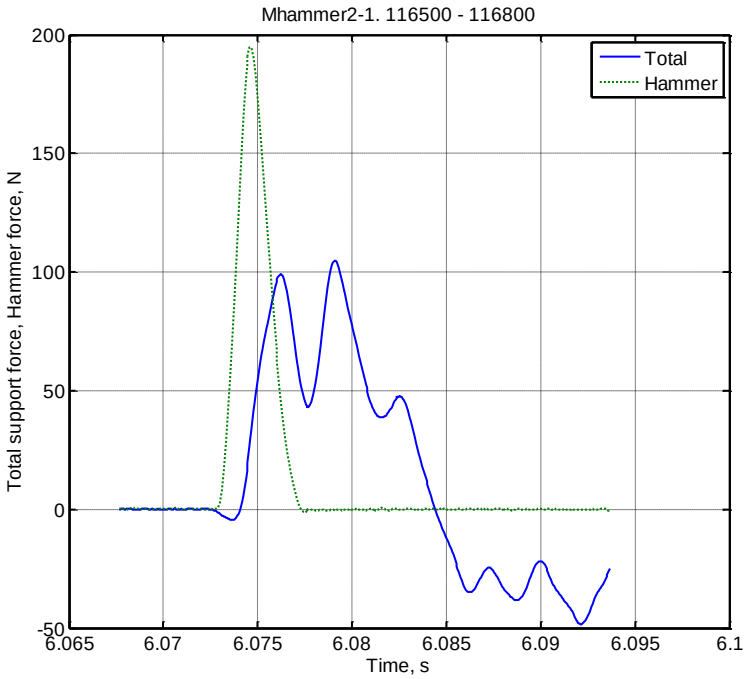

Figure 22. The impuls hammer force and the total response of the structure – expanded time view.

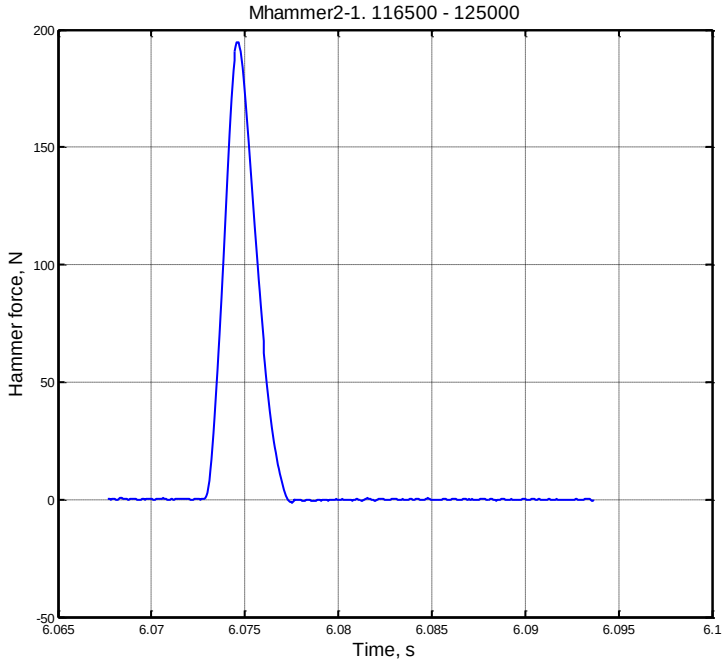

Figure 23. The transfer function concept used on the "Total" response force, Figure 20.

3.3. FRF applied to the wave slamming response forces.

We have applied the outlined procedure to obtain the wave slamming force for specific response force time series, MF054e200_2 and MF054e265_1, wave frequency 0.54 Hz, wave period T = 1.85 s, as obtained by Miriam Aashamar for her Master thesis. We have further analyzed the time series MF048e280_1 of Miriam Aakhamar's test data, wave frequency 0.48 Hz, wave period T = 2.08 s.

It should be noted that the analysis is a simplified analysis based on the assumption that we have a single degree of freedom system subjected to a "Total" force. We have filtered away the low frequency part of the response force as shown in Figure 17 and 18. The low frequency part is assumed to be Morison type forces.

The IFFT of S(ω)/H(ω), Figure 24,for the test series MF054e200_2 has a high frequency component. This high frequency component has been filtered away and we obtain a force time series as shown in Figure 25. This time series resembles the time series shown in Figures 17 and 18, except that the forces are smaller. This indicates that the applied forces are smaller than the response forces. The total force will be the high frequency forces plus the Morison forces.

Comparing Figures 25 and 18 it is seen that the ratio between the maximum response and the maximum force is approximately 9.5 N/6,5 N = 1.46. If we assume that the slamming force impulse is sinusoidal in shape, Figure 12 indicates that the ratio between the duration of the impulse and the natural frequency of oscillation is approximately 0.5 or duration time $t_1 \approx$ 0.01 s. This again means that the duration time is significantly larger than indicated in Chapter 2, $t_1 \approx 0.003$. This duration time is based on wave slamming on a single cylinder. A possible reason for the apparent longer duration time for the truss structure may be because the wave hits at slightly different time points at different parts of the structure.
The apparent highest response for all the tests was measured for the test series Mf054e265_1, wave frequency f = 0.54 Hz, wave period T = 1.85s. Figure 26 shows the whole time series of the total response force for this series, while Figure 27 shows a time expansion around t = 4 s. Figures 28 and 29 show response forces and waves, and waves respectively. This response is especially interesting since in this case the wave broke ahead of the structure and surged against the structure illustrated by the small wave height at the structure for the largest response, Figures 27 - 29.

The deep water wave height for test series Mf054e265-1, Figure 29, is approximately H_{deep} = 35 cm, while for test series MF054e200, Figures 15 and 30, the deep water wave height is approximately H_{deep} = 25 cm. This indicates that wave slamming forces may occur for a range of deep water wave heights.

It is mentioned again that since the waves break the wave measurements at the structure is somewhat uncertain, Figure 27.
As the response force is higher for tests MF054e265, when the waves break ahead of the structure, than for test MF054e200, when the waves break more directly on the structure, the surging wave for MF054e265 may give relatively higher forces on the bottom force transducers than for the tests MF054e200. Figures 31 and 32 show that this is the case.

We have selected the part of the time series of Figure 25 where the response is highest, or around t = 4 s. Figure 33 show an expanded part of the time series of Figure 25. It is noted that the wave crest height is lower in this case than for the tests series Mf054e200_1, Figure 15.

We have treated the time series of Figure 33 as we treated the time series of Figure 15. Figure 33 shows the total force response, filtered force response, high frequency part of the response and wave height, while Figure 34 shows the filteredfiltered force response and wave separately.

Finally Figure 35 shows the low pass filtered Inverse Fast Fourier Transform of $S(\omega)/H(\omega)$ for the response force, Figure 34.

Similarly the low pass filtered time series for the IFFT of the low frequency force for the test series MF054e265_1, Figure 35, shows a smaller force than the response force, Figure 34. In both of these analyzed time series the hammer pluck Mhammer2_1 has been applied. We have further applied the hammer pluck Mhammer5_1 to analyze MF054e265_1. Figure 36 shows the result of this analysis. It is seen that the maximum force of approximately 20 N is the same in Figures 35 and 36. But the subsequent forces are smaller in Figure 36 than in Figure 35.

If we compare Figure 35 and Figure 34 it is seen that the ratio between the maximum response and the maximum force is approximately 42N/20 N = 2.1. If we assume that the slamming force impulse is sinusoidal in shape, Figure 12, we are beyond the response ratio for this assumption.

Part of the test series Mf048e280 (f=0.48 Hz or T = 2.08 s) was filmed. The film shows clearly that the wave broke ahead of the structure. We have analyzed the wave that gave one of the highest responses for this test series. Figure 37 shows the total response force and the wave measured at the structure, while Figure 38 shows the “total response – filteredfiltered” response. Figure 39 shows the obtained wave slamming force. It is interesting to note again that the wave slamming force is approximately half of the wave slamming force response.

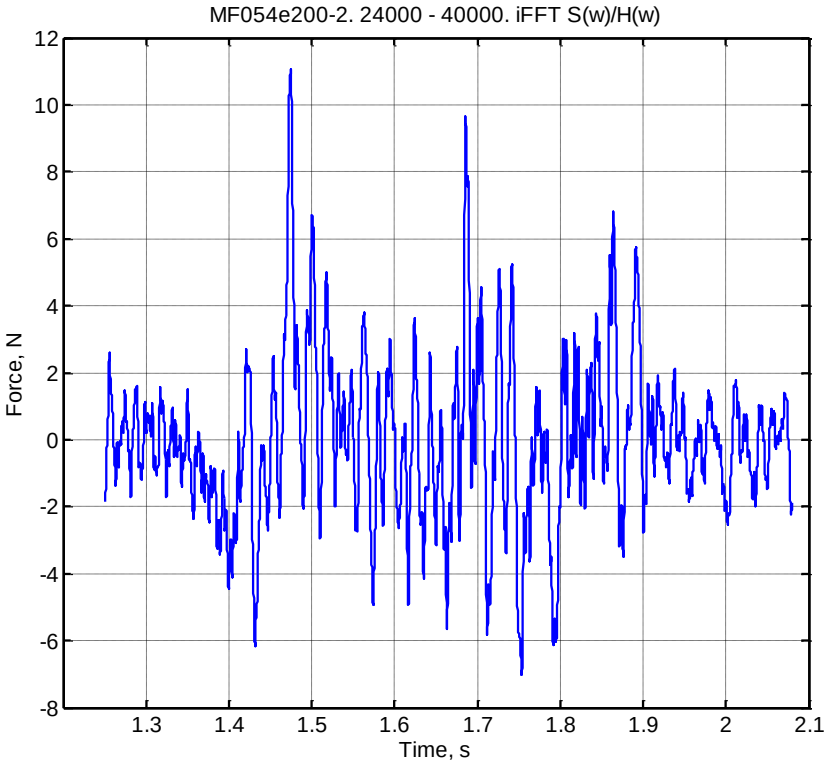

Figure 24. Inverse Fast Fourier Transform of S(ω)/H(ω) for the response force, Figure 17.

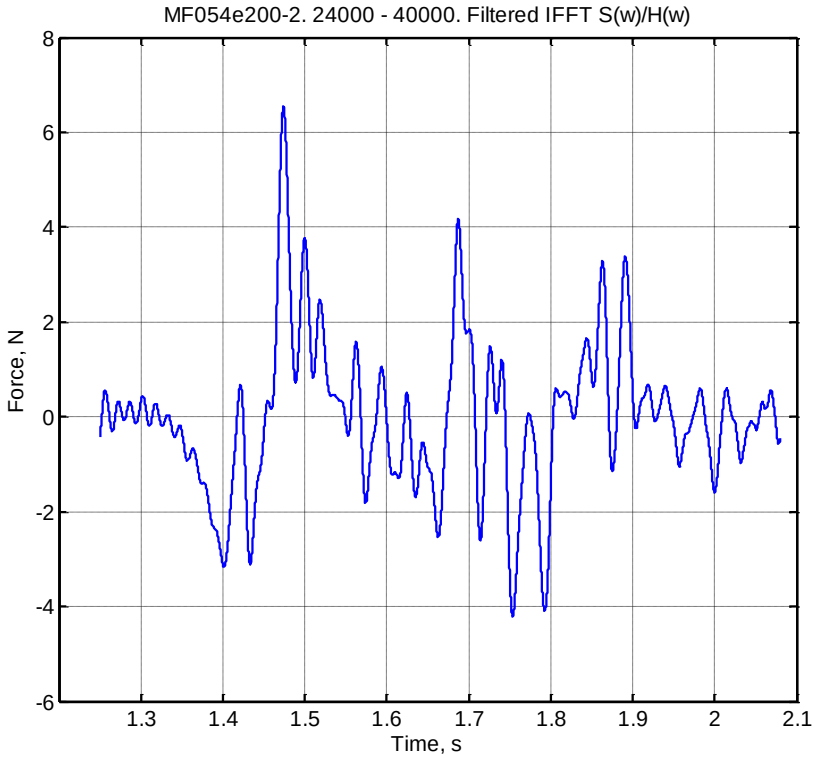

Figure 25. Lowpass filtered Inverse Fast Fourier Transform of Figure 23.

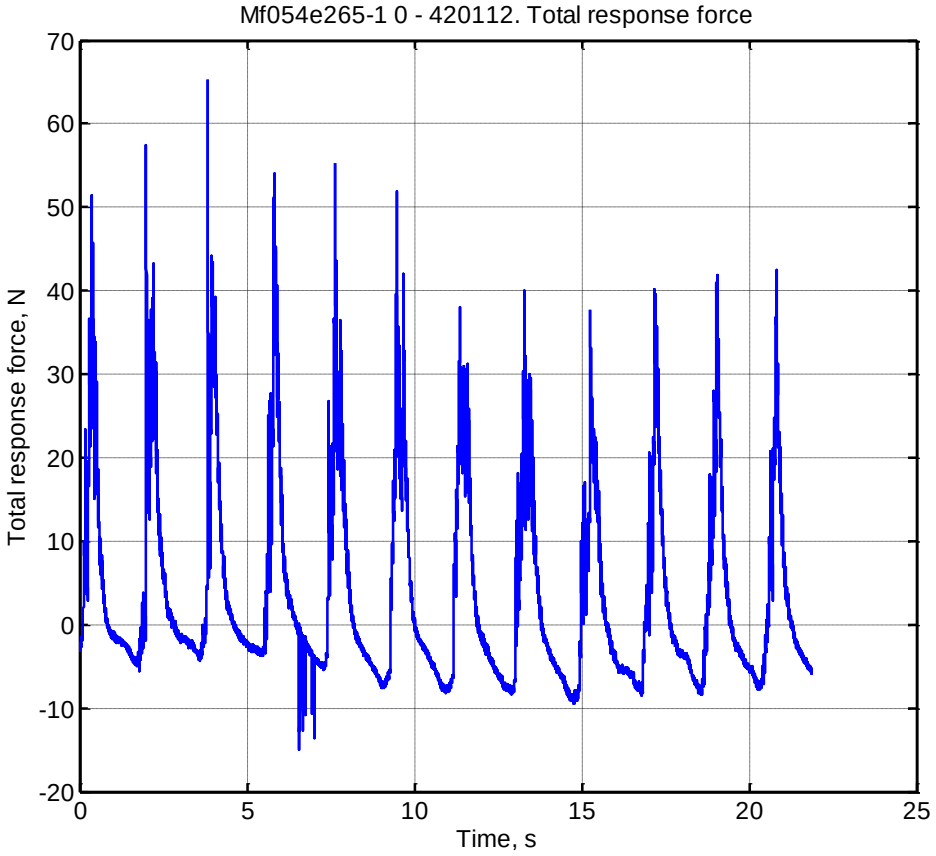

Figure 26. Time series were the highest total response force occurred.

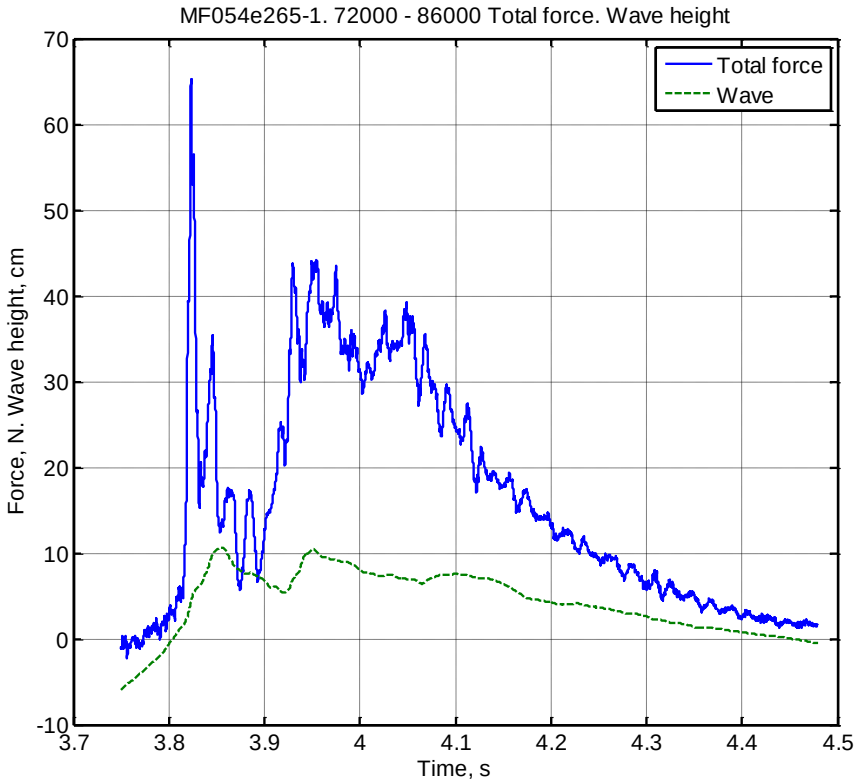

Figure 27. Time expansion for the highest response, Figure 26.

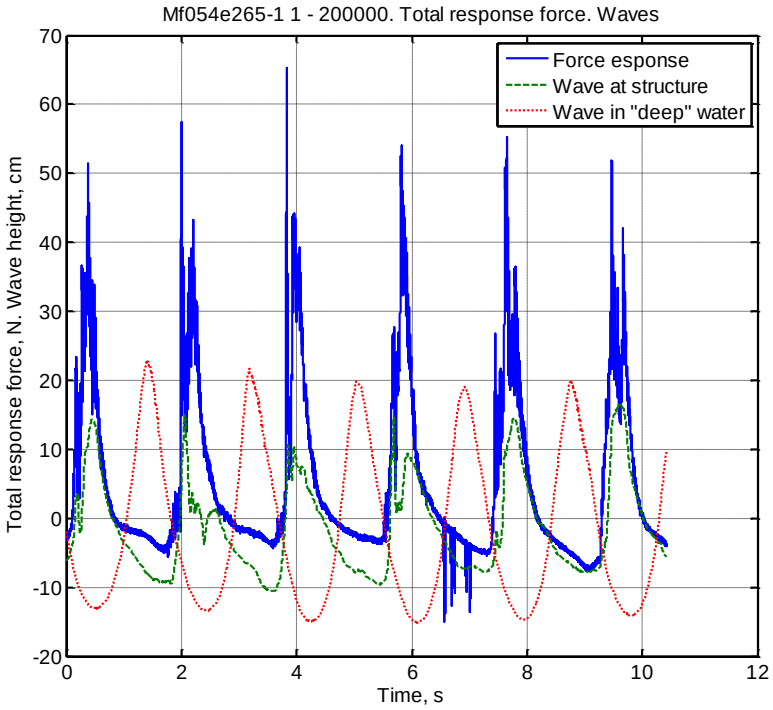

Figure 28. Total force response for the time series Mf054e285-1 and waves at the structure and in "deep" water.

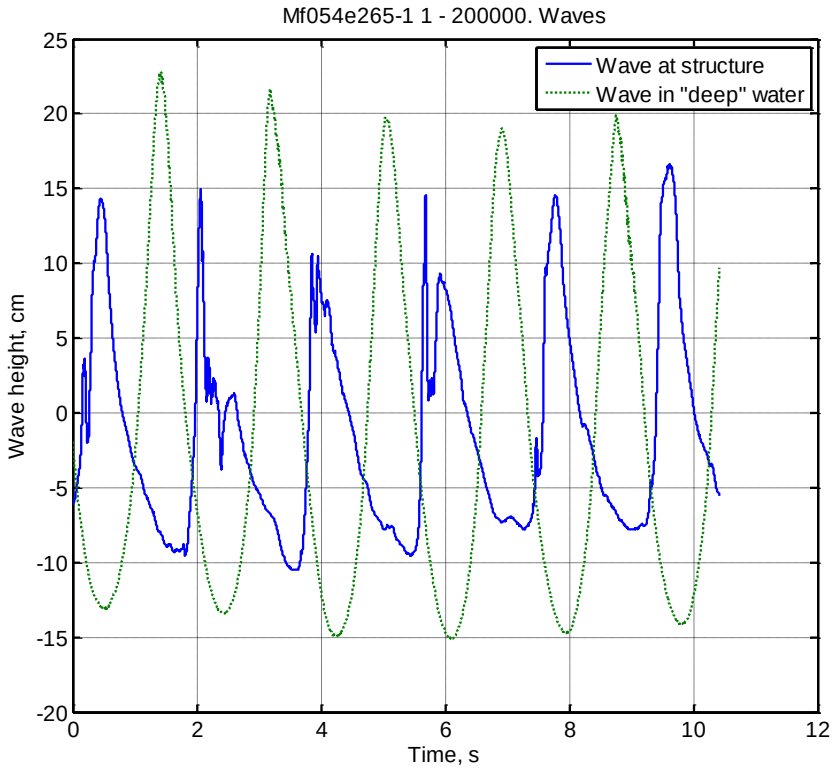

Figure 29.Time series Mf054e265-1. Waves at the structure and in "deep" water.

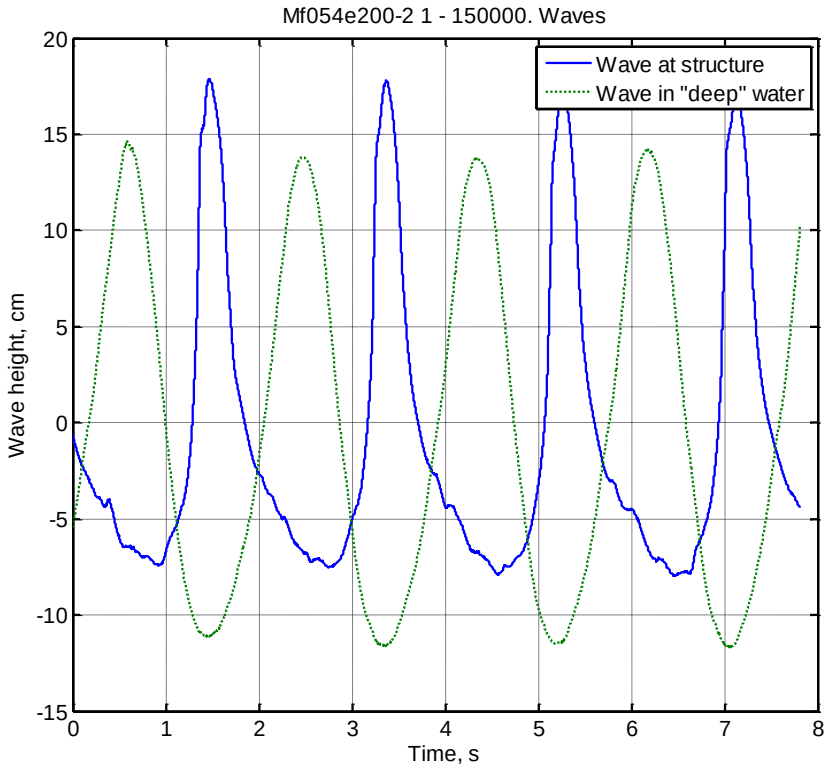

Figure 30. Time series Mf054e200-2. Waves at the structure and in “deep” water.

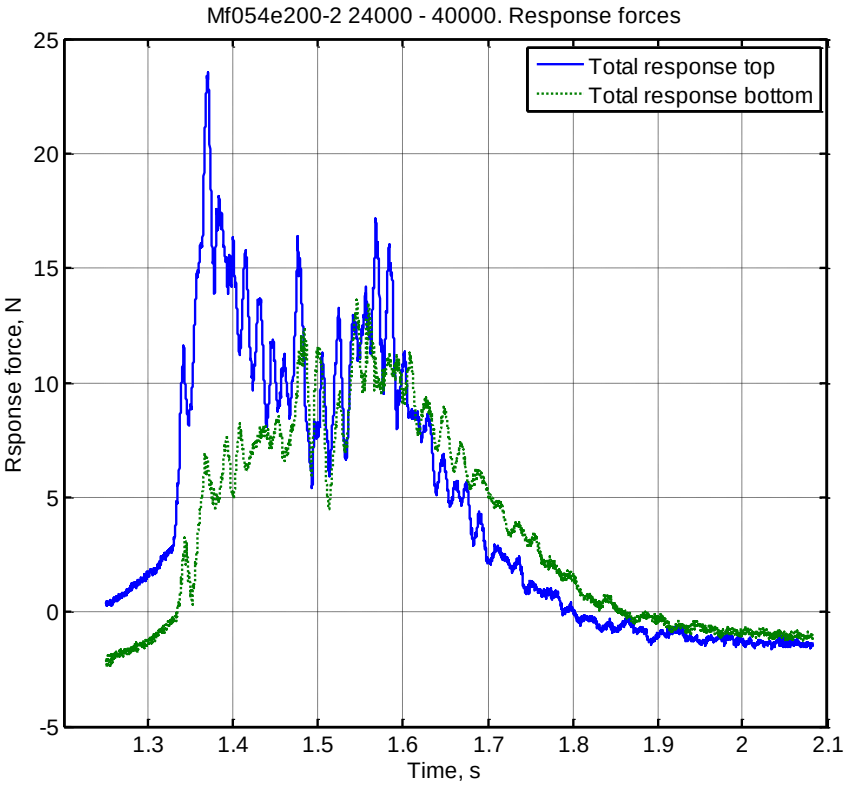

Figure 31. Time series Mf054e200-2. Total response at the top and bottom force transducers.

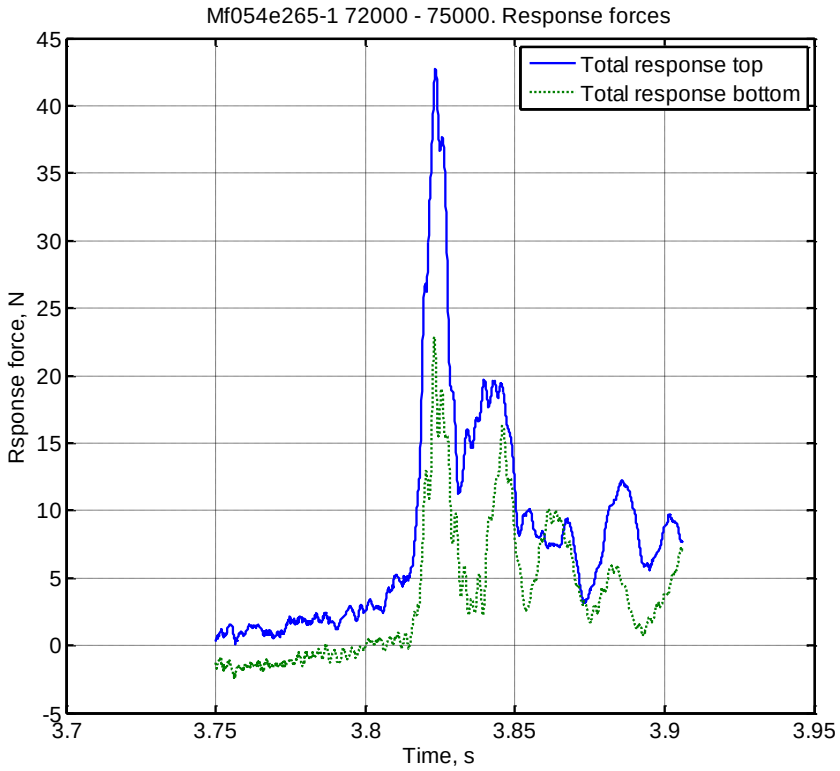

Figure 32. Time series Mf054e265-1. Total response at the top and bottom force transducers.

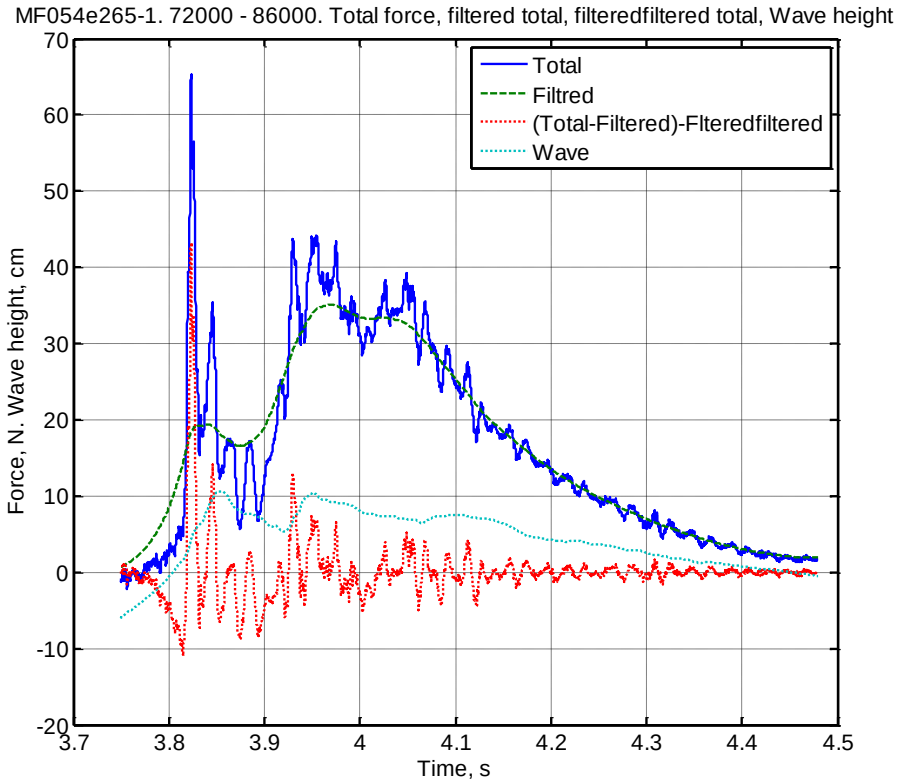

Figure 33. Total force response, filtered force response, high frequency part of the response and wave height.

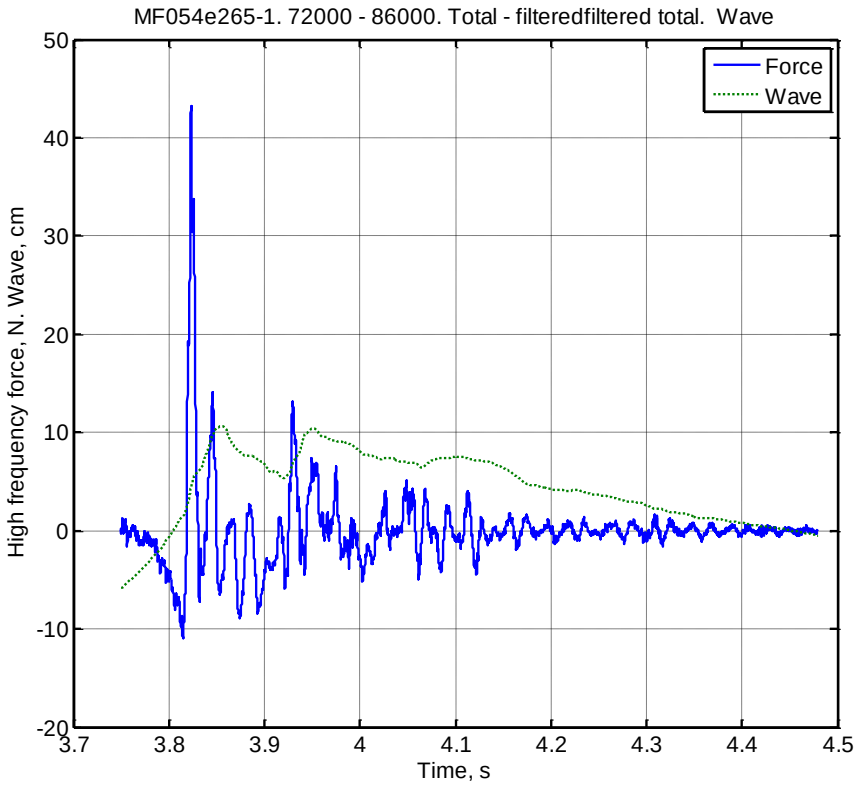

Figure 34. Total response - filteredfiltered force response, and wave at structure.

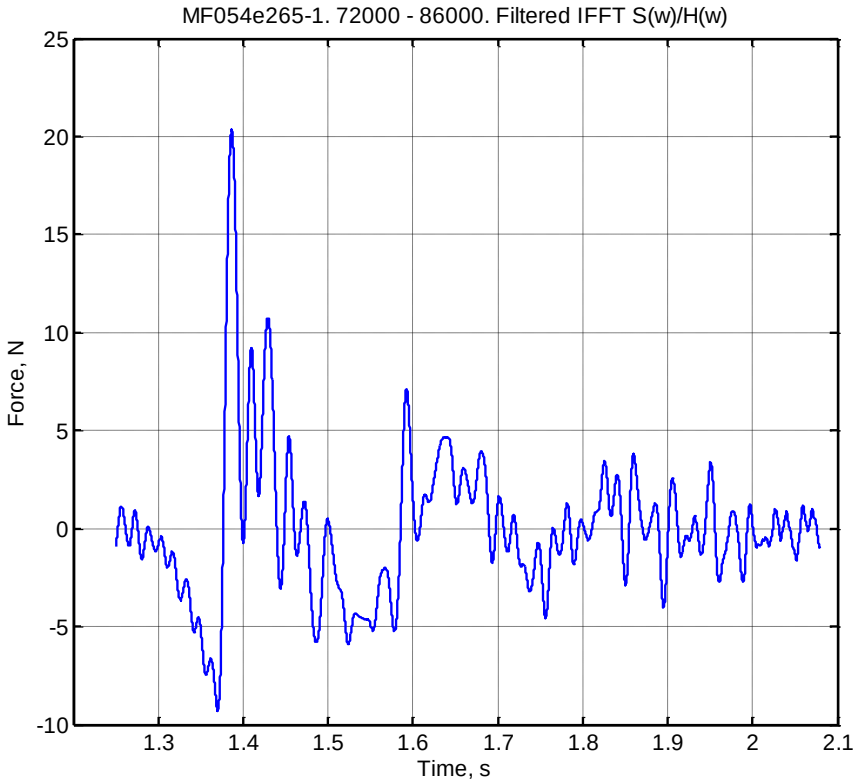

Figure 35.Low pass filtered Inverse Fast Fourier Transform of S(ω)/H(ω) of the response force of Figure 34, using hammer plucking Mhammer2-1. MF048e280.

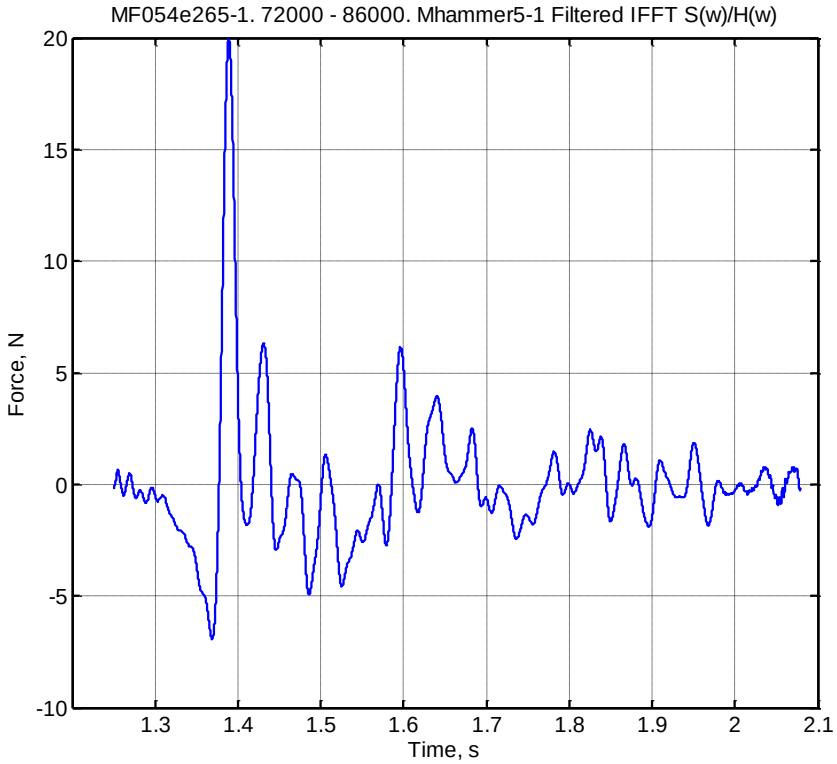

Figure 36 .Low pass filtered Inverse Fast Fourier Transform of S(ω)/H(ω) of the response force, Figure 34,using hammer plucking Mhammer5-1. MF048e280.

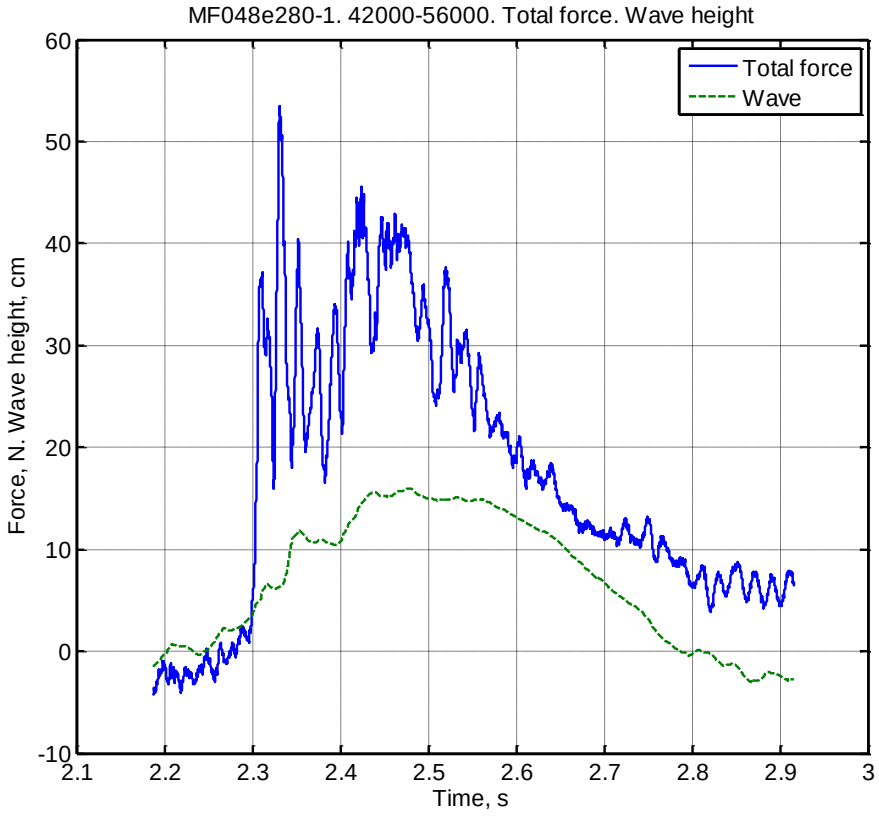

Figure 37. Total force response and wave height. Mf048e280.

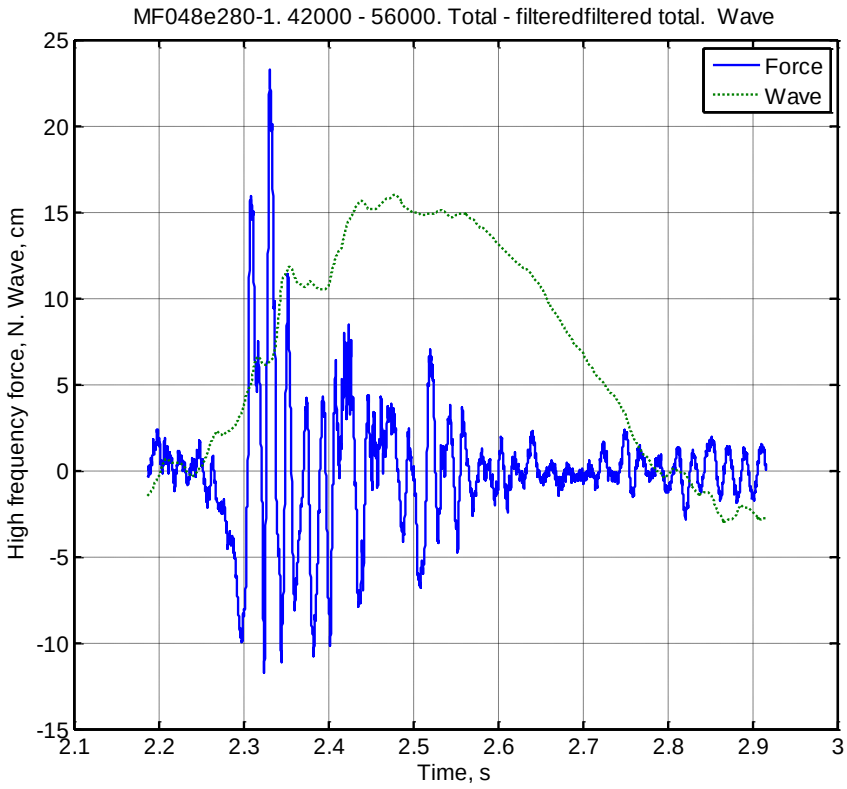

Figure 38. Total response - filteredfiltered force response, and wave at structure. Mf048e280.

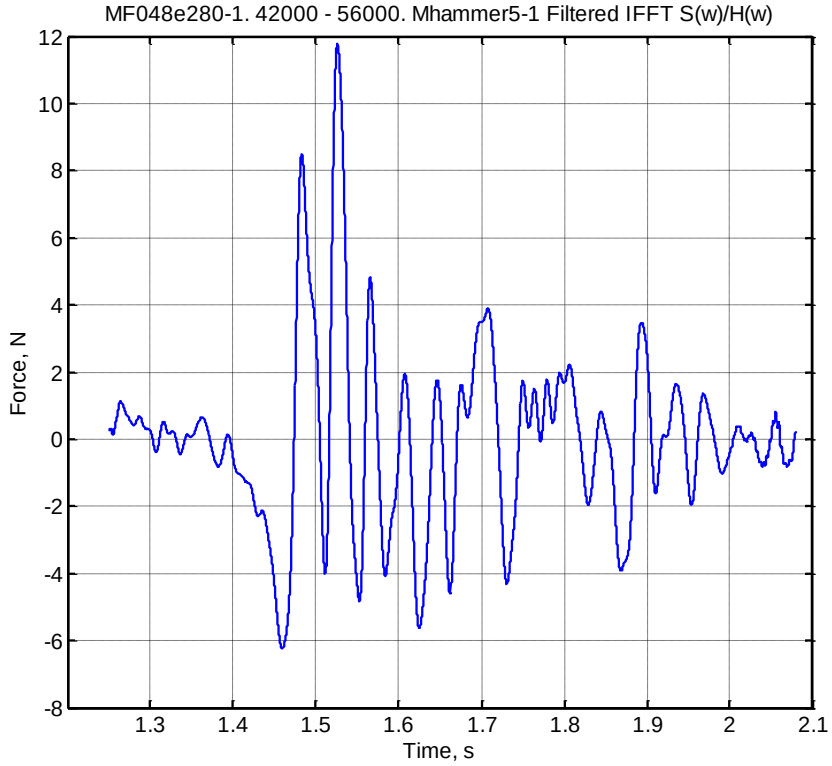

Figure 39. Low pass filtered Inverse Fast Fourier Transform of S(ω)/H(ω) of the response force, Figure 37,using hammer plucking Mhammer5-1. MF048e280.

5. DISCUSSION OF THE RESULTS

As Figure 25 shows there is a significant variation of the response forces from wave to wave, similarly as Ros (2011) also found, Figure 8, for the local force meters on a single pile.

It is interesting to note that the largest force response occurred when the wave broke some distance ahead of the structure. This was also found by Sawaragi and Nochino (1984) for a single vertical cylinder. After breaking the wave in our case surged against the structure and imposed forces with a slamming character in both the top and bottom transducers, Figure 32, while for a case when the wave plunged directly on the structure there were indications of less slamming on the bottom transducers, Figure 31. May be we have to reconsider the concept of Figure 1?

Previously the duration time of the slamming force has been derived partly from the idealized conditions when a horizontal falling cylinder is hitting still water. There are indications from our analysis that the duration time in our case is larger than obtained from this ideal approach. One possible reason for this may be because the wave may hit different parts of the truss structure at slightly different time points.

Most of the previous tests on breaking wave slamming forces has been on cylinders where the ratio cylinder diameter/wave height, D/H, has been larger than in our case. Apelt and Pierowicz (1987) found that the maximum slamming force occurred when D/H was approximately D/H = 2.0. Their investigation covered D/H as low as approximately 0.5. For D/H = 0.5 the wave slamming force was approximately 40 – 50% of the maximum slamming force, depending to some extent on the wave steepness. In the Wienke and Oumeraci case, Wienke and Oumeraci (2005) the minimum D/H value was approximately 0.7 m/2.0 m = 0.35, while in our case the minimum D/H is approximately 1.6cm/24 cm = 0.066. Extrapolations from Apelt and Pierowics indicate that it is expected to get significantly lower wave slamming forces on our truss structure members than on a mono-pile.

Other factors that may influence the results are scale effects. There is significant air entrained in the water during the breaking process and which may influence the results differently in the model and in reality. However, the tests of Sawaragi and Nochino (1984) and Ros et al (2011) were carried out with waves of the same height as has been used by Miriam Aashamar and the results of these tests are comparable to what Wienke and Oumeraci (2005) obtained from their tests on a larger scale in the Large Wave Channel in Hannover.

Although this has been a simplified analysis, the used method is promising. Further analysis should be made by using the other hammer plucking tests and look at the individual response forces for each force transducer. May be one has consider the system as a “Multi degree system”.

Slamming forces is supposed to occur on the vertical legs as well as on the bracings of a truss structure. It is thus a challenging task to resolve the slamming forces on the individual members of the truss structure. It may not be possible without carrying out the planned tests in the Large Wave Chanel in Hamburg.

ACKNOWLEDGEMENT

The writer acknowledges the many helpful discussions with professor Mauri Määtenän, who made him aware of the applied analysis method. The writer also appreciates the discussions with and help from PhD student Torodd Nord.

REFERENCES

Arntsen, Ø. Ros, X. and Tørum, A. (2011) Impact forces on vertical pile from plunging breaking waves. Proc. International Conference on "Coastal Structures, Japan, 2011.

Goda, Y., Haranaka, S., and Kitahata, M., (1966). Study of impulsive breaking wave forces on piles. Report of Port and Harbor Research Institute, Japan, Vol. 5. No. 6, pp. 1–30 (in Japanese). Concept also in English language in Watanabe, A. and Horikawa, K. (1974): Breaking wave forces on large diameter cell. Proc.14th Intern. Conf. on Coastal Eng. pp 1741–1760.

Määttänen, M. (1979): Laboratory tests for dynamic ice-structure interaction. Proceedings "Port and Ocean Engineering under Arctic Conditions" (POAC), Norwegian Institute of technology, 1979.

Ros,X. (2011). Impact forces from plunging breaking waves on a vertical pile. Master thesis, Technical University of Catalonia, Barcelona, Spain, carried out at the Department of Civil and Transport Engineering, NTNU, Trondheim, Norway, under the Erasmus Socrates student exchange program. In preparation (December 2010).

Sawaragi, T. and Nochino, M. (1984). Impact forces of nearly breaking waves on a vertical circular cylinder. Coastal Engineering in Japan, Vol. 27, pp 249–263.

Tanimoto, K., Takahashi, S., Kaneko, T. and Shiota, K., (1986). Impulsive breaking wave forces on an inclined pile exerted by random waves. Proc. 20th Intern. Conf. on Coastal Eng. pp 2288–2302.

Wienke, J. and Oumeraci, H., (2005). Breaking wave impact force on vertical and inclined slender pile-theoretical and large-scale model investigations. Coastal Engineering 52 (2005) pp 435–462.